HUNGARIAN UNIVERSITY OF AGRICULTURE AND LIFE SCIENCES

Pre-treated pine waste as an alternative energy source

DOI: 10.54598/001160

PhD dissertation

by

Alok Dhaundiyal

Gödöllő
2021

Doctoral school denomination: Doctoral School of Mechanical Engineering

Science: Mechanical Engineering

Leader: Prof. Dr. Farkas István, DSc
Institute of Technology
Hungarian University of Agriculture and Life Sciences, Gödöllő, Hungary

Supervisor: Prof. Dr. Laszlo Toth, DSc
Institute of Technology
Hungarian University of Agriculture and Life Sciences, Gödöllő, Hungary

Dr. Nobert Schrempf, PhD
Institute of Technology
Hungarian University of Agriculture and Life Sciences, Gödöllő, Hungary

....

Affirmation of head of school Affirmation of supervisor

CONTENTS

LIST OF SYMBOLS AND ABBREVIATIONS 5
1. INTRODUCTION, OBJECTIVES 6
1.1. Introduction 6
1.2. Objectives 9
2. LITERATURE REVIEW 10
2.1. Biomass processing 10
2.1.1. Mechanism of torrefaction 10
2.1.2. Characteristic of processed biomass 13
2.1.3. Operating parameters 14
2.1.4. Morphology of torrefied biomass 15
2.2. Thermo-chemical process 17
2.2.1. Classification of pyrolysis 18
2.2.2. Mechanism of pyrolysis 21
2.2.3. Modelling of pyrolysis 24
2.3. Densification of processed material 31
2.4. Summary of literature review evaluation 33
3. MATERIALS AND METHODS 34
3.1. Fuel preparation and densification by pelletising 34
3.2. Improvisation of a Joule heating system 37
3.3. Construction detail of a packed-bed reactor 39
3.4. Thermogravimetric/ Differential thermal analyses 43
3.5. Field emission scanning electron microscopy 46
3.6. Physical and chemical measurement 47
3.7. Thermo-chemical formulation 52
3.7.1 . Dynamics of a system 52
3.7.2. Chemical kinetics of pyrolysis reactions 53
4. RESULTS AND DISCUSSION 57
4.1. Investigation of physicochemical characteristic 57
4.1.1 Physical and chemical traits of processed pine needles 57
4.1.2. Physical and chemical traits of processed pine cones 62
4.2. Morphological analysis of pine waste 66
4.2.1. Structural evaluation of pine needles 66
4.2.2. Structural evaluation of pine cones 67
4.3. Thermal analysis of torrefied material 68
4.3.1. Thermal performance of pine needles in a small-scale reactor *68*

4.3.2. Thermal performance of pine cones in a small-scale reactor 72
4.3.3. Thermo-chemistry of torrefied pine waste 75
4.3.3.1. Thermogravimetry of pine needles 75
4.3.3.2. Enthalpy of reaction for pine needles 77
4.3.3.3. Thermogravimetry of pine cones 78
4.3.3.4. Enthalpy of reaction for pine cones 80
4.4. Chemical kinetics of thermally processed pine waste 81
4.4.1. Chemical kinetics of pine needle 82
4.4.2. Chemical kinetics of pine cones 86
4.5. Energy distribution and economic feasibility of the pre-treatment process 90
4.5.1. Energy allocation of end products derived from pine needles 90
4.5.2. Energy allocation of end products derived from pine cones 91
4.6. Validation of experimental results 92
4.7. New scientific results 93
5. CONCLUSION AND SUGGESTIONS 95
6. SUMMARY 96
7. ÖSSZEFOGLALÁS (SUMMARY IN HUNGARIAN) 97
8. APPENDICES 98
A1. Bibliography 98
A2. Publications related to the dissertation. 108
9. ACKNOWLEDGEMENT 110

LIST OF SYMBOLS AND ABBREVIATIONS

Y	Mass yield	%
Z	Energy yield	%
HHV	Higher heating value	MJ-kg^{-1}
T	Temperature	°C
t_p	Torrefaction time	min.
K	calibration factor	mW-μV^{-1}
ΔP	Pressure-drop	Pa
FCR	Fuel consumption rate	kg-s^{-1}
SPR	Specific pyrolysis rate	kg-s^{-1}-m^{-2}
$SGPR$	Specific gas production rate	m-h^{-1}
Re	Reynold's number	-
Pr	Prandtl number	-
L	Length of bed	m
D	Diameter of a copper tube	m
ε	The void fraction of a packed bed	-
μ	Dynamic viscosity of gas	N-s-m^{-2}
U	Superficial velocity	m-s^{-1}
d_p	Diameter of particle	m
ρ	Density of material	kg-m^{-3}
m_t	Mass of pine waste after torrefaction	kg
m_b	Mass of raw pine waste	kg
ψ	Sphericity of a pellet	-
A	Frequency factor	min^{-1}
E	Activation energy of reaction	kJ-kg^{-1}
β	Heating rate	°C-min^{-1}
a	Subscript denotes apparent activation energy	-
g	Subscript represents gas	-
f	Subscript denotes solid fuel	-
p_v	The partial pressure of water vapour	Pa
p_s	Saturated pressure of water vapour	Pa
b	Subscript denotes the bed	-
T_m	Maximum temperature peak in DTG curves	K
R	Universal gas constant	kJ-mol^{-1}-K^{-1}
α	Conversion of biomass	-
$k\,(T)$	Rate constant	-
$f\,(\alpha)$	Differential form of conversion	-
$g\,(\alpha)$	Pressure function	-
$q\,(\alpha)$	Integral form of conversion	-
c	Subscript represents cold gas	-
h	Subscript denotes hot gas	-
t	Subscript stand for thermal efficiency	-
η	The efficiency of a reactor	-
S_s	The surface area of a spherical pellet	m^2

S_p	The surface area of a pellet	m^2
ω	Specific humidity	kg(w.v)-kg(d.g)$^{-1}$
γ	Degree of saturation	-
τ	Time required to consume biomass	h
$\bar{h}$	The average value of the heat transfer coefficient	W-m^{-2}-K^{-1}
$y(\alpha)$	The generalised reduced reaction rate	-
p	Pressure exerted by producer gas	Pa
Ac.s	Cross-sectional area of a reactor	m^2
H	Height of a reactor	m
Ω_t	Energy density of torrefied material	GJ-m^{-3}
Ω_b	Energy density of raw material	GJ-m^{-3}
ΔH	Heat of reaction	kJ-kg^{-1}
$\left(\frac{dm}{dt}\right)$	Rate of decomposition of cellulose	mg-min^{-1}
$\left(\frac{dm}{dt}\right)$	Rate of evaporation of moisture	mg-min^{-1}
$\left(\frac{dm}{dt}\right)_L$	Rate of decomposition of Lignin	mg-min^{-1}
FCR	Fuel consumption rate	
SPR	Specific pyrolysis rate	
TG	Thermogravimetry	
DTA	Differential thermal analysis	
DTG	Derivative thermogravimetry	
FESEM	Field emission scanning electron microscopy	
TCD	Thermal conductivity detector	
SGPR	Specific gas production rate	
CHNS	Carbon-Hydrogen-Nitrogen-Sulphur	
ICTAC	International confederation for thermal analysis and calorimetry	
ASTM	American society for testing and materials	
HBM	Hottinger Baldwin Messtechnik	
WD	Working distance	
HFW	Horizontal field width	
TEM	Transmission electron microscope	
KAS	Kissinger-Akahira-Sunose	
FWO	Flynn-Wall-Ozawa	
FC	Fixed Carbon	
VC	Volatile Content	
HHV	Higher heating Value	
EDEF	Energy density enhancement factor	
WGSR	Water-gas shift reaction	
GHG	Greenhouse gas	
OPFP	Oil palm fibre pellet	

1. INTRODUCTION, OBJECTIVES

The significance, novelty, and objectives of the research work have been discussed in this chapter.

1.1. Introduction

By definition, biomass refers to how much tissue mass for a population is available at a particular instant of time or averaged over several periods. It is often reported either in the context of mass (g) or energy (J) per unit area (Benke and Heryn, 2007). The broader perspective includes the organic matter of plants (under and above the ground), but it is not limited. The organic matter in the soil does not fall in the biomass domain, yet some of them come under the purview of it: bacteria, fungi and meiofauna. However, soil biomass covers less than 5% of soil organic matter (Houghton, 2008).

Moreover, the relevance of lignocellulosic biomass can also be known by the fact that it comprises 50% of the carbon that converts into carbon dioxide during oxidation and putrefaction. Carbon dioxide is one of the major reasons for global warming, which is also generated from human activity. Through proper processing of biomass, the emission issue can be resolved to some extent. It is a common misnomer among people that biomass is static in nature. It is dynamic, and most forests have copious biomass (and carbon) due to their expansion. Amassing carbon during their life cycle brings an eco-balance by offsetting carbon dioxide emissions from natural and anthropogenic means. The involvement of the global carbon cycle makes the dynamic characteristic of forest biomass to be more significant. As an energy source, their compatibility with modern industries relies upon the quality of the feedstock and the effectiveness of the power plant. A shift in the ingestion of biomass with ‘ingestion’ of technology causes a low yield of the secondary products. Hence, it becomes indispensable to process the biomass and resuscitate the technology so that both can be efficiently linked up. From the application point of view, as aforementioned, the biomass has an organic matter and the ability to carbon sequestration that warrants its participation in energy generation.

Certain limitations are also appended vis-à-vis with some benefits, which can be addressed through the treatment process. Higher alkali and halogen percentage carrying biomass results in corrosion and formation of deposits. Although, adulteration of biomass with certain additives that are rich in silicon, aluminium, calcium and potassium would ease the severity of these problems. (Nikolaisen and Jensen, 2013). Another evidential issue is higher ash and moisture content in the forest waste. The agglomeration of ash and its melting point is decided by application. In the case of higher temperature application, where the secondary products are prioritised such as carbonisation, the ash melting point should be lower than a furnace temperature so that fusible ash can be easily eliminated from the system. On the opposite, it must be appreciably high if the material is heated below its melting point as it could be easily cast out from the grate.

The problem arises due to ash whilst the thermal decomposition of biomass is very much similar to those for combustion. The high moisture content material generates a substantial amount of flue-gas, increases the start-up and burn-out time, and enhance the residence time of volatile in the reactor, which in turn influence the working ability of the unit. Some species are highly hydrophilic, and they have a negative impact on the groundwater cycle (Dhaundiyal and Gupta, 2014). It is also noticed that the geometrical characteristic of biomass also governs the thermal decomposition behaviour and pressure inside the reactor (Thunman and Leckner, 2005). The other

external factors, such as the constriction of biomass and angle of repose, are impacted by the physical characteristic of the material (Mattsson, 1989).

Some methods are taken into consideration to improve the physical and chemical traits of the bio-waste. The deposition of ash on the surface of a reactor affects the convective heat transfer of the unit and accelerates the metal degeneration and enhance the energy consumption required for cleansing the gas. Besides, the percentage of aerosol and fumes in the environment are also quantified. Some anti-slagging additives like aluminium (Steenari and Lindqvist, 1998), phosphorus (Grim et al., 2011), sulphur (Jimenez and Ballester, 2005) and calcium (Thy et al., 2006), could be used as a chemical binder (Alkali-getter effects). Kaolin is one of the aluminium silicate-based additives, which converts KCl into a more complex aluminate silicate that has a melting temperature of about 1500 to 1600 °C (Steenari and Lindqvist, 1998; Steenari et al., 2009).

Similarly, zeolites, emathlite and bentonite are some of the Al-based additives used to handle the corrosive agent potassium chloride (Uberoi et al., 1990). Another source of Al-based additives is Sewage sludge. It also contains different aluminium silicate, silica and alumina, which can be added to reduce the fouling of components of the reactor (Wang et al., 2011). But the addition of additives must not put the running cost up for a plant (Tobiasen, L. et al., 2007). Another perspective can be the cofired power plant that can do the same at a relatively low cost. But the moisture content of material added with coal makes the system a more energy-intensive process. Co-firing of coal with 20% dried straw produced 6.4% less alkali than that with Ulva Lactuca (Nikolaisen and Jensen, 2013).

It was found that a single lot of wood chips might have a 20-40% variation in its moisture, whereas a densified fuel had a relatively low deviation in its moisture content. In other words, the fractional change in moisture and ash was lower as compared to the raw biomass (Møller and Esbensen, 2005). While performing pyrolysis, the movement of biomass causes elutriation and the formation of the ash at the grate. It influences the time required for the complete conversion of a single particle into the end products, which also depends on moisture content, temperature and retention period on the grate. Therefore, the size of the particle should comply with the geometry and dynamics of the pyrolysis reactor. Besides the biomass size distribution, the biomass can be further enriched to reduce the transportation cost and the running cost of the power plant.

Apart from the chemical processing of biomass, some physical processes have gained ground in the 21st Century. One of them is torrefaction or thermal pre-treatment. The biomass is thermally processed at a temperature range of 200–300 °C during the dry torrefaction. The finished product has outstanding handling, milling and co-firing (with other conventional fuels in power stations) properties. However, the enriched form of biomass has been so far confined to a pilot scale. Some technical and economic issues are yet to be addressed before implementing torrefaction for commercial purpose. During 2010–2012, this scheme made a place for itself where several plants were commissioned in Europe with a capacity of 10,000–60,000 tons per year. The potential of processed biomass is assumed to have a mammoth share in the energy market in the coming time as the product is very flexible and compatible with all types of thermal plants. The demand for processed biomass has gained momentum under Europe's new 2030 target (National Renewable Energy Action Plan). It has been categorically instructed that the application of coal must be curtailed by 70% in the coming 10 years. Consequently, it will increase the import of biomass (wood) to Europe. The expected advantages, which are to be proven, of torrefied biomass, are co-

firing by replacing coal with 50% of processed biomass, the outdoor storage of torrefied material for a reasonable amount of time. Unlike wood pellets, the energy used in transportation is lower than for wood pellets. The calorific content per kilogram is higher, better milling characteristic (size and energy use) than raw biomass and a slow biological decomposition compared to raw biomass. Therefore, for societal benefits, it is necessary to utilise the fecundity of such organic matter, which provides a significant source of clean energy without disturbing the life cycle of humankind. The increase in energy demand is illustrated in Fig.1.1.

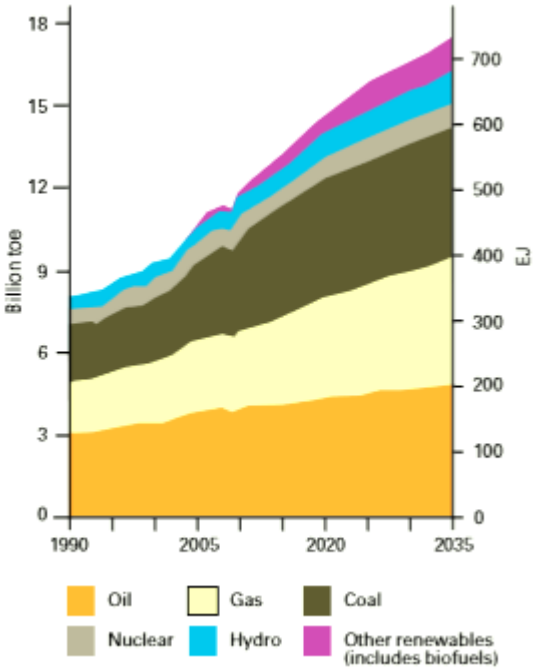

Fig. 1.1. The increase in energy demand in billion tonnes of oil equivalence and projections until 2035 (BP, 2014)

The novelty of research work

A prevailing methodology for thermal pre-treatment of the material focuses on the application of micro-waves, which pivoted around varying power output and varying operating frequency. The ramification of micro-wave torrefaction leads to cold spots within the material and poor texture due to intermolecular friction. Apart from the material properties, the risk of contamination and leakage of radiation poses a serious health hazard (Zhi et al., 2017). Some studies have also been carried out on the modified version of the micro-wave system. It was reported that the energy yield of swedge sludge and Leucaena had been surged by 21% and 7%, respectively. However, the increasing power level caused an opposite effect on the heating value of Leucaena (Huang et al., 2016). The influence of thermal condition on the feedstock behaviour was missing throughout their work. In another study, Lemongrass was torrefied in a micro-wave oven at 200–300 °C. The fixed carbon percentage was shot up to 58.72–124% during the processing time of 30–40 minutes. It is to be noted that the binding agent was added with torrefied biomass for the pelletisation process (Tan et al., 2017). Yu et al. (2020) adopted the same technology for wet torrefaction of microalgal hydrolysate for bioethanol production. They used a relatively very low-temperature range for a period of 5–10 minutes. The obtained yield of biofuel was found to be 7.61% and the effect of thermal condition on the productivity of ethanol was overlooked.

It was found that the past research work focussed primarily on the quantitative aspect of torrefaction, and the interaction of surrounding with the system was neglected. All the discussed factors encourage to take up this cause, and a dramatic change in torrefaction technology is sought in a Joule heating system rather than in the microwave oven. The remarkable change in the physical, chemical and structural properties of biomass makes the torrefaction process far more promising than any other chemical treatment method. Furthermore, the novelty of this research work hinges on the thermal condition adopted to carry out the thermal pre-treatment of biomass. So far, the result was derived from the ramped thermal history of the furnace. The mutual relationship between thermal condition and the diffusion of volatile species has not yet discussed anywhere. The method relies on the quasi-static torrefaction of the material. The waste materials used in this study have been retrieved from the Austrian pine. It has been prepared, densified and processed for examining its suitability in a newly developed pyrolysis reactor. The physicochemical characteristic depends on the operating factors, time and temperature, which play a crucial role to decide the optimal condition for performing thermal pre-treatment; therefore, these factors should also be scrutinised in this research work.

1.2. Objectives

The research work encompasses the detailed analysis of the thermal pre-treatment process and its effect on the physical, chemical and structural characterisation of the waste materials. The quasi-static technique was adopted whilst performing torrefaction in the modified Joule heating system, and based on the factors mentioned above, the objectives of this research are elucidated as follow:

- The effect of the operating condition on physicochemical traits of the processed substrate obtained by the new methodology.
- The change in the morphology of raw pine waste upon varying thermodynamic state of pine waste.
- Thermal performance of the torrefied material in a packed-bed pyrolysis reactor.
- Alteration in the reaction pathway of the pyrolysis process upon thermal pre-treatment.
- Energy economics of the derived material after the quasi-static torrefaction.

2. LITERATURE REVIEW

The literature review is based on the existing technology, physical and chemical traits of processed material, the parameters that impact the process, and the structural behaviour of the material. In the torrefaction process, the critical investigation of the thermo-chemical process, pyrolysis, has also been performed.

2.1. Biomass processing

Torrefaction is a pretreatment technology that thermally decomposes biomass in an inert atmosphere at the reaction temperature of 200–300 °C (Chen et al., 2015; Uemura et al., 2011; Bach et al., 2016). This process does not only remove the moisture content from biomass but also cause the thermal degradation of cellulose, hemicellulose and lignin in lignocellulosic biomass in the extraordinary condition of torrefaction (Commandré and Leboeuf, 2015; Williams et al., 2016), however, mainly the hemicellulose which is easily hydrolyzed, is affected the most (Shafizadeh and McGinnis, 1971).

Due to high moisture content, the auto-thermal operation gets deterred, and consequently, the torrefaction range also increases. Hence, the moisture content should not be more than 10–15%. Despite weight loss being about 30%, the energy loss is only 10%, and the biodegradable and water uptake is minimised, making it less energy-intensive. In the case of algal biomass, carbohydrates, protein and lipids are also affected (Deng et al. 2009). Consequently, the produced biochars have lower atomic H/C and O/C ratios (Almeida et al., 2010), whereas it improves grinding ability and hydrophobicity (Couhert et al., 2009; Chai and Saffron, 2016; Lorio et al., 1995). Emission of carbon dioxide and volatile matter during combustion of biochars is relatively low to the unprocessed biomass (Strom et al., 2002). Owing to physio-chemical changes, the final product obtained after torrefaction considers as upgraded biomass. Also, the transportation and inventory cost of holding biomass waste is curtailed to some extent (McKendry, 2002; Zheng et al., 2013)

Therefore, torrefaction can be considered as one of the most precise and useful pretreatments for pine waste. The pine waste is highly energetic due to higher resin content (Linden, 1984) in its bark and needles, used to extract turpentine and prevent it from beetle attack (Lédé et al., 2012; Sluiter et al., 2008; Lv et al., 2015). In the subsequent sections, detailed modus-operandi of torrefaction and its effect on the physical and chemical properties of the material have been reviewed.

2.1.1. Mechanism of torrefaction

In the beginning, the moisture content of biomass is expelled through a subcontractor so that the moisture content can be limited within the range of 10–20 %. The biodegradable waste is kept in a cubic box which a crane hoists to the top floor of the pilot facility (Fig. 2.1.), where it is collapsed down to the belt conveyor. The upper deck of the drying section has a controlling system that allows batches of ingoing waste to be bathed with nitrogen before discharging into the drying section. The mass flow controller controls the purge flow rate of nitrogen. The rate of flow of biomass in an hour is decided by the bulk density of biomass used. The working conditions of the torrefaction process mainly depend on the moisture content and the physical properties of feedstock. The biomass is heated till 150–200 °C by direct contact with recycled steam at a

maximum temperature of 220 °C. Consequently, the dried biomass enters the torrefaction section of the pilot plant reactor. The biomass is heated directly by a circulating torrefaction gas stream at

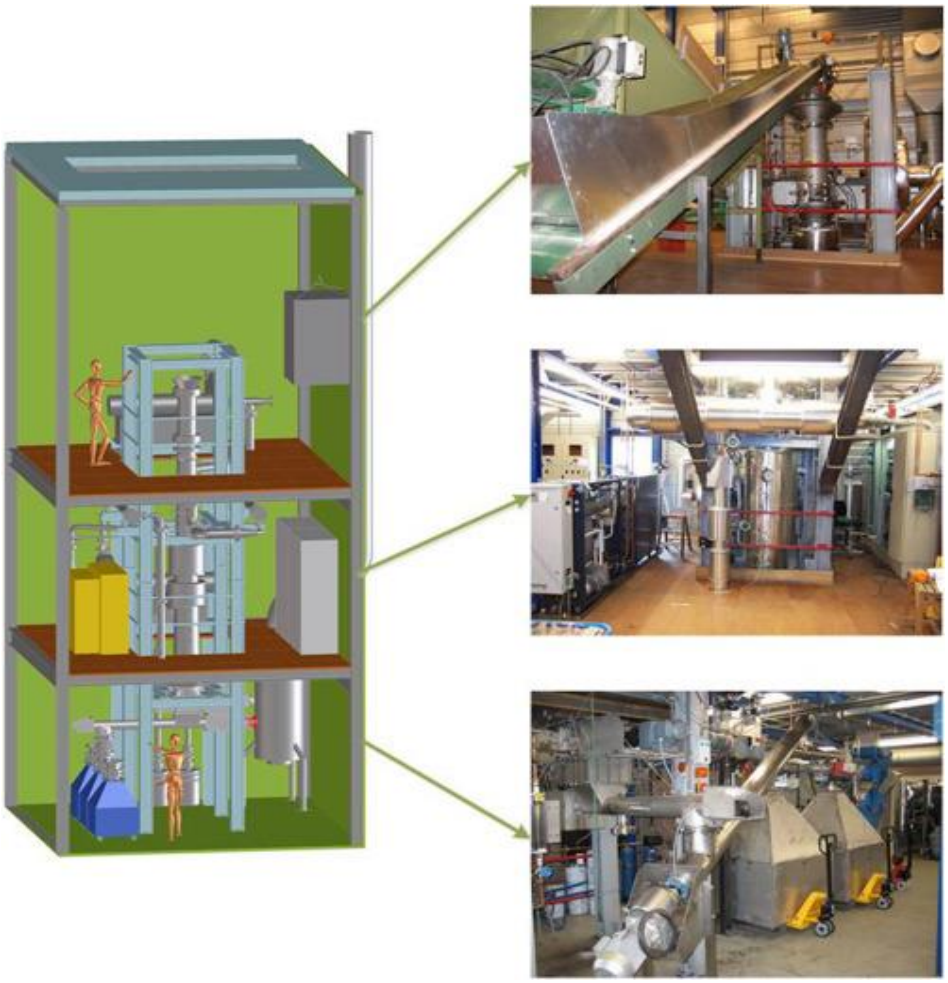

Fig. 2.1. Torrefaction plant. Top: Feeding and drying section, Middle: Torrefaction reactor, Bottom: Product collection (Nanou et al., 2016)

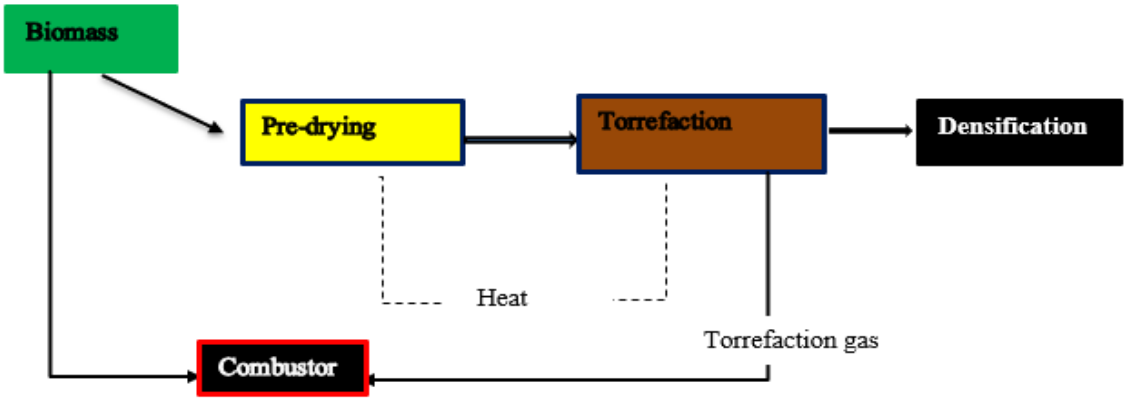

Fig. 2.2. Overall torrefaction process sketch. Navy blue units need heat and the red unit release heat

The torrefaction process can be categorised by the method of heating the biomass. The biomass can be heated either directly or indirectly. The classification of the torrefaction reactor is illustrated in Fig. 2.3.

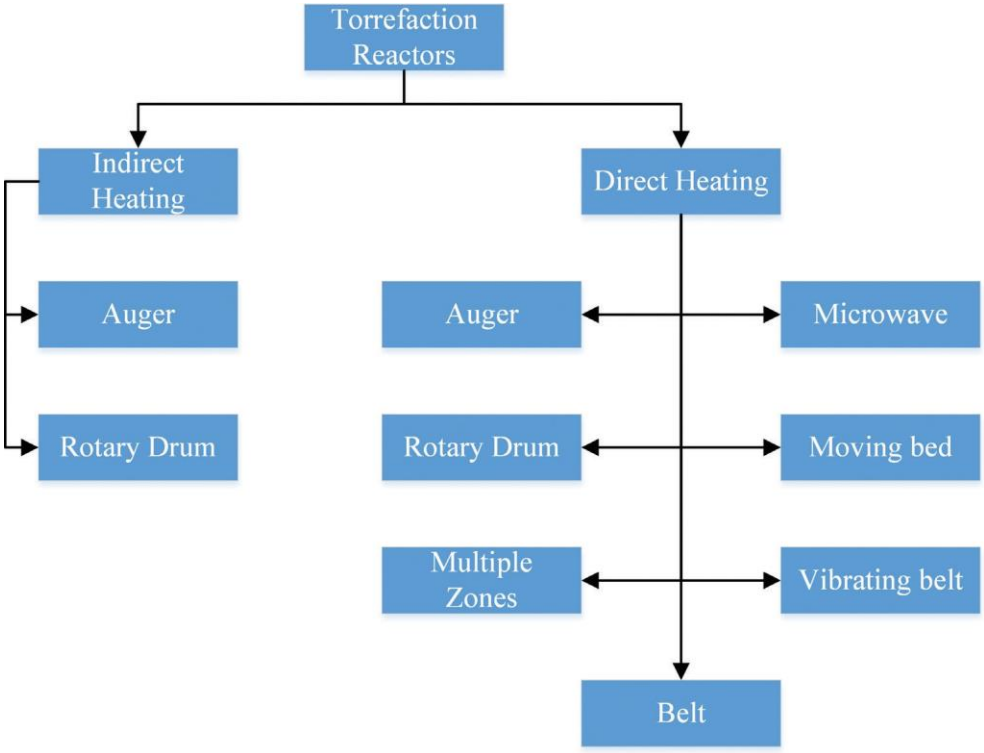

Fig. 2.3. Classification of torrefaction based on supplying heat (Dhungana et al., 2012)

Auger reactor

The auger-based reactor comprises one or more screw conveyors whose location relative to the ground could be vertical, horizontal or at a particular angle. The function of the auger is to transport biomass into the reactor. In this type of reactor, the biomass is indirectly heated by a heating medium or directly by the heating element juxtaposed to the reactor wall. However, both modes of heating supply provide uneven heating to biomass and excessive charring of the product. It occurs due to heterogeneous mixing of the substrate and non-uniform heating of the material. The residence time of biomass depends on the length and speed of the conveyor. The primary advantages of this type of reactor are its relatively low price, flexibility in industrial usage, and less demand for inert gas. The demerit of an Auger-based reactor is its limited production capacity.

Rotary drum

A rotating reactor is a type of reactor that is incessantly operating during loading or unloading. Likewise, in the auger reactor, the heat supply can be either direct or indirect. The heat is mainly provided by the circulating gas produced during the torrefaction process and heated by the heat generated via combustion of surplus tar gas, whilst the drum walls perform the direct heating. Drum torrefaction reactors are controlled by rotating speed adjustments or length and angle of drum inclination. Unlike the auger reactor, homogenous mixing and uniform heating are provided to the biomass. This reactor generates large amounts of biomass fines formed by friction between walls and the substrate. Drum reactors also have a lower processing rate than fluidised bed reactors. It is approximately in the range of 1.5–4.5 mg-h^{-1} (Nhuchhen et al., 2014)

Microwave-based reactor

This type of reactor involves microwave radiation. The micro-wave reactor can be distinguished from others by its rapid and uniform heating of the material. The duration of treatment relies on type, size and microwave radiation absorption capacity of the processed material and reactor power rating (Nhucchen et al., 2014). The loophole in this technology is the higher energy consumption for the production of microwave radiation. The generated tor gas cannot be utilised for processing purpose, which eventually influences the process efficiency and the running cost of the reactor.

2.1.2. Characteristic of processed biomass

The objective of the pretreatment of biomass is to obtain good quality fuel, reliability of end product and extensive industrial application. Prins et al. gave a kinetic model so that the kinetic mechanism of torrified biomass can be adopted for the Industrial torrefaction process (Prins et al., 2006). There is some physical attribute of biomass that is greatly affected by the pretreatment process. It is indicated that the volatile content of rice husk reduced by 30% during the torrefaction process. The fixed carbon and ash content of rice husk increases gradually with the removal of volatile matter (Chena, 2018). In another experiment on highly moisturised Licorice residue, the behaviour of fixed carbon and ash content was reported to similar to rice husk torrefaction. A rapid decrease in the molar ratio of H/C and oxygen content was observed from 210–240 °C (Xin et al., 2018). It was concluded that hemicellulose decomposition played a significant role in rearranging hydrogen and oxygen molecules (Yang et al., 2007). Besides, it was noted that hemicellulose had ample carboxyl groups, and the decarboxylation reactions liberate oxygen-containing compounds, such as water, CO_2, CO and oxygenated organics (Chaikumpoller et al., 2004; Pushkaraj et al., 2011; Shen et al., 2010). The removal of water and oxygen eventually increases the heating value of biomass; therefore, physical rearrangement of molecules attributes as a considerable improvement in the quality of biomass. Moreover, the inability of OH groups to make hydrogen bond confers biomass hygroscopic nature and torrified biomass get immunised from ingression of moisture (Pastorova et al., 1993).

Another essential facet of torrefied biomass is to improve the grinding ability of raw material. Li et al. (2004) reported that modification of microstructure in torrefied biomass provided a better grinding ability than unprocessed. The same trend was reported in the previous studies of the microstructure of sunflower seed shell (Bilgic et al., 2016; Xiao et al., 2015). Specific grinding consumption of untreated and treated biomass is compared. It was observed that the specific energy required to grind treated biomass was significantly reduced with increasing torrefaction temperature. The specific grinding energy consumption of torrefied biomass was linearly correlated with torrefaction temperature; therefore, the grinding quality of torrefied biomass improved dramatically. The effect of torrefaction on the geometric mean particle size of biomass also provides additional information about the physical behaviour of the end product. The mean particle size of torrefied biomass decreases with the increase in the torrefaction temperature. The reduction in the particle size of biomass led to increased bulk density and particle density (Phanphanich and Mani, 2011). It happened on account of a reduction in both inter and intra-particle void spaces generated after milling (Mani et al., 2004; Esteban and Carrasco, 2006). The bulk density and the particle density are loosely related physical characteristics of biomass. It was reported that the particle density of torrefied biomass relatively to untreated biomass does not change during the torrefaction process.

In contrast, the decreasing trend was recorded until the torrefaction temperature reaches 250 °C. After that, it increases up to the torrefaction temperature of 300 °C (Phanphanich and Mani, 2011). The fact was established through literature that the chemical and mechanical properties are highly correlated with torrefaction conditions. Therefore, it is inevitable to examine these conditions critically.

2.1.3. Operating parameters

During the torrefaction process, biomass retains most of its energy. It simultaneously loses its hygroscopic properties, making it the best fuel for multi-purpose usages, but how does it happen? So, there are various operating parameters of torrefaction that affects the energetic and gravimetric aspects of biomass.

Parameters related to the treatment process are temperature, residence time, inert gas flow and heating rate. In contrast, the particle size, moisture content and relative fraction of biomass polymer are related to the raw material subjected to torrefaction. Out of these parameters, the temperature has a significant role in the physio-chemical transformations happening within the biomass. Energy and mass yield are two critical outcomes of biomass pretreatment. Mass loss of biomass during torrefaction is mainly due to the removal of water and volatile content. The solid yield of biomass is not affected unless it reaches a critical temperature of decomposition of hemicellulose, a highly unstable biomass component. In the temperature range of 210–240 °C, there is a negotiable decrease in solid yield by 10%. On the other hand, the solid yield decreases by 35.6% when the same sample undergoes thermal treatment at 270–300 °C (Chena et al., 2018).

It was reported that the residence time and higher heating rate have a significant effect on the carbon content of solid waste. High temperature causes a low mass yield but provides a high-density fuel. Besides variation in the physical aspects of biomass, rearrangement in the chemical composition of biomass also takes place. As the torrefaction temperature elevates, the fixed carbon in biomass increases. In contrast, the fraction of hydrogen and oxygen decreases due to breakage of inter and intramolecular and emission of hydrophilic extractives (Bridgeman et al., 2008). It was reported that variation in the mass yield was proportional to an exponential function of the temperature and residence time (t). Thus the thermal gradient was formed between the surface and the particle's core (temperature inside particle more than that of a surface) (Ciolkosz and Wallace, 2011). Another energetic facet of torrefaction is the heat of reaction. In an experimental evaluation of the energy balancing of torrefaction of beech wood, it was observed that with increasing reaction temperature, the torrefaction process becomes less endothermic (Strandberg et al., 2015)

In another study, it was found that the yield of the solid product decreases with the temperature and the residence time, whereas the gas, tar and water yields increased. The carbon content and the calorific value of torrefied biomass increased at elevated temperature and longer residence time, whilst it has the reverse effect on the O/H ratio. The sample of wood introduces more solid products than the agricultural residue (bagasse) after torrefaction. Also, the calorific value and composition of gaseous products (especially CO, CH_4 and hydrogen carbons) increases as the residence time dilated. There is no substantial evidence of the influence of inert gas on the torrefaction process reported (Pach et al., 2002). The effect of particle size influences the heat transfer as well as residence time. The residence time gets minimised when the heat transfer rate to and within the particle is faster than the reaction rate. It implies that the solid temperature must

be essential homogenous throughout the reactor; thus, the overall controlling factor is the intrinsic kinetics only. It happens only when the Biot number much smaller than unity; therefore, heat conduction within the particle is much faster than heat convection to the particle decomposition of biomass components such as glucomannan, 60–70% of hemicellulose fraction in softwoods. The pyrolysis number (Pyle and Zaror, 1984a)should be sufficiently larger than unity so that the overall rate of reaction torrefaction is rate-limiting (Prins et al., 2006). It was suggested that the nature of biomass also affects the mass yield. Based on hemicellulose content, it was concluded that the mass yields of hardwood and softwood differ drastically from each other under similar torrefaction conditions (Prins et al., 2006; Basu, 2018). Since xylan is the active constituent (80–90%) of the hemicellulose of hardwood, whereas it is 15–30% in softwood, therefore the mass yield of hardwood is relatively less to softwood. The xylan of hemicellulose is highly unstable during torrefaction and it decomposes faster than other solid components of the biomass, thus the mass loss is mainly influenced by the xylan content rather than other contents of hemicellulose alone. The moisture content of biomass is another important factor that affects the mass yield of processed biomass. The torrefaction experiment was conducted on two different samples of corn stove (having a moisture content of 3% and 22 %) at 200 and 250 °C. It was observed that the high moisture content of the corn stove increased the dry matter loss by 10% (Turner et al., 2010). There is a high likelihood of the concentration of water molecules correlates with the rate of hydrolysis during torrefaction, so it has been emphasized to conduct studies on the thermal behaviour of biomass at different concentration of oxygen (Saadon et al., 2014). Chen and Kuo (2011) assessed the torrefaction behaviour in the oxidative environment and they observed that the thermal reactivity of biomass gains huge momentum due to the acceleration of mass loss at the initial stage of torrefaction. Another important deciding factor of mass yield is the heating rate. The heating rate in torrefaction is kept low, therefore it is one of the important aspects that make it different from the fast pyrolysis process. Tran et al. (2013) reported that the slower heating rate is good for obtaining a high solid yield. The optimum heating rate observed to be 10 °C-min^{-1} for fetching high energy density fuel and high mass yield, therefore the heating rate should not be more than 50 °C-min^{-1} (Bergman et al., 2005). The operating range of temperature should be in-between 200 and 300 °C and the process must be conducted at low heating rates and low residence time under inert conditions (Basu, 2010; Chen et al., 2013; Chew and Doshi, 2011). Overall assessment of the torrefaction process depicts that the temperature and heating rate are the major key factors for materializing the energetic aspects of biomass pretreatment.

2.1.4. Morphology of torrefied biomass

Whilst torrefaction of corncobs, it was reported that there are not only physiochemical but also structural transformations that occur in biomass: hemicellulose, cellulose and lignin (Zheng et al., 2013). Xylan has a mass loss of 12.2–28.5% during torrefaction for 10 minutes at a temperature of 220–250 °C, whereas Lignin decomposition largely depends on oxygen-containing compounds (phenols, methoxyl, aliphatic alcohols, carbonyl and ether), therefore it decomposed over the broad temperature range. Cellulose remains thermally stable at a torrefaction temperature of 220 °C. A 3 % mass loss of cellulose was recorded for 5 h of treatment at 220 °C (Lv et al., 2015). The effect of torrefaction on the cellulose component leads to an overall increase in the aromaticity of biomass. The reason for high stability at a low temperature is carbonization and cross-linking reaction which makes it mechanically and thermally immune (Lédé et al., 2012; Sluiter et al., 2008).

Due to variation in the chemical structure of basic polymers of biomass (cellulose, hemicellulose and lignin), their reaction pathways, as well as thermal decomposition, are different from each other. Biomass Torrefaction is not just related to expelling the moisture content out of biomass, but it also causes decomposition of basic constituents of biomass (hemicellulose, lignin and cellulose) to some extent, which is later become the reason for mass loss (Sluiter et al., 2008; Thangalazhy et al., 2011). It has been extensively examined that the cleavage of β-O-4 linkages liberates phenolic group from etherified phenolic hydroxyl and resulting in an increase in the aromaticity of lignin during thermal processing (Zheng et al., 2013; Sluiter et al., 2008; Thangalazhy et al., 2011; Mohan et al., 2006). The variation in the aromaticity of torrefied biomass attributes cleavage of lignin ether bonds and decomposition of carbohydrates which could re-condense to form 15 aromatic C-C and C-H bonds (Yang et al., 2014; Bai et al., 2014; Chaiwat et al., 2008). Based on factual evidence, it has been concluded that the thermal treatment leads to the depolymerization of different components. Moreover, the constituent that is highly affected due to temperature ramping is lignin. The cleavage of β-O-4 linkages of lignin initiate above 245 °C, therefore it becomes indispensable not to overlook structural transformation of biomass during torrefaction, as it changes the reactions of different polymers and affect the yield of the end products (Melkior, 2012). It is visible in Fig 2.4 and Fig. 2.5 how the thermal pretreatment does influence the bio-oil yield (Chaiwat et al., 2008; Sierra et al., 2008). The structural array of constitute of biomass is shown in Fig. 2.6.

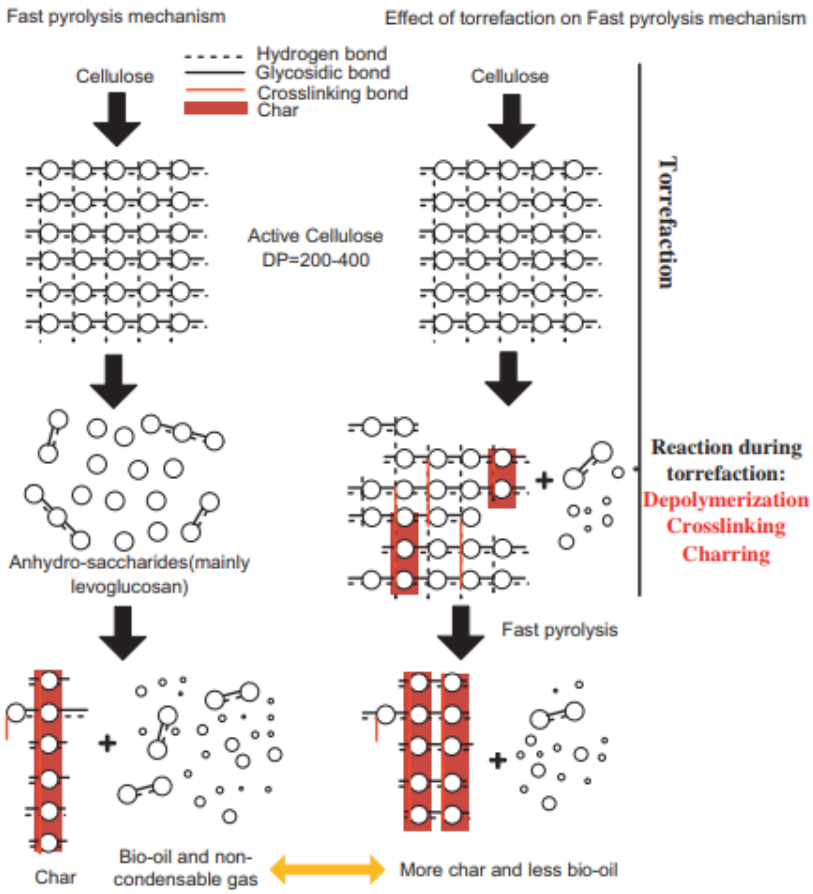

Fig. 2.4. Effect of torrefaction on the cellulose structure of biomass (Chaiwat et al., 2008)

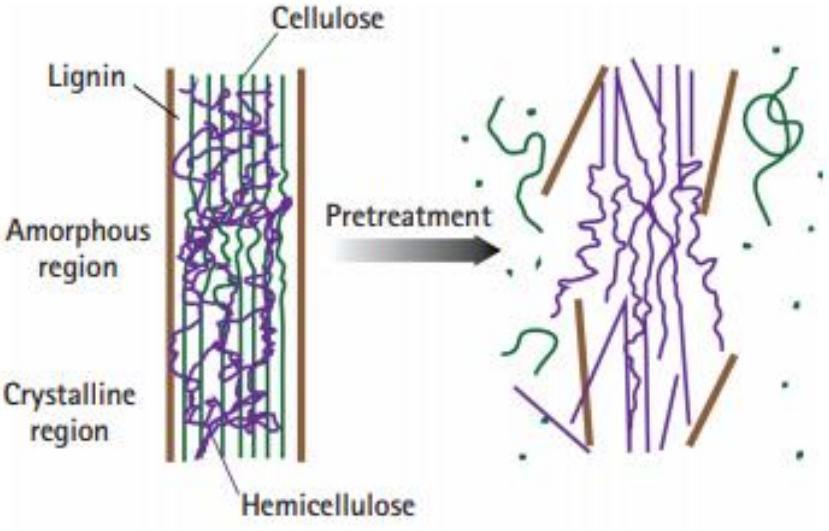

Fig. 2.5. Pre-processing affects the biomass structure (Sierra et al., 2008)

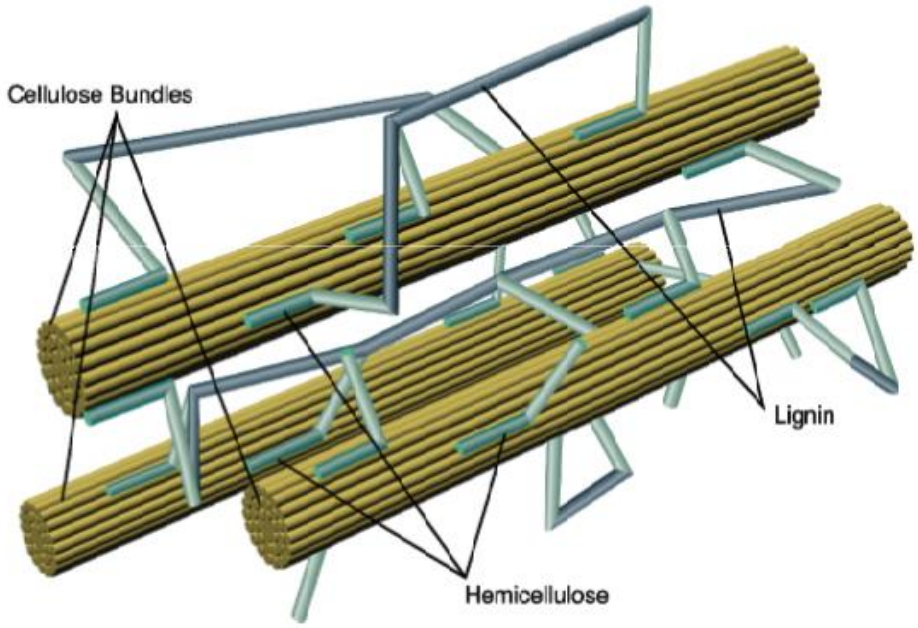

Fig. 2.6. The structural array of cellulose, hemicellulose, and lignin in biomass (Murphy and McCarthy, 2005; Shaw, 2008)

2.2. Thermo-chemical process

Pyrolysis is one of the thermochemical treatments carried out in the absence of oxygen. In this process, the material subjects to a high temperature ranging from 300 to 500 °C. It undergoes a chemical and physical transformation which allowing to receive products of fine quality than original residue. Unlike combustion and gasification that involve complete or partial oxidation of material, pyrolysis initiates by the indirect heating of the material in the absence of air. This makes it an endothermic process to some extent and allows to explore the behaviour of constituent parts of biomass. It was observed that the heat variation during the pyrolysis process was associated

with thermal degradation reactions, which may influence the course of pyrolysis. Several endothermic and exothermic peaks were observed during experimentation (Dhaundiyal et al., 2018a; Tang and Neikl, 1964; Stamm and Harris, 1953). It was reported in several papers that cellulose pyrolysis follows an endothermic pathway (Nassar and Mackay, 1984; Brown et al., 1952), whereas lignin pyrolysis was exothermic in nature (Demirbas et al., 1996). Distinguishing pyrolysis from other similar processes, such as torrefaction and carbonization, is quite subtle, but a dichotomy does exist among them. In the thermal sciences of treatment processes, pyrolysis can be considered as an umbrella term (torrefaction, slow and fast pyrolysis, catalytic and non-catalytic, carbonisation) whose main objective is to maximise the bio-oil yield, whereas the motive of torrefaction and carbonization are to retain the solid products in the best possible ways. The mass yield and energy density of the biomass is the major yardstick to access the pre-treatment process, torrefaction, which can also be defined as isothermal pyrolysis of biomass. On the contrary, carbonization is very similar to torrefaction in many aspects but it repels most of the volatiles, whereas torrefaction possesses most of it and eliminate only the low energy-dense compounds along with breakage of water molecules. Therefore, whilst torrefying the biomass, the carbonization reactions that expels the volatiles should be discouraged. Finally, the most noticeable difference is that the carbonization, which provides smoke-less fuel, does not retain the maximum amount of energy of biomass than the torrefaction process (Kihedu, 2015). It is clear from literature analysis that pyrolysis has a broad spectrum and torrefaction, or other similar processes are schism, which can be demarcated from each other through temperature constraints.

2.2.1. *Classification of pyrolysis*

Motivation and processing conditions of the substrate decide the course of the chosen technology. Therefore, the classification of treatment methodology becomes indispensable. Pyrolysis is differentiated based on biomass characteristic, involvement of catalyst, the end products and the operating conditions. As torrefaction is governed by temperature and residence time, so is the thermochemical process. The characteristic of pyrolysis is based on the temperature range experienced by the samples of a substrate (Fig 2.7). In the case of slow pyrolysis, the residence time of vapour in the pyrolysis reactor is in the order of minutes or prolonged. This condition is promising to maximize the oil yield. Carbonisation and torrefaction also share a trait of slow pyrolysis. Torrefaction related to the low and narrow range of temperature, whereas carbonization occurs at the high and wide range of temperature. In the contrast, in fast pyrolysis, the vapour residence time is in the order of seconds or milliseconds. This process is mainly used to produce bio-oil and gas. According to literature reports, fast pyrolysis produces less char but more gas than slow pyrolysis. The high yield of gas indicates that the fast pyrolysis could intensify the decomposition of small pyrolysis oil components into gas products. In similar thermal conditions, fast pyrolysis provides heavier oil but relatively less light oil than slow pyrolysis. It is also concluded that the major portion of light oil is water (Ben and Ragauskas, 2011). Hence, automotive and biochemical industries could take vantage of heavy oil yield derived through fast pyrolysis. The effect of fast pyrolysis is not limited to end yield, but it also influences the structural transformation of biomass. The content of methoxyl groups in biomass is decreased by 76% in pinewood during the fast pyrolysis at 600 °C. The carbonyl group decreased by 76% and it is nearly expelled out of pine wood. An 86% increase in the aliphatic C-O bonds formed during the fast pyrolysis than that of slow pyrolysis (Ben and Ragauskas, 2013). It is examined that percentage of C-C bonds is relatively reduced to C-O bonds as the heating rate increases

(Debdoubi et al., 2006). Comparatively, the fractions of aromatic C-H bonds and polyaromatic hydrogen carbons are increased during the fast pyrolysis. As a result of increasing molecular weight and aromaticity, it could be a burden to the refining process. Finally, it gives a clear picture that fast pyrolysis triggers depolymerization at a higher rate than slow pyrolysis. The relative yield of heavy oil from pine wood is 125% to yield obtained from the slow pyrolysis and cleavage of several functional groups also increased. The nature of end products after pyrolysis of Bagasse is illustrated in Tables (2.1), (2.2) and (2.3) (Arni, 2018). These processes come under noncatalytic pyrolysis or the traditional way of carrying out pyrolysis.Another way of demarcation is based on the external agent used to carry out pyrolysis. Catalytic pyrolysis is an upgraded manner of performing pyrolysis. It is one of the solutions to fetch a good quality of biofuel in terms of heating value, oxygen content, viscosity and stability. Catalytic pyrolysis is conducted by introducing the catalyst into a fast pyrolysis process to induce several catalytic reactions during pyrolysis, which in turn provide a fuel that is partially or entirely different from non-catalytic bio-fuel. In a study, it has been observed that adding catalytic helps in decomposing the higher hydrocarbon and removing the oxygen which results in a good quality of bio-oil with a better viscosity index (Chen et al., 2017). In the presence of a catalyst, the released volatiles underwent deoxygenation (dehydration and decarboxylation,) that results in the formation of hydrocarbon as well as generates carbonaceous solid, coke. The effect of the formation of coke during pyrolysis decreases the yield of liquid product (Fig 2.8) (Carlson et al., 2008; Gayubo et al, 2004). The amount of coke formed during the process solely depends on the biomass, type of catalyst and process temperature. It has been found that the coke does not influence the primary and non-volatile product of pyrolysis, char (Czernik, 2012). The catalytic process affects the composition of producer gas. It promotes the formation of carbon dioxide, methane and alkene hydrocarbon gases, whereas the normal thermal process emanates carbon monoxide and hydrogen and alkane hydrocarbon. Moreover, the presence of the catalyst significantly increases the formation of aromatic hydrocarbons. Relation of aromatic HC yield from catalytic pyrolysis is directly proportional to the weight of cellulose, but inversely to torrefied biomass. Catalytic fast pyrolysis of biomass is mainly performed in the presence of zeolite catalyst which is the most reliable way of getting a good quality of bio-oil. Furthermore, it has good thermal and hydrothermal stability as well as it is the most effective catalyst for aromatic hydrocarbon production from the pyrolytic vapour (Jae et al., 2011).

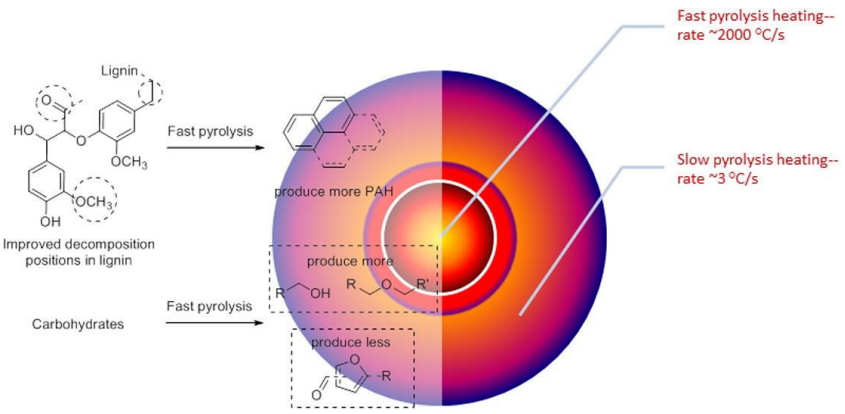

Fig. 2.7. Graphical representation of pyrolysis (Ben and Ragauskas, 2013)

Table 2.1. The effect of slow pyrolysis on the end products of Bagasse (Arni, 2018)

End Products	Temperature (K)									
	663	753	803	853	873	893	953	1143	1203	1253
Char	33.67	37.64	35.67	33.33	32.33	31.67	27.67	27.33	31.30	30.67
Tar	27.11	26.11	24.13	22.67	26.67	29.33	21.67	20.33	19.20	19.33
Gas	26.43	25.10	26.20	30.50	29.40	26.30	35.67	41.33	36.10	37.50
Losses	12.79	11.15	14.00	13.50	11.60	12.70	14.98	11.00	13.40	12.50

Table 2.2. The fractional yield of Bagasse during Fast Pyrolysis (Arni, 2018)

Products (%)	Temperature (K)				
	653	753	853	953	1053
Char	28.33	25.34	29.86	29.53	27.26
Tar	47.13	50.89	42.81	39.77	38.11
Gas	11.33	14.12	15.46	17.94	21.32
Losses	13.21	9.65	11.87	12.76	13.31

Table 2.3. Syngas composition at fast and slow pyrolysis (Arni, 2018)

Syngas (vol%)	753 K		853 K		953 K	
753 K	Fast	Slow	Fast	Slow	Fast	Slow
CH_4	21.5	17.6	6.9	31.1	17.0	7.2
H_2	8.7	9.6	15.2	21.3	45.3	28.8
CO_2	52.4	11.7	58.1	20.7	14.4	23.9
CO	13.9	60.1	18.7	25.1	20.5	37.7
$C_2H_4 + C_2H_6$	2.2	0.6	0.7	1.3	1.7	0.9
C_3H_8	1.4	0.4	0.4	0.5	1.1	1.6

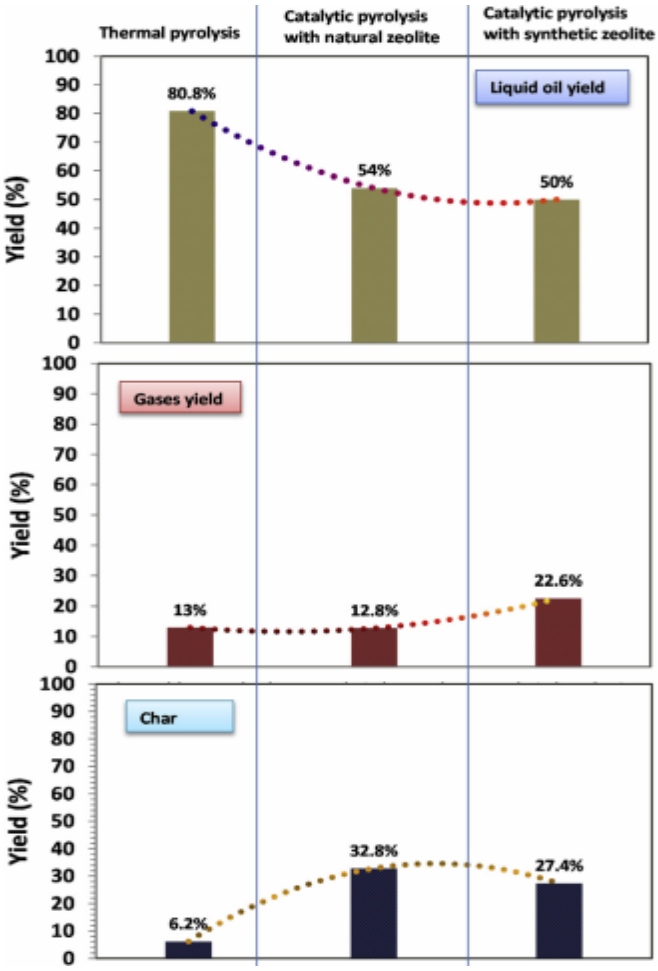

Fig. 2.8. The yield of liquid oils, gases and char from thermal catalytic pyrolysis (Rehan et al. 2017)

2.2.2. Mechanism of pyrolysis

The basic phenomena that occur during pyrolysis are transferring of heat from the heat source which results in an increase in temperature inside the fuel and the initiation of pyrolysis reactions due to the increased temperature. The raised temperature causes the formation of char and the release of volatiles. The flow of volatiles towards the ambient resulting in heat transfer between hot volatiles and unpyrolysed fuel (cooled portion). Condensation of some of the volatiles in the cooler region of fuel causes the formation of a black slimy substance, tar. Besides the production of tar, it also triggers auto-catalytic secondary pyrolysis reactions owing to such interactions. Dhaundiyal et al. (2018b and 2019a) gave a mathematical solution to solve auto-catalytic reactions by introducing the bivariate function.

The major component of any woody biomass includes cellulose (a polymer glucosan), hemicellulose (a polysaccharide producing wood sugars), and lignin (a multi-ring organic compound). There is some relative variation in the percentage of constituents in different species of biomass, but cellulose is considered to be the majority part of any biomass (50%), whereas both hemicellulose and lignin hold 25% each by dry weight (Krishna et al., 1985). All the biological origin such as wood and agro-wastes contain the same principle constituents (Iyer et al., 1997).

The end products of pyrolysis are a combination of the products expected from the separate pyrolysis of each of the three major constituents of biomass. Pyrolysis of individual constituent is itself a complex process depending on many factors. A process with a combination of all the three constituents makes it more complicating to solve as the various influencing factors that govern the rate of the numerous reactions brings a huge range of possible products. However, modelling and demarcation of such a complex system based on temperature have been successfully done to assess the kinetic behaviour of each constituent (Dhaundiyal and Tewari, 2017).

The destructive reaction of cellulose initiates at a temperature lower than 300 °C and is identified by a decreasing polymerization degree. Thermal degradation of cellulose proceeds in two different ways: a gradual decomposition and charring at a lower temperature, and rapid volatilisation along with the formation of levoglucosan at a higher temperature. The glucose chains are the first which cleaved to glucose. Subsequently, glucosan is formed by knocking out one of the water molecules. As cellulose and levoglucosan have the same chemical formula, therefore the yield of levoglucosan, the major component of tar that vapourised and then decompose as temperature increases, is 100%. The initial decomposition reactions include depolymerization, hydrolysis, oxidation, dehydration, and decarboxylation (Shazadeh and Stevenson, 1982). Lewellen et al. (Lewellen et al., 1969) gave a comprehensive sketch of the possible pathway chosen during the pyrolysis of cellulose that may a key factor of weight loss during pyrolysis (Fig.2.9). Under this scheme, cellulose decomposes rapidly into intermediate levoglucosan. It may follow path 1. To give tar, or may repolymerized, crack, or become cross-linked to yield char via path 2. There is also a possibility that it follows path 3 to produce light volatile products CO, CO_2, fixed gases, organic acids, ketones, esters, aldehydes and free radicals, some of them impair char formation through path 4, or follow autocatalyze step 3 through path 5. The light stable products can be escaped from the matrix through path 6 to yield volatiles. Hence, there are numerous possible pathway for the pyrolysis of cellulose alone, which implies the complex mechanism of pyrolysis of biomass as a whole (Lewellen et al., 1969)

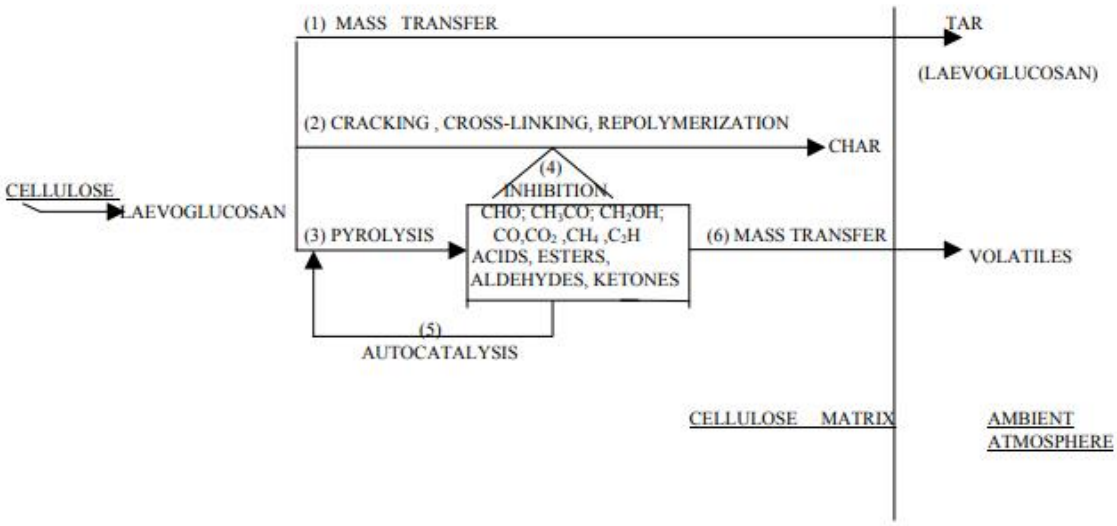

Fig. 2.9. Pathway of pyrolysis reactions (Lewellen et al., 1969)

Another constituent of biomass is hemicellulose which is a mixture of polysaccharides (composed of glucose, mannose, galactose, xylose, arabinose, 4-0 methyl glucuronic and galacturonic and residues). Generally, its molecular weight is lower than cellulose. Unlike cellulose, it is amorphous

in structure. Its susceptibility towards thermal treatment is very high and it decomposes in the temperature range of 200-260 °C (Soltes and Elder, 1981). Decomposition of hemicellulose is carried out in two steps. Firstly, the decomposition of the polymer into soluble fragments, and secondly, the transformation of them into monomer units that eventually decomposes into volatile components. Relatively, hemicellulose provides more volatiles, less tar and char to cellulose. The composition of tar has acidic groups (acetic acid and formic acid) and a few furfural derivatives. Gabor et al.(1997) explained TG/DTG curves at different heating programs with least square methods. They suggested the proposed method would provide a better fit if the transformation of cellulose to active cellulose from the cellulose decomposition pyrolysis model, propounded by Broido-Shafizadeh, was excluded. It was conceived that the transformation of cellulose to active cellulose does not play any role whilst decomposition of cellulose and therefore, there is no evidence of the existence of this during thermal decomposition of biomass (Gabor et. al., 1997).

Similarly, lignin is also amorphous in nature and polymer of naturally occurring phenolic phenylpropanoid or 'protolignin' that can be treated to provide aromatic products. It is assumed to be the main binder for the aggregation of fibrous components. The percentage of lignin in biomass varies from 15 to 30 %. It decomposes in the temperature range of 280–500 °C. Among the end products of lignin pyrolysis, the char is the most abundant constituent with a yield of 55% (Soltes and Elder, 1981). It is produced in a large amount during pulping, but an iota fraction of lignin is utilised for chemical purposes (Vuory et al., 1988). Lignin is mainly used for the generation of a low-grade fuel for an industrial process (Nassar and McKay, 1984). The mechanism of lignin is known for its pyrolysis products. The guaiacol is chiefly obtained through a coniferous kind of biomass, whereas guaiacol and pyrogallol dimethyl ether derived from deciduous woods. Phenolic compounds released from lignin during cracking of the phenyl propane units of macromolecule lattice. Phenols obtain through pyrolysis is more substituted on a selective basis, as the syringyl and propane units are loosely linked to the lignin skeleton than the less substituted group gaiacyl-propane and phenyl propane (Brown, 1958). Composition of the product of lignin pyrolysis, pyroligneous contains 20% aqueous components and 15% tar residue. The aqueous portion is composed of ketone and alcoholic groups (Methanol, acetic acid, acetone), and water on dry lignin basis. The gaseous products have a 10% share of lignin and are composed of methane, ethane and carbon monoxide.

The holistic approach of pyrolysis of biomass is accompanied with dehydration (160 °C) and decomposition of hemicellulose (200–280 °C), cellulose decomposition (280–500 °C), and the characteristic peak of lignin (after 320 °C). The end products of hemicellulose are mainly volatile contents, such as carbon dioxide, carbon monoxide and condensable vapours, whereas tar, char and other gaseous product are predominant during cellulose degradation. The decomposition rate of lignin increases drastically after 320 °C, however, the lignin decomposition rate is relatively slower than the other two constituents. Indication of lignin is known by a rapid increase in the carbon content of the residual solid mass (Roberts, 1971). Thus, the decomposition of cellulosic material passes through a complex series of chemical reactions, along with heat and mass transfer processes. There are 200 intermediate products were reported by Emmons and Atreya (Emmons and Atreya, 1982). Roberts (Roberts, 1971) demarcated the number of products over 100. As cellulose is the major component of any biomass, therefore it is important to comprehend the mechanism of pyrolysis. The simplified form of the cellulose pyrolysis pathway (Fig. 2.10) is suggested by Shafizadeh (Shafizadeh, 1982).

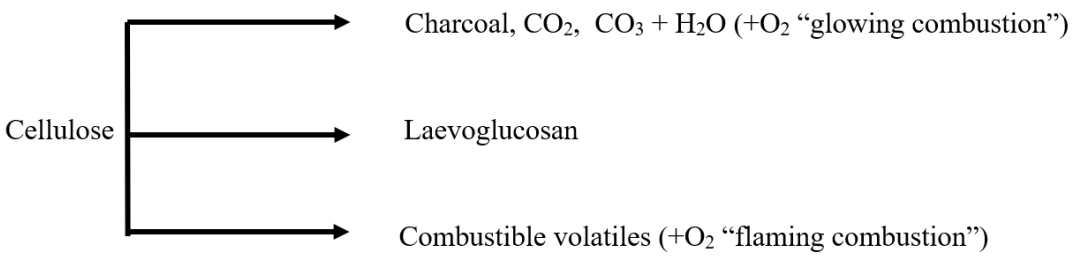

Fig.2.10. Pyrolysis mechanism of cellulose (Shafizadeh, 1982)

2.2.3. Modelling of pyrolysis

Modelling of pyrolysis delineates the chemical and physical phenomena encompassing pyrolysis in a mathematical form. In another sense, pyrolysis is to be elaborated as a system of equations that are taken together to provide in-depth information about the valuable quantitative and qualitative facets of the process. Chemically, pyrolysis is a huge network of inter-linked reactions that enhance the degree of complication during the modelling process. One of the most key issue whilst modelling the pyrolysis process is the interdependence of reactions. Therefore, there is a dire need to discover some robust and precise way to sort out problems of the pyrolysis process. Modelling of pyrolysis is closely related to the mechanism of pyrolysis reaction, therefore the different classes of mechanism to describe the course of pyrolysis reactions are required (Blasi, 1993).

The models are classified into three main groups: one step global models; one stage, multi-reaction models; and two-stage, semi-global model. The first group assumes the pyrolysis as a single step first-order reaction and represented as

$$\textbf{Solids} \xrightarrow{k} \boldsymbol{a}\ \textbf{Gases} + \boldsymbol{b}\ \textbf{Tar} + \boldsymbol{c}\ \textbf{Char} \qquad (2.1)$$

where k is the rate constant of the reaction and a, b and c are yield coefficients of the different products of pyrolysis. Having reviewed literature, it was found that the obtained values vary from each other by an appreciable margin for the same species of wood and the kinetic constant are very susceptible to the experimental conditions under which the values are estimated (Blasi, 1993). The second group of models rely upon the simultaneous and competing first-order reactions in which biomass degrades into the different components of pyrolysis products, tar, char and gases. This model is mainly focused on the small particles of woody biomass (Samolda and Vasalos, 1991). The third category of models considers the pyrolysis to be a two-stage reaction, wherein the products of the first stage disintegrate further in the presence of each other to form the secondary pyrolysis products. These models are described for cellulose and lignin (Bradbury et al., 1979), and wood by Koufopanos et al. (Koufopanos et al, 1991).

Besides proposing the models for pyrolysis and applying for different kind of biomasses, they are underlying key factors that influence the pathway of the pyrolysis process, such as heating rate, the residence time of volatiles, heat of reaction, reaction scheme, structural effect, grain orientation, moisture content, particle size, and material properties.

Heating rate

The rate of heating affects the reaction pathway; therefore, the final products may drastically change. Pyrolysis is generalised as slow and rapid/fast/flash pyrolysis. The heating rate of the order 10 °C-min^{-1} is considered as slow pyrolysis, whereas the heating rate approaching 1000 °C-min^{-1} represents rapid pyrolysis. Through experimental observations, it is suggested that the char yield is supported at low heating rates, whereas the yield of volatiles increases remarkably with increasing heating rates. According to the pathway suggested by Lewellen et al. (Lewellen et al., 1969) in Fig. 2.8. under rapid heating rates and thin sample conditions, pathways 1 and 3 along with 4 and 6 could be flagged as the path determining steps of pyrolysis with the little char yield. On the other hand, especially for the large samples, the residence time of all primary products within the pyrolyzing matrix would take lead and furnish the appreciable char yield at a low heating rate. It was reported that condensation reactions of cellulose are supported at low heating rates (Shafizadeh, 1982). The interior part of the particle is also influenced by the slow heating rate. Any pressure drive flow rate is reduced; whereas the intraparticle residence time of volatiles and the condensation and char formation reactions are increased at the slow heating rate.

Heat of reaction

Whether pyrolysis reactions are endothermic or exothermic plays a crucial role in modelling. The work of Lee et al. (Lee et al., 1976) is the most plausible to comprehend the effect of the heat of reaction. It is indicated when an incident heat flux of 31920 kJ-m^{-2}-s^{-1} is applied parallel to the grain direction, the pyrolysis region is separated into three regimes: an endothermic primary decomposition regime at T < 250 °C; an exothermic partial zone at 250 °C< T < 340 °C; an endothermic surface char zone at 340 °C < T< 520 °C. At higher heat fluxes conditions, the overall heat of the reaction exhibit the exothermic nature of reactions and its magnitude depends upon the direction of heating relative to the grain orientation of the particle. It is observed that the heating orthogonal to the grain orientation has a higher heat of reaction than that of heating parallel to the grain orientation. Whilst heating orthogonal to the grain orientation, pyrolysis gases have sufficient residence time in the solid matrix to trigger the secondary pyrolysis reactions, which are supposed to be exothermic in nature. It is also concluded that exothermic is highly influenced by lignin content (Roberts, 1971)

Residence time

It is observed that the residence time of volatile inside pyrolyzing cellulose matrix is very significant to determine conversion. It decides the extent of secondary pyrolysis and competitive pathways, such as evading of volatiles from the matrix, inhibition of char formation and auto-catalysis of secondary pyrolysis may exist whose kinetics solely reply upon residence times of certain products within cellulose (Lewellen et al., 1969).

Reaction scheme

The pyrolysis reaction proceeds in two distinct ways, namely, primary and secondary. Primary pyrolysis implies the decomposition of any of the three major components of biomass. Hence, primary reactions may proceed in parallel with the simultaneous decomposition of lignin, cellulose and hemicellulose in distinct zones of the fuel. It depends only on the local solid temperature. These reactions are characterised by a very low enthalpy change (Pyle and Zaror, 1984b). On the other hand, secondary pyrolysis reactions encompass the decomposition products of primary

reactions. The products of primary reactions are char and volatiles that catalyse the secondary reactions. Dhaundiyal et al. (2018b and 2019a) assumed these reactions to be independent of primary reactions for modelling biomass pyrolysis. They suggested that the secondary reactions are merely influenced by primary pyrolysis reactions, but their occurrence are mutually exclusive to each other. They used Archimedean families of copula to solve the multi reaction models. Their work was centred around the concept proposed by Kansa et al. (Kansa et al., 1977). It was concluded that the modelling of secondary pyrolysis reactions is to be done in such a way that mitigates the difference between experimental observations and model predictions (Kansa et al., 1977). These reactions occur when the hot volatile products come in physical contact with pyrolysed biomass. The correlation of the secondary reactions with the residence time of volatiles inside the solid matrix makes the computation process complicating. Even not only the secondary reactions but the primary pyrolysis reactions also require many simplifications. In earlier days, a one-step first-order global reaction scheme would be used by models (Bamford et al., 1946; Matsumoto et al., 1969; Maa and Bailie, 1973).

It is concluded that such a simple scheme is notably different from an accurate model (Lee et al. 1976). It is proposed to follow the multi reaction scheme (Eqs. (2.2) and (2.3)) as follow:

$$\mathbf{Wood} \xrightarrow{\mathbf{Heat}} \mathbf{Char} + \mathbf{Tar} + \mathbf{Gases} \tag{2.2}$$

$$\mathbf{Wood} \xrightarrow{\mathbf{Char}} \mathbf{Char} + \mathbf{Gas} + \mathbf{Heat} \tag{2.3}$$

It is clear from the above reaction scheme that the char catalyzed decomposition reaction would be responsible for the apparent residence time dependency of the exothermic pyrolysis reactions and secondary char formation (Lee et al. 1976). The same insight about a single-step scheme that is not sufficient enough to model secondary reactions, is shared by many researchers (Panton and Rittman,1971; Murty and Blackshear, 1967; Akita, 1959). For the special case of flash pyrolysis under rapid heating (400–1000 °C-min^{-1}), the single-reaction scheme is adequate (Shafizadeh, 1982). This is due to fact that residence time is very small and autocatalytic secondary reactions are abstracted.

Grain orientation

Anisotropy of material affects grain orientation as well as the heat of reaction. It was reported that the permeability of flow along the grains is 10^4 times more than that across the grain. Similarly, thermal conductivity along the grain is twice that across the grains, therefore it must be taken into account for modelling of the secondary reactions (Roberts, 1971).

Moisture content

Another key factor that influences modelling problems is moisture content in the biomass, which affects the thermal history of fuel due to endothermic evaporation (Pyle and Zaror, 1984b). It is emphasised to consider the moisture factor for energy balancing (Chan et al., 1985). In another finding, it is concluded that water evolution has a crucial role in the intra-particle energy balance (Kelbon, 1983). Omission of water content is led to overprediction of temperature in the numerical solution, therefore it is necessary to consider moisture content whilst modelling pyrolysis of biomass (Chan et al., 1985). The effect of expelled moisture, which is mainly a low-temperature phenomenon, on temperature profile and pyrolysis rate must be considered in the energy balancing

equation. It is observed that the dehydration reactions occur in parallel with char formation and due to the low temperature, it is considered to back up the char formation (MacKay and Roberts, 1982).

Material properties

Material properties are one of the major key issues for modelling pyrolysis. Thermal conductivity and heat capacity are some of the significant factors which affect the process of pyrolysis directly. As particle density is easily measured, therefore it can be easily introduced heat and mass transfer models. In most of the models, char and wood yield are linearly correlated to thermal conductivity, which eventually depends upon the instantaneous value of density. It was reported that variation of thermal conductivity of char affects the temperature and mass loss predictions, therefore it is assumed to be very sensitive with the anisotropic behaviour of biomass (Kung, 1972).

Structural effect

Cracking of the woody biomass during pyrolysis influence the pathway of reactions (Roberts, 1971; Pyle and Zaror, 1984b; Kansa et al., 1971). As soon as the temperature at the centre reached the furnace temperature, it has observed that the pressure at the centre of the wooden dowel has risen sharply and then suddenly dropped to zero (Tinney, 1965). Due to sudden falling of pressure, serious structural defects, such as longitudinal and channelling and surface cracking observed. The phenomenon of surface cracking leads to the variation of the heating characteristics. Moreover, heat transports more rapidly to the interior part of the material due to the presence of cracks on the surface, whereas the total heat transfer remains the same. These structural failures account for variation in local porosity and permeability, therefore the flowing ability of fluid is also changed.

Particle size

As large the particle size be, so is the fluid residence time increased. Consequently, the secondary reactions come into the action and make the modelling complicating (Bamford et al., 1946; Matsumoto et al., 1969). The large particle also indicates dilation in the thermal gradient. The moisture content also compounds the problem of surface cracking, as it escapes violently and causing cracks on the surface. Local condensation of water and moisture is occurring on these sites; however, the multi-step scheme models can assess the overall tar formation, but they get failed to explain the local condensation of volatiles to produce tar.

These are the pivotal part of modelling which is to be considered for the mathematical model of the thermal treatment process.

By-products of thermochemical reactions

It is noted that torrefaction results in decreasing the total tar content of torrefied spruce woods and a negotiable increase in the total tar content of torrefied ash woods. It indicates that the composition and fraction of major constituents of woody biomass affect the tar yield (Asmadi et al., 2017; Yu et al., 2014). It was reported that hardwood provides more tar than char and the yield of tar established a trade-off relationship with the duration of pyrolysis, therefore tar-to-gas conversion rates are smaller than that of softwood (Fig. 2.11). The main reason for such anomaly is the yield of acetic acid, which is very high in the hardwood. So due to the low gasification reactivity of acetic acid, it gasifies at the later stages, thus the tar reduction takes a long period (Asmadi et al., 2017). Another factor that affects the tar yield is demineralization whose influence

is derived by yield ratio (yield from demineralized wood/ yield from original wood). To record the influence of demeralisation, the value of yield ratio greater than one indicates the rise in tar yield by demineralization and vice-versa. Several papers reported that both char and gas yield is decreased by demineralisation, whereas the tar yield increases (Scott et al. 2001; Radlein et al. 1991; Piskorz et al. 1989). Upon torrefaction, the total tar content reduction was 30% found for spruce wood (softwood), whereas hardwood provided the same results at 260 °C or higher temperature (Morf et al., 2002; Tsalidi et al., 2017). As the major fraction of tar derives from the holocellulose and the hemicellulose mass fraction is only affected in the torrefaction (Weiner et al., 2014), therefore the volatile content could not decrease to that possible extent which can reduce the formation of tar species (Woytiuk et al., 2017). Tsalidi et al. (Tsalidi et al. 2017) did the tars classification based on their solubility, chemical composition and condensation behaviour. It was reported that classes 3 and 4 tars are mainly formed during gasification. Moreover, they say that these classes are formed due to primary tar that is generated due to the decomposition of holocellulose and lignin and increasing torrefaction only increases the phenolic content (Class 2 tars) (Tsalidi et al. 2017).

In the context of operating parameters, experimental studies reveal that the rise in the bed temperature increases hydrogen volume fraction and H_2/CO ratio, and thus a decrease in the tar content of the product gas (Kurkela et al., 2004; Li et al., 2004). Moreover, the use of oxygen and steam (Siedlecki et al., 2011) seems to improve product gas quality to volumetric increasing of hydrogen fraction and decreasing of the tar content. Oxygen provides the heat for endothermic processes due to oxidation reactions and steam influences the product gas quality through the water-gas shift, char gasification and steam reforming. The typical value of the equivalence ratio during gasification is in a range of 0.2–0.4. The lower values of equivalence ratio result in low carbon conversion efficiency; whereas higher values result in combusting the product gas. Sikarwar et al., 2016 reported that a higher equivalence ratio helps in lowering the total tar content of the product gas, cold gas efficiency, and increase the carbon conversion efficiency.

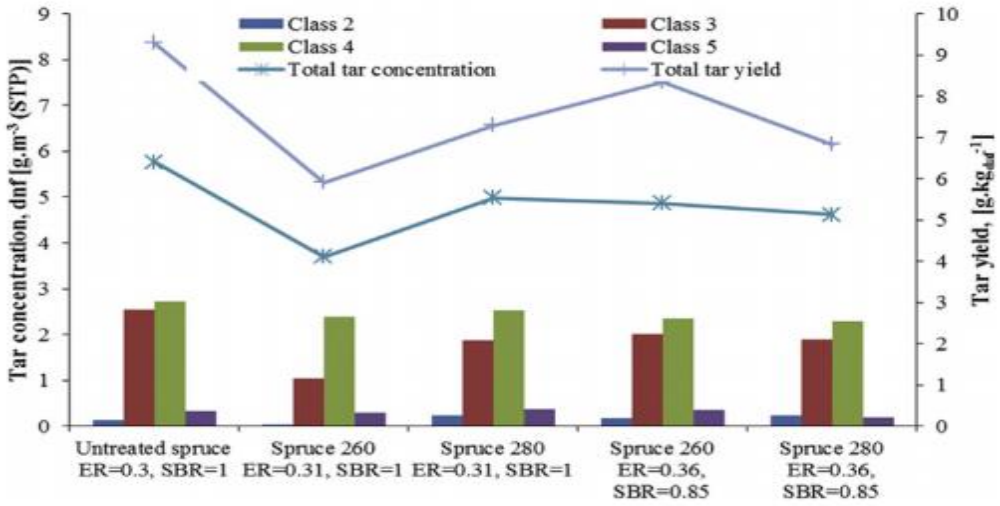

Fig.2.11. Content and yield of total tar and tar classes of Spruce wood (Taslidi et al., 2017)

Effect of ambience on the process

In many research conducted on the pretreatment process, torrefaction, the effect of torrefaction environment on physical and chemical biomass is overlooked at the first sight of experimentation. During the pretreatment of coniferous and deciduous species in a different atmosphere, it was found that the thermal breakdown of coniferous species was changed when the chamber was purged by carbon dioxide. A noticeable difference in cellulose peak was observed whilst carrying out cellulose breakdown in the CO_2 atmosphere. The reason for the shifting of the peak is due to the loss of hydrocarbons during torrefaction, as torrefied biomass contains less volatile matter when pyrolyzed in CO_2. A remarkable shift was also observed in the peak of lignin decomposition at a higher temperature regime when CO_2 was used. The same behaviour was observed for deciduous species (Dustin et al., 2013).

It is mainly due to the higher specific heat of carbon dioxide when compared to nitrogen (Thanapal et al., 2012). Moreover, it has been noticed that the carbon dioxide environment provides the smallest amount of fixed carbon and the lowest higher heating value than that of the nitrogen environment. The rate of mass loss increases using carbon dioxide as the torrefaction medium with increasing temperature. It happens due to the behaviour of ash components. There is a likelihood of inorganic contents in ash, which act as a catalyst in the carbon dioxide environment, resulting in higher weight loss. Dustin et al. (Dustin et al., 2013) suggested that the Boudouard reaction might be the cause of such a peculiar behaviour, as the fixed carbon in the char reacts with carbon-dioxide gas. Moreover, the carbon dioxide environment has enhanced the grinding ability of torrified biomass by 40.2 %, whereas it is 22.1 % for nitrogen (Dustin et al., 2013). It was reported that torrefaction causes the surface of the biomass to become smoother due to the loss of hemicellulose (Chen et al., 2011).

In another experimentation on oil palm fibre, it is found that there is an overall increase in fixed carbon in an oxidative environment, whereas it renders lower volatile matter as compared to a non-oxidative atmosphere. The reason is the higher reaction extent of volatile matter in oxidative torrefaction, consequently, results in higher fixed carbon and lower volatile matter than non-oxidative. However, the torrefaction process triggers carbonization to some extent which becomes the reason for a relative increase of fixed carbon to raw material, but the oxidative environment enhances the same process at elevated temperature. Irrespective of the atmosphere, it is noticed that fixed carbon is larger than volatile matter when torrefaction temperature is higher or equal to 300 °C (Fig. 2.12). As compared to the non-oxidative torrefaction, the oxidative torrefaction indicates the abrupt increases in higher heating value at 275 °C (Chen et al., 2016).

Whilst experimenting on the oil palm fibre, coconut fibre, eucalyptus and Cryptomeria japonica at oxidative and non-oxidative atmosphere with different superficial velocities, it was reported that some alteration in heat and mass transfer, as well as surface reactions, took place. In a nonoxidative atmosphere, it was observed that the solid yield of biomass is not affected by the superficial velocity of N_2 at a given temperature which shows that the thermal degradation is governed by heat and mass transfer mechanism; whereas air superficial velocity decreases the solid yield, especially in oil palm fibre and coconut fibre. It also implies that the torrefaction reaction of biomass is controlled by surface oxidation, therefore there must be some limiting condition for the superficial flowing velocity of air to prevent decrement of solid yield. It is also suggested that the thermal degradation is no longer dominated by surface oxidation rather than controlled by internal

mass transport if superficial velocity goes beyond the critical value (Chen et al. 2013). By the definition, superficial velocity is defined as the volumetric flow rate of carrier gas divided by the cross-sectional area of the cylindrical chamber (Saravanakumar et al., 2007). Chen et al. 2013 suggested that the reaction is controlled by heat and mass transfer in biomass when the experimentation undergoes in a nitrogen atmosphere, whilst surface oxidation is the controlling mechanism in air. The surface oxidation accelerates the internal heat and mass transfer when the temperature and superficial velocity are augmented (Fig. 2.13). Consequently, this phenomenon leads to an appreciable drop in solid and energy yields. Moreover, there is an upper limit for surface oxidation when superficial velocity changes without disturbing the temperature scale (Chen et al., 2013).

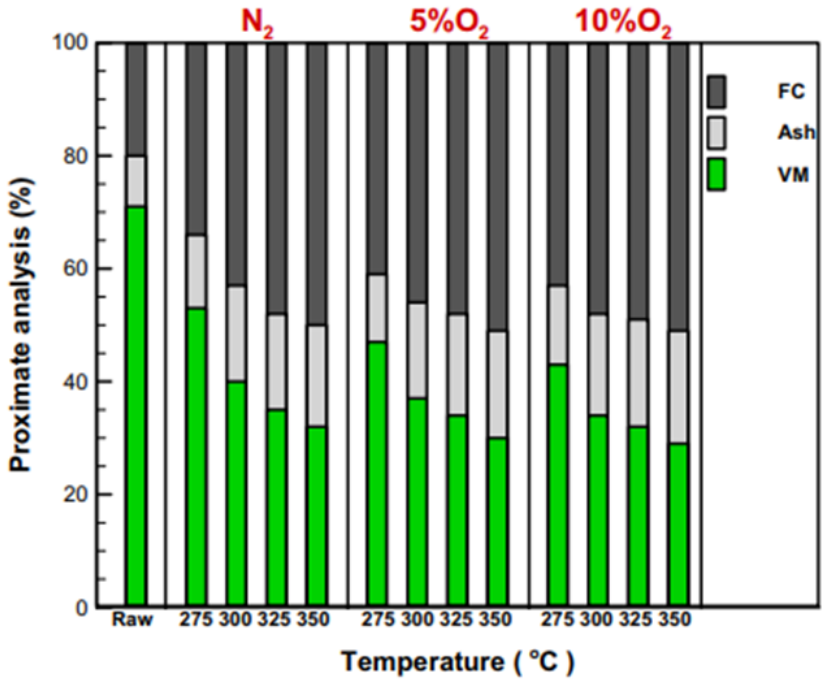

Fig. 2.12. Profiles of proximate analysis of raw and torrefied OPFP (Chen et al., 2016)

Table 2.4. Properties of Mesquite and Juniper in N_2 and CO_2 at 240 °C (Dustin et al., 2013)

Parameters (%)	N_2 medium		CO_2 medium	
	Mesquite	Juniper	Mesquite	Juniper
Moisture	4.84	5.69	4.30	6.25
Volatile matter	69.5	74.6	71.1	73.2
Fixed carbon	23.3	18.6	22.2	19.4
Ash	2.39	1.08	2.34	1.13
Carbon	53.4	53.6	53.3	53.2
Oxygen	33.2	34.1	33.9	33.8
Hydrogen	5.33	5.42	5.37	5.41
Nitrogen	0.81	0.19	0.77	0.17
Sulphur	0.05	0.01	0.04	0.02

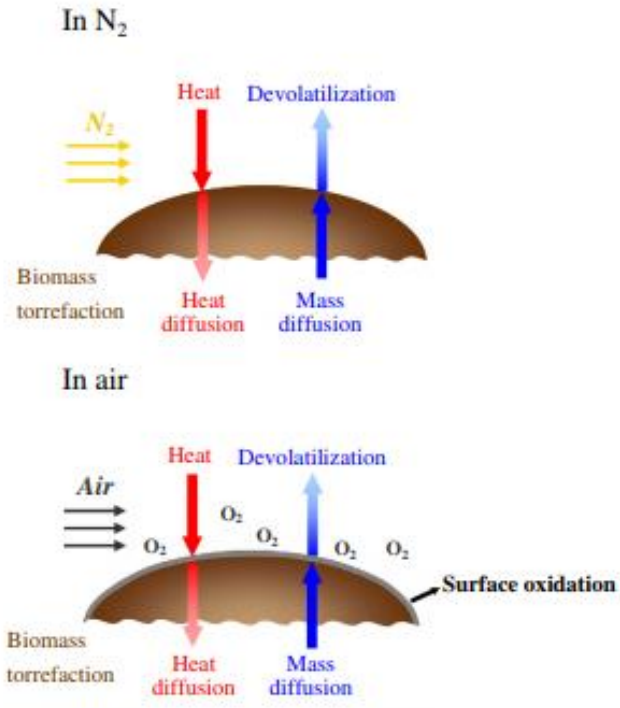

Fig. 2.13. The effect of ambience on the surface oxidation as well as heat mass transfer (Chen et al. 2013)

2.3. Densification of processed material

The densification process involves compacting the milled form of raw or processed biomass into a well-defined shape and size. Though, the torrefied biomass requires an artificial binder during pressing or extrusion. It mainly happens due to alteration in the protein and starch structure; therefore, gelatinisation of starch is required to impart a better textual property to the processed biomass. The starch predominately undergoes reactions of gelatinisation, pasting and retrogradation during a crucial stage of the densification process. It is a highly irreversible process, and it is mainly impacted by heat, water, shear and residence time (Thomas et al., 1999). The addition of starch in processed biomass depends on the ratio of amylase to amylopectin. During gelatinisation of the starch granule, amylase forms double helices, which allow them to hydrogen bridges, and upon cooling it retrograde and forming a semi-crystalline region to assist in binding.

The detailed mechanism and why it happens can be known by the fact that the denaturalisation of protein structure by the external stress (applied heat) causes the formation of new bonds and realign with other protein, lipids and starch, available in the biomass and improves the binding capacity (Thomas et al., 1998; Nyanzi and Maga, 1992). It was found that the increasing fraction of protein enhances the durability of pelleted biomass (Briggs et al., 1999; Wood, 1987). The physical properties of a pellet were determined to be better for biomass with the raw protein than the denatured protein. Transformation of protein structure also occurs during the extrusion process when a non-covalent, as well as covalent bonds of the secondary structure of a protein, gets ruptured. Consequently, it leads to the formation of new intermolecular bonds (Lampart-Szczapa et al., 2006). Tabil et al. (1996) reported that the natural protein strengthens the binding abilities of biomass if biomass has a satisfactory level of protein content. It was reported that starch along with protein influence the mechanical properties of biomass. The higher is the fraction of starch and protein in the biomass the denser and more stable pellet would be obtained than that of the

biomass with a high composition of cellulose (Sokhansanj et al., 2005). The structural form of cellulose is another issue that is faced during pelletisation. Cellulose forms crystalline microfibrils that are surrounded by amorphous cellulose inside the cell (Chen et al., 2004). The cohesion within the cellulose structure is owing to hydrogen bonding that exists between glucose monomers (Goldstein, 1981). It was noticed that the strength of binding mainly relies on the conversion of cellulose into an amorphous state. As cellulose is semi-crystalline in structure and strongly bonded with hydrogen, therefore it cannot be dissolved easily in the conventional solvents and it is hard to restructure it unless it undergoes thermal degradation. Furthermore, only cellulose is a constitute of the biomass that does not serve the purpose of adhesion, so it is necessary to break hydrogen bonds (Hon, 1989). On the other hand, Lignin is a random-network polymer that contains miscellaneous linkages of phenyl-propane units and it is derived from aromatic rings of two amino acids, phenylalanine and tyrosine (Zandersons et al., 2004; Nelson and Cox, 2005). The objective of the lignin molecule is to impart structural stability and adhesion to cellulose fibres. The presence of lignin makes biomass material support the densification process. It was reported lignin had a thermosetting behaviour at a working temperature of 140 °C above and acted as intrinsic resin in binder-less board production (Van Dam et al., 2004). It was noticed that moisture content of 8 to 15% in biomass assisted in reducing the softening temperature to 100–135 °C by plasticising the molecules chain and make it less viscous (Lehtikangas, 1999). The adhesive characteristic of thermally softened lignin imparts a good strength to densified lignocellulosic materials (Granada et al., 2002).

Besides structural chemistry, physical behaviour is also affected during the densification process. Densified material is either produced in form of a briquette or pellet. The average length and diameter of a briquette vary from 75–300 mm and 50–90 mm, respectively, whereas the pellets of diameter 6–8 mm and length of 40 mm are commonly used for thermal application (Nunes et al., 2014). The size of a finished product also decides its application as the briquettes are confined to large and medium scale industrial application. On the other, pellets can be comfortably utilized in a smaller reactor. The density, handling and storage and transportation cost are some of the salient features that could be materialised via the densification process. A screw extrusion of a milled form of biomass is illustrated in Fig. 2.14.

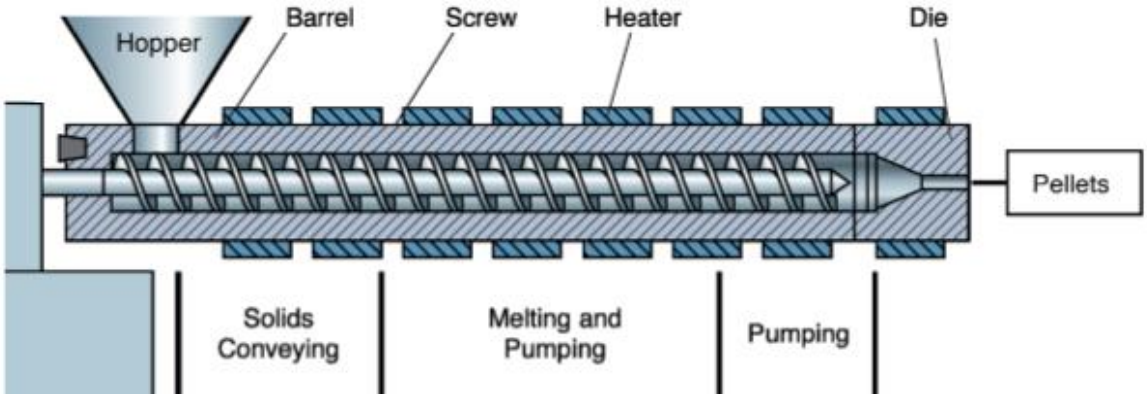

Fig. 2.14. Screw extrusion process for pelletising the biomass (**http://matse1.mse.uiuc.edu/polymers/prin.html**)

2.4. Summary of literature review evaluation

After an exhaustive analysis of literature, it has been found that torrefaction is the most promising pre-treatment process of biomass, especially when the dearth of conventional fuel and burden of climate change policies are the main concerning factors. A research gap was seen as to how operating condition and surface properties affect the torrefaction process. Some refurbishment related to the torrefaction is also required. The literature review is dichotomised based on the qualitative and quantitative aspect of the torrefaction process. Alongside torrefaction, an in-depth assessment of various factors has been perused to carried out the research work. The operating parameters of processing technology and surface chemistry of biomass are highly intertwined with each other. Based on modelling issues and the effect of external ambience, an initiative is taken to make such inextricable features of process technology tangible. State variables of thermodynamics and heat mass transfer not only affects the surface properties of biomass but also influence the energy and mass yields. It is suggested to carry out torrefaction at a relatively low heating rate and temperature so that the mass and energy are not drained away in the pre-treatment process alone. The most significant part of torrefaction is that the mechanical properties of processed biomass are drastically magnified, which make it a competitive fuel in the conventional energy market. However, the influence of torrefaction on energy density is marginal and largely depends on biomass characteristics. Apart from thermal criterion, the surface topography also affects the yield of the end products and in some cases, it makes the mathematical modelling process very complicating. The tar and ash yields are mainly concern with the holocellulose content of the biomass, that is it depends on the species of biomass that is subjected to be analysed. Ash fouling or ash deposition is also another facet of torrefaction; therefore, it can be reduced by selective demineralization. The higher fraction of lignitic ash, which has an abundance of calcium and magnesium oxides than ferrous oxide, causes fouling. On other hand, it is necessary to identify the ash component before and after torrefaction. If we somehow expel calcium and magnesium oxides out of torrefied biomass, it can drastically elevate the fusion point of ash. Removing alkali metal can be one of the solutions to shake off the unwanted oxides from ashes. Another way of solving the ash problem is to minimized ash contents, but as the temperature rises ash content and fixed carbon increases gradually. So, there is a need to find the optimal temperature at which torrefaction can be done without an appreciable rise in the ash content of biomass. The effect of non-inert ambience on the biomass characteristic shows negotiable variation in mass loss but the higher heating value is drastically improved. Oxidative atmosphere recorded the same behaviour along with a change in the surface mechanism of biomass. According to mathematical modelling of pyrolysis reactions, secondary reactions should be deterred which is highly influenced by heating rate, particle size, structural behaviour and residence time.

Also, densification could provide economic leverage to biomass processing if the morphological study is conducted alongside it. It has been determined that the crystalline structure of cellulose does not play any crucial role in the binding process, and it is lignin, starch and protein content in biomass that provides structural support to a densified lignocellulose.

3. MATERIALS AND METHODS

The material and methods are classified according to the operation conducted upon the waste material derived from black pine. The techniques used to analyse the samples of material are also covered under this heading. The sophisticated measurements were performed in the Indian Institute of Technology, Roorkee, Uttarakhand, India, whereas some physical analyses were partly carried out in the National Agriculture and Innovation Centre, Hungary and the Energy Laboratory of Institute of Process Engineering, Szent Istvan University, Hungary.

3.1. Fuel preparation and densification by pelletising

The net 10 kg of pine waste (pine needles and pine cones) was collected from the Pest county of Hungary. After collecting the raw material, it was sundried for a week in a sieved frame. The collected material is illustrated in Fig. 3.1. For the milling purpose, a 3-phase heavy-duty 1.5 kW rotor milling machine (6-disc rotor) (Retsch SM 2000) was considered. The milling machine used during the preliminary preparation of the raw material is shown in Fig. 3.2. The material was fed tangentially through a standard hooper (80 mm × 80 mm). For a given material, the feeding rate was kept between 200 to 300 $g.h^{-1}$. The material experienced a plastic deformation through a sieve size of 1.5 mm. The net material collected at the end of the milling process with an average processing efficiency of 70% was 7 kg. The milled form of pine material for the densification process is shown in Fig. 3.3. After milling the feedstock, the moisture content was measured. It is to be noted that 1–2% of water is supplied to the milled form of material, which is thereby heated to approximately 70 °C. The heat ensures that the lignin in the wood is released and it would contribute to increasing the binding of the particles in the end-product.

Fig. 3.1. The collected pine waste (pine needles and pine cone)

Fig. 3.2. Grinding machine for the milling process

Fig.3.3. The prepared pine waste for the densification

The densification of the prepared pine waste was performed using a ring-type pellet machine (CL3, Pellet mill). The laboratory-based pellet machine is shown in Fig. 3.4. A screw extrusion of prepared feedstock was initiated by feeding the fine powder into a barrel through a long material hooper (feeding capacity of 0.014 m^3). The objective of the screw is to push the material into the chamber where a roller presses the material radially outward through the cylindrical grooves provided on the circumference of the ring die. The ring die is shown in Fig. 3.5. The estimated length and diameter was calculated to be 25.95 mm and 6.39 mm, respectively. During the process, the temperature of the pellet was constantly measured and it varied from 49 to 60 °C throughout the whole process. The gap between the die and roller impacts the quality of the pellets, the wearing of the machine components and the consumption of energy in the process. A 1 mm increase in the gap would approximately increase the energy consumption by 20%, but meanwhile, it also reduces

the dust content by 30% in the final product. Another factor is the pressure required during pressing the material. The compacting process enhances the temperature of the input feedstock. A material that requires a higher pressure would eventually block the holes in the die and thereby hamper the pelletising process. The densified form of pine material is depicted in Fig. 3.6. Upon densification of the pelletisation, the collected pellets were subjected to a dust cleaning process where a sieve of 1–2 cm was used to remove the broken fragments of the pellets. The net pine waste determined after densification was 5.81 kg. The process efficiency of the pellet mill was estimated to be 83%.

Fig. 3.4. The ring-type-laboratory-based pellet machine

Fig. 3.5. The ring-die used for the densification by pelletisation

Fig. 3.6. The pelletised form of pine waste for dust removal

3.2. Improvisation of a Joule heating system

The torrefaction process was performed under a pilot scheme. A digitally programmed furnace (Nabertherm Gmbh) based on the Joule heating was modified to carry out the thermal pre-treatment in the quasi-static condition. The furnace used during the testing process is illustrated in Fig. 3.7 (a). The technical drawing of the furnace is provided in Fig. 3.7 (b). For scavenge process, the nitrogen gas was allowed to flow with a volumetric rate of 42 L-min^{-1}. The flow of nitrogen deters the diffusion of the present oxygen and prevent the surface oxidation reaction at the surface of the material. The mass measurement was performed by connecting the mass holder to the weighing machine via a mechanical link. The lid (313.15 mm × 250 mm) for the furnace was fabricated in such a manner that could hold the pine pellets without heating them. A hollow cylinder having a length of 559.8 mm along with a ramrod was provided with the lid for carrying the material unless the furnace attains the desired temperature. To hold the lid with the furnace, a steel bracket was used. Apart from the cylindrical accoutrement, the nitrogen ducts of 21.5 mm each in diameter were carved out on the hollow cylinder and the rectangular frame of the lid. To cool down the system, a fan was bolted along the structure to inhibit the heating of protruded cylindrical section. The flow rate of nitrogen was measured with the gas flow meter (Ganz 2000). To make the process quasistatic, the sample is kept at the outer dead centre, and the ram was used to feed the densified material into a provided vessel placed inside the furnace. As the furnace attains the desired temperature, the sample was immediately prodded into the chamber and the processing time was recorded by a stopwatch. The effect of ramping rate of temperature was in this way was bypassed and torrefaction was conducted at a quasi-static condition, where an infinitesimal deviation from the isothermal condition was noticed due to the flow of nitrogen gas and prevention of combustion reactions. It is to be noted that the thermal profile was controlled by a digital console that was pre-set for a particular duration of time by a switching device. Upon completion of the torrefaction process, the physical and chemical investigation was performed by the ultimate and proximate analysis. The thermally processed material derived after quasi-static torrefaction is shown in Fig. 3.8. The torrefaction of the samples (pinecone and pine needles) was carried out at a temperature range of 210–250 °C. Each quasi-static thermal history was applied for a time of 5–15 minutes. The pellets were torrefied only at the optimised operating condition.

(a)

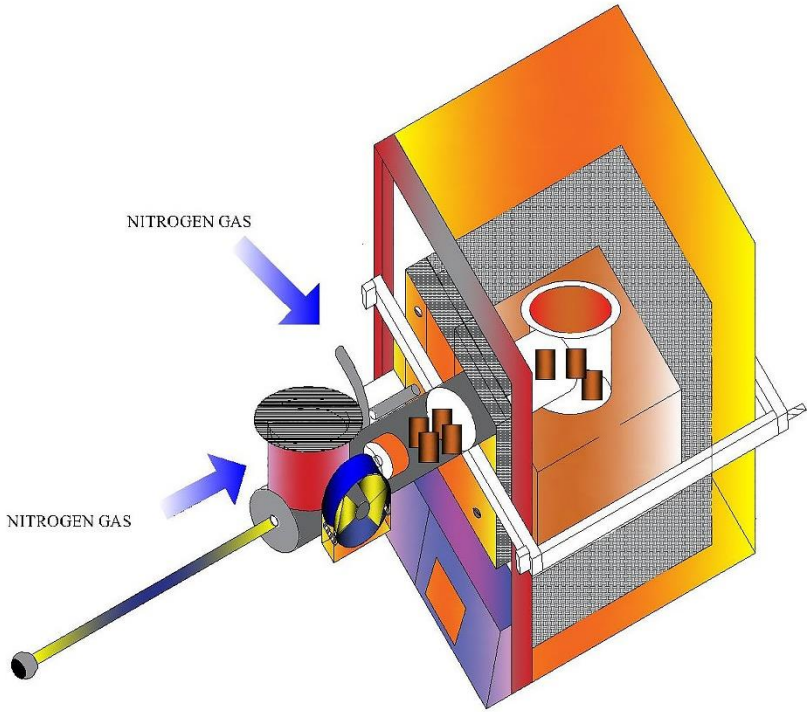

(b)

Fig . 3.7. Torrefaction unit for pre-treatment of pine waste (a: Improvised Joule heating system, b: Technical drawing of heating system)

Fig. 3.8. The upgraded pine waste after thermal pre-treatment

3.3. Construction detail of a packed-bed reactor

The preliminary drafting of the reactor was executed in AutoCAD (Autodesk, 2019). The inner shell of the reactor was fabricated from 1.45 mm thick welded carbon steel. The height of the reactor from the base was decided to be 430 mm, whereas the inner length was estimated to be 400 mm. A clearance of 30 mm was provided between the inner shell and the outer shell. The rock wool having a thickness of 41.5 mm was coated around the inner shell to fend off the heat loss across the outer shell of the reactor. The material used for manufacturing the outer shell was a galvanised steel sheet. The diameter of the outer and inner shells of the reactor was estimated to be 165 mm and 85.2 mm, respectively. The technical sketch of the reactor is provided in Fig. 3.9 (a), whereas the physical form of the reactor is shown in Fig. 3.9 (b). The six measurement ports for thermocouples were etched along the diametrical axis of the shells. However, the four measurement ports (A, B, C and D) were only used during the measurement process (Fig. 3.9 (a)). The distance between ports was made to be 43.8 mm. For pressure measurement, a small duct of diameter 5 mm was welded on the top stainless-steel cover plate. The pressure sensor used for measurement was a current-based transducer (Huba Control). The outer diameter of the plate was estimated to be 93.7 mm and it was riveted tightly to provide the inner shell proper insulation from the ambient air. A lid was also fabricated for additional heat insulation to the main body. The length and diameter of the lid were calculated to be 71.6 mm and 118.4 mm, respectively. A grate of 79.55 mm diameter was formed to carry the ash and char of feedstock. The heating element for providing the indirect heat to the feedstock was formed by a concentric ceramic casing for holding the nichrome wire. The depth of helical grooves was etched in such a manner that would prevent the heating element to touch the outer casing. The total height of the heating unit was estimated to 153 mm from the bottom of the inner shell. The inner and outer diameter of the concentric casing was evaluated to be 47 mm and 73 mm, respectively. An opening flange of the inner diameter of 26.8 mm has been provided for the electrical networking to the heating system. To avoid the ingression of air, an airtight gasket was provided between a lid and flange.

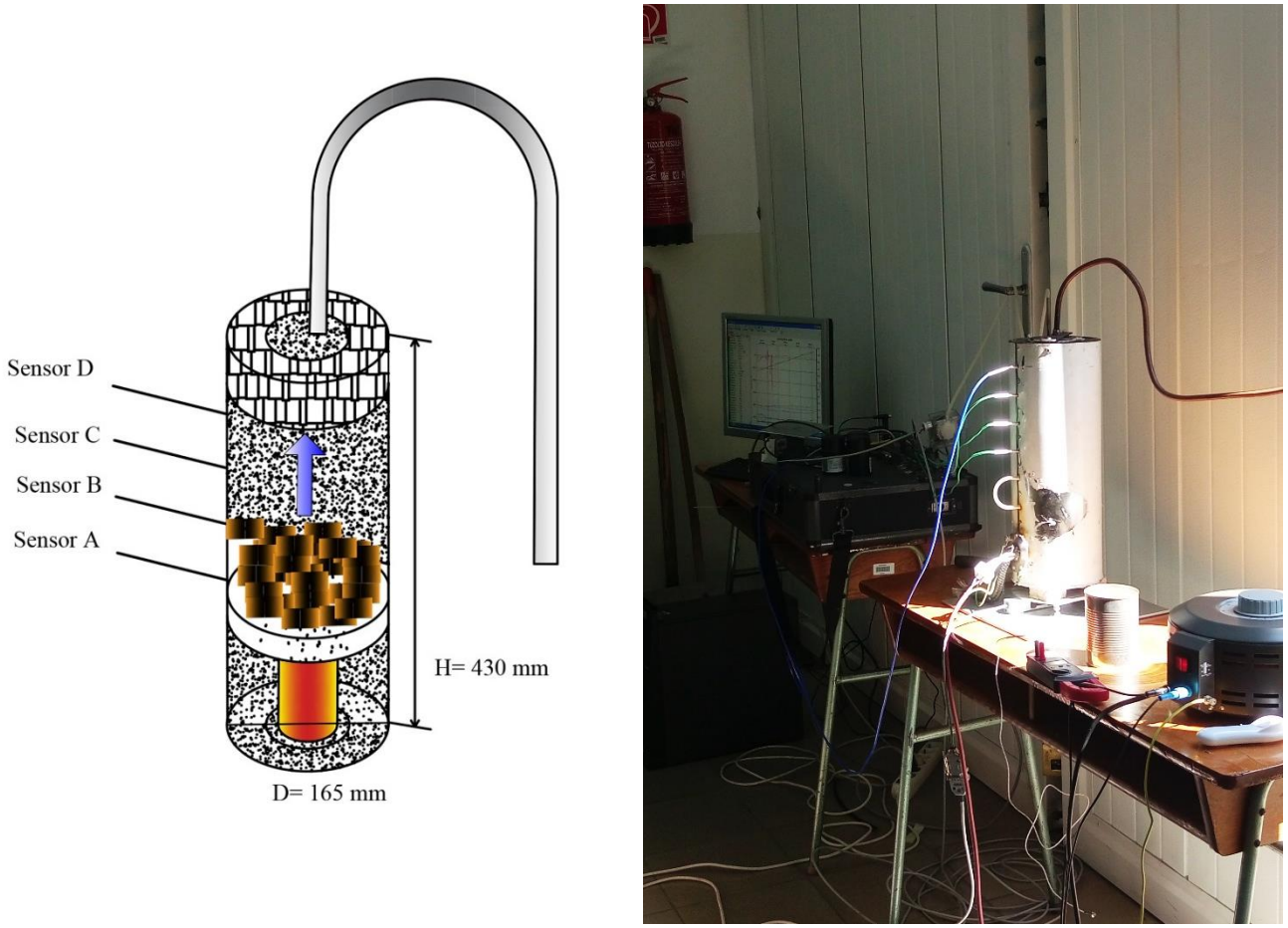

(a) (b)

Fig. 3.9. A fixed bed pyrolysis reactor (a: Technical drawing of pyrolysis reactor, b: The reactor retrofitted with the ancillary components)

The measurement of thermodynamic properties of the system was done by a 16-channel data acquisition unit (HBM). The thermogravimetric evaluation was carried out by a strain gauge (HBM) (voltage type, full-bridge Wheatstone, type II). To calibrate the strain gauge, a 500 gram of iron weight was taken to determine the accuracy and precision of the mass measurement system. The thermocouples type K (Ni-Cr) were used to determine the temperature at the designated ports (A, B, C and D) provided along the circumference of the outer shell of the reactor. The producer gas measurement and its sampling were performed with the help of the wood gas analyser (VISIT-03 H, Messtechnik EHEIM Gmbh). The sampling rate was preset at a volumetric rate of 0.7 L-min^{-1}. The wood gas analyser considered during the gas measurement is shown in Fig. 3.10.

Fig. 3.10. The wood gas analyser for the producer gas measurement

The gas analyser not only determines the % fraction of producer gas but also provides the gas wash to cool the hot gas. The gash wash bottles filled with refined oil and the distilled water were used to trap the gaseous by-products formed during pyrolysis reactions. Once the gas got cleaned, it went for further processing in the wool filter, activated carbon, and activated alumina soaked in potassium permanganate so that the dry producer gas could be obtained. The remaining condensate formed during the cleansing process was expelled out through the water port provided on the console of the gas analyser. It is be noted that before letting the gas be washed, a condensate trap was provided to remove the pyrolytic oil formed during thermal degradation of processed pellets (pinecone and pine needles). Similarly, the dust and tar collection were performed at a sampling rate of 0.6 L-min^{-1}. A 50 mL of isopropanol was used to dissolve the collected tar in the bottle kept in an ice bucket. Before beginning the sampling process, the volumetric suction rate of the pump was calibrated with the help of a gas meter. The schematic diagram of the pyrolysis unit is provided in Fig. 3.11. A diagram illustrating the tar collection system is provided in Fig. 3.12.

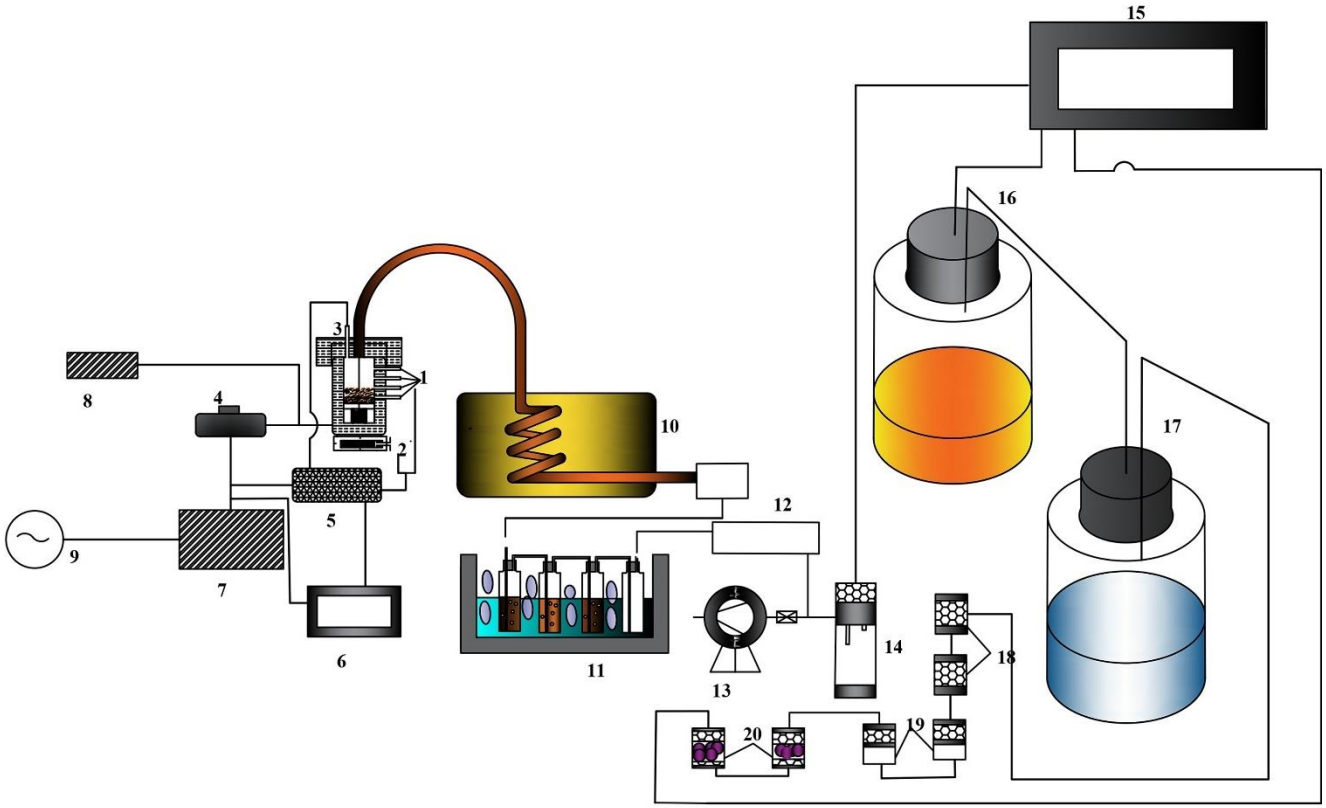

Fig. 3.11. Schematic diagram of pyrolysis unit (1: Temperature Sensor, 2: Strain Gauge, 3: Pressure transducer, 4: Variable transformer, 5: Data acquisition system, 6: Display unit, 7:Isolation transformer, 8: Electrical network analyser, 9: A.C supply, 10: Water bath, 11: Tar sampling unit, 12: dust collector, 13: Vacuum pump, 14: Condensate trap fitted with water stop filter, 15: Gas port, 16: Gas wash bottle filled with oil, 17: Gas wash bottle filled with distilled water, 18: Wool filter, 19: Activated carbon filter with Wool filter, 20: Activated alumina impregnated with potassium permanganate ($KMnO_4$)

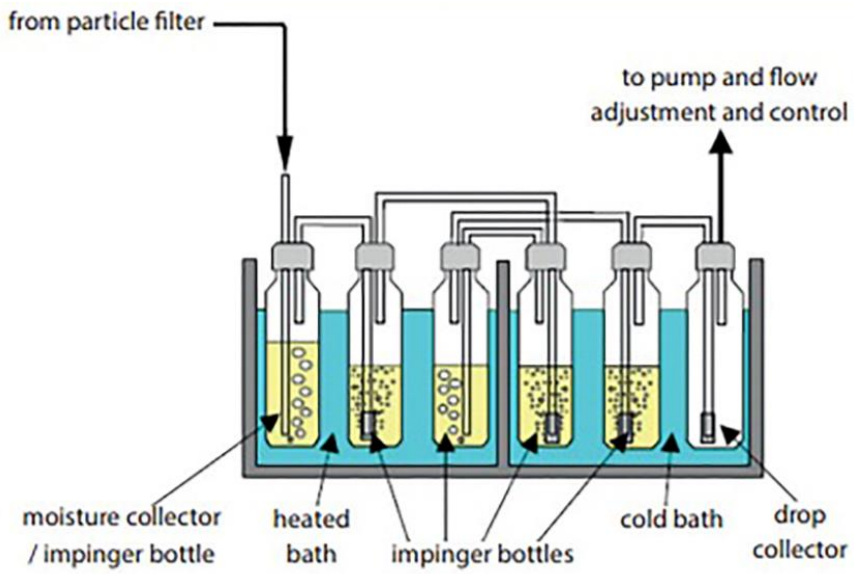

Fig. 3.12. The collection of tar sample in the impinger bottles (Dhaundiyal and Tewari, 2016)

3.4. Thermogravimetric/ Differential thermal analyses

The analytical experiments were conducted at the premises of the Indian Instrumentation Centre, Indian Institute of Technology, Roorkee, Uttarakhand, India. To determine the thermo-chemistry of the thermally processed pine waste, thermogravimetry (TG) and differential thermal techniques were adopted. The milled form of the torrefied pine waste samples underwent thermal degradation in a small-scale pyrolysis reactor. The schematic diagram of the thermogravimetric analyser is shown in Fig. 3.13. The linear ramp profile was considered to decompose the processed material. The heating rate of 5 °C-min^{-1} and 15 °C-min^{-1} were considered for thermal degradation of pine waste in the nitrogen atmosphere. The purge rate of nitrogen in the furnace was estimated to be 0.2 L-min^{-1}. Unlike in the macroscopic study, the thermocouple 'R' type was used in the thermogravimetric analyser. The reference material chosen for differential thermal analysis was Alumina powder. The 10 mg of pine waste samples underwent thermal degradation at a temperature range of 308–873 K. The operating range chosen for the microscopic system was 60 min. The weight of the reference material selected in horizontal thermobalance was also 10 mg. The heat of reaction determined by DTA was determined by Eq. 3.1. The calibration factor (K) was estimated through the peak area of the reference material. The heat of fusion of Al_2O_3 was calculated to be 1092 kJ-kg^{-1}. The calibration factors for the torrefied pine needles samples at the heating rate of 5 ˚C-min^{-1}, 10 ˚C-min^{-1} and 15 ˚C-min^{-1} were estimated to be 0.1495 mW-μV^{-1}, 0.1542 mW-μV^{-1} and 0.158 mW-μV^{-1}, respectively (Dhaundiyal et al., 2021).

$$\Delta H = \pm K.\,\text{Peak area of DTA} \tag{3.1}$$

Similarly, the calibration factors for the torrefied pine cones at the ramp rate of 5 °C-min^{-1}, 10 °C-min^{-1} and 15 °C-min^{-1} were, correspondingly, 0.1427 mW-μV^{-1}, 0.1547 mW-μV^{-1}and 0.1628 mW-μV^{-1} (Dhaundiyal et al., 2020).

The important aspect of a thermogravimetric analyser is the measurement of mass as a function of temperature, heating rate, and time. A suitable thermobalance is often needed to measure the change in mass with accuracy and precision.

A thermobalance is a combination of a suitable electronic microbalance with a furnace, a temperature programmer and a computer for control, that let the sample be simultaneously weighed and heated or cooled in a controlled manner, and the mass, time and temperature data to be recorded. The balance should be in a suitably enclosed system so that the nature and pressure of the atmosphere surrounding the sample can be guided. It is to be noted that the balance mechanism in an inert atmosphere must be maintained closely at the ambient temperature. Movement of the beam alters the light intensity on the photocell, and the amplified output from the photocell restore the position of thermobalance to its null position, and concurrently, is a measure of change in the mass of the sample. The restoring mechanism is electromagnetic in nature. The beam has a ribbon suspension and a small coil at the fulcrum, located in the field of a permanent magnet. The objective of the coil is to exert a restoring force on the beam, which is proportional to the current from the photocell. A common issue that arises during mass measurement is the change in buoyance of the system.

To avoid the buoyance effect on the balancing mechanism, the horizontal differential TG/DTA was used. The reason is the deviation of the balance beam from the null position. During operation, buoyancy occurs due to a lack of symmetry in the weighing system. If the asymmetry can be determined in terms of a gas volume *V*, the mass of displaced gas (ideal gas behaviour) is $\frac{PMV}{RT}$ (where *p* is the pressure and *M* the molar mass). The buoyance thus depends not only on the asymmetry *V* but also on the pressure, temperature and nature of the gas. So, it is always aiming to minimise the *V*, or correction can be estimated, or an empirical correction may apply by heating an inert sample under a similar condition to those considered in the study of the sample of interest. Gallagher et al. (1998) reported that the masses of air, carbon dioxide and hydrogen, at room temperature and pressure, were 120 g, 9 g, 196 g, respectively. Mainly, during the evolution of volatiles buoyancy effects will change. Another reason is the thermomolecular flow problem at low pressure (10^{-2} to 270 Pa) that occurs when there is a temperature gradient along with the sample holder and support. This gradient causes ‘streaming’ of molecules from hotter to colder direction, that is towards the suspension point, which eventually provides a spurious mass change. Thermomolecular flow is minimised by allowing the inert gas or by changing the furnace design and sample placement, including the use of the symmetrical balance design with a twin furnace, or by evaluating the correction required, using an inert sample, as provided in buoyancy case.

Differential thermal analysis, DTA, relies on the temperature difference, between the sample a reference material is captured whilst both are subjected to the same thermal history. In DTA, a single block with symmetrical cavities for the sample and reference is heated in the furnace. The block is considered in such a manner that would sink heat, and a sample- holder of low thermal conductivity is included between the block and the sample to make sure that an adequate differential temperature signal would be fetched during the thermal event. If an endothermic thermal event ($+\Delta H$), such as melting happens, the temperature of the sample will lag behind the temperature of the reference under a similar thermal profile. Similarly, should an exothermic thermal event occur, the response will be in the opposite direction. The area under the DTA curve represents the change in the enthalpy of the system during the thermal event.

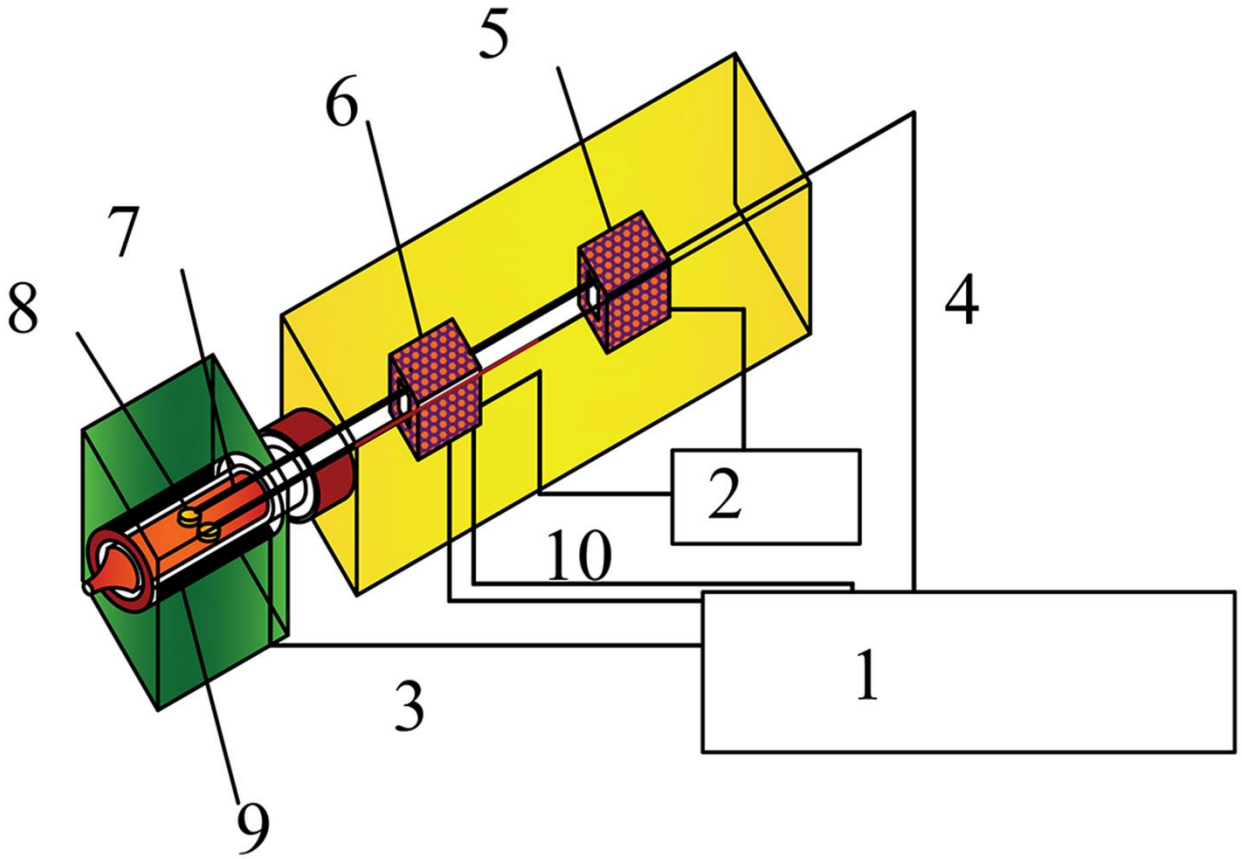

Fig. 3.13. Schematic diagram of horizontal thermogravimetric (TG)/ differential thermal (DTA) analyser (1: TG/DTA module CPU, 2: Balance circuit, 3: Heater power, 4: Thermogravimetric signal, 5: Deflection sensor, 6: Fulcrum housing, 7: Balance arm, 8: Sample, 9: Furnace, 10: DTA signal)

3.5. Field emission scanning electron microscopy

An SEM analysis of torrefied, as well as raw materials, was performed at the Indian Instrumentation Centre, Indian Institute of Technology, Roorkee, India. Before carrying out morphological analysis, the specimens of processed pine waste material were prepared. The specimens were initially dried so that they could be compatible with the vacuum produced during SEM analysis. The presence of water influences the vacuum as well as the imaging of the samples. The massive deformation and collapsing of a structure are some of the obnoxious effects of water molecules. As dehydration might bring a structural change, the specimens were first fixed to preserve their structural characteristic. However, fixation could be achieved using chemical methods such as fixation with glutaraldehyde or physical methods such as cryofixation in liquid nitrogen. Thereafter, ethanol dehydration of the specimens was performed. The specimens were then dried using the critical point method so that the nano and microstructures were not impacted. The reason for critical drying is that the tangential forces caused by the surface tension of solvent can harm the structure during phase transformation, therefore, to preserve the morphology of the sample, drying at the critical point was suggested. Upon finishing drying, the dried specimens were coated with a conducting material usually gold to make the surface conducting and allow it to emit more secondary electrons.

The state-of-art of technique can be determined by the source of energy provided by the electron gun. In a Transmission electron microscope (TEM), the electron source is a tungsten filament which was placed in a Wehnelt cylinder or Wehnelt cap. The filament is located immediately above the aperture provided in the Wehnelt cap. A negative potential is applied to the Wehnelt cap that allows the electron emitted by the filament to focus as a narrow beam. Therefore, an electron gun acts as an electron source and as a lens. Below this cap, an anode is laid that could accelerate the emitted electron. The brightness of tungsten filament is defined in current density per unit solid angle and it is nearly 10^9 A-m^{-2}-sr^{-1}. This can be further increased by 10-fold if lanthanum hexaboride (LaB_6) is used in place of a tungsten filament. Unlike other thermionic electron emissions, field emission uses a single tungsten crystal that has a very fine tip point. Rather than heating the tungsten filament, the emission of an electron in the FESEM is generated by applying a very strong electric field also called an extraction voltage. The brightness of the field emission gun is around $>10^{13}$ A-m^{-2}-sr^{-1}.

The micrographs and the energy dispersive spectroscopy detail are obtained by FESEM (Carl Zeiss). The schematic diagram of SEM is provided in Fig. 3.14. As an interface, the smart SEM software is used to control the functioning of FESEM. The specimen chamber was ventilated by nitrogen gas so that the desired vacuum level could be obtained. The working distance (WD) ranging from 11.1 to 11.6 mm was considered between the focussed specimen and the end of the objective lens for surveying the specimen, whereas the horizontal field width (HFW) of the scan was subjected to vary from 37.30 μm to 0.60 mm. The voltage of 5 kV was applied to investigate the topology of the processed pine waste.

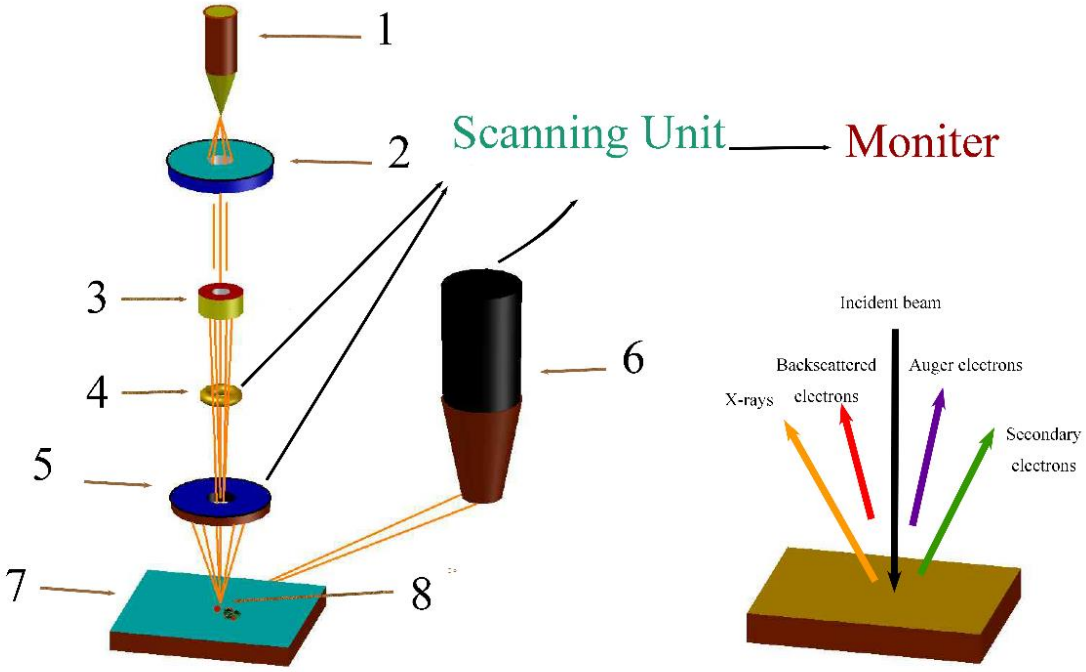

Fig. 3.14. Schematic diagram of FESEM (1: The electron gun, 2: Anode, 3: Magnetic lens, 4: Scanning coils, 5: Backscattered electron detector, 6: Secondary electron detector, 7: Stage, 8: Specimen)

3.6. Physical and chemical measurement

The physical and Chemical analysis was performed at the National Agriculture and Innovation Centre, Hungary. The physical analysis of torrefied, as well as raw materials, is divided into two parts: ultimate and proximate analyses and fractional distillation of pyrolysis oil obtained after pyrolysis of pine waste. The proximate analysis of the torrefied, as well as raw pine waste, was determined by heating them in a muffle furnace. The furnace used for proximate analysis is illustrated in Fig. 3.15. The moisture measurement was performed by heating the 1 g of each sample until 105 °C for a period of 1 hour, the loss in weight of each sample provided the moisture content in pine waste samples. Similarly, for evaluation of volatile content, the same 1 g of each sample was heated up to 950 °C for 7 minutes. At the end of the process, the loss of weight due to the elimination of moisture and volatile matter was determined. To measure the ash content, by subjecting 1 g of each sample in an uncovered crucible to the temperature of 720 °C until the samples were not completely burnt, the constant weight of the samples was reached, which indicates there is only ash remaining in the crucible. The fixed carbon is determined by subtracting the ash, moisture and volatile content from 100. The following equation was used to determine the fixed carbon in the samples (torrefied as well as raw pine waste).

$$\mathrm{F.C} = 100 - \mathrm{Ash\%} - \mathrm{M\%} - \mathrm{V.C\%} \quad (3.2)$$

The ultimate analysis of the samples (torrefied and raw pine waste) was performed using a CHNS analyser (Vario MACRO elementar).

Fig. 3.15. The muffle furnace for proximate analysis

Initially, the analyser was heated up to 1200 °C for 30 minutes. Meanwhile, the samples were encapsulated in a tin foil with tungsten (VI) oxide (WO_3) that acted as a reagent in the chemical reaction and facilitated the oxidation of the samples. To calibrate the CHNS analyser, the birch leaf standard was used to check the working condition of the system. Once the furnace reached the pre-combustion temperature, the samples were fed into the chamber via a multi-sample injector. The role of oxygen was to maintain the catalytic combustion, whereas helium gas was acted as a carrier gas. The objective of the carrier gas was to carry away the products of combustion to different reduction columns. These tubes were placed in the middle of combustion and the signal-processing unit. The elements of gas were isolated with the help of purge or trap chromatography. The separated elements were individually detected by a thermal conductivity detector (TCD). The function of TCD is to create the electric pulse that is proportional to the concentration of the elementary components of the samples. The CHNS analyser is depicted in Fig. 3.16. The schematic diagram of the CHN analyser is provided in Fig. 3.17.

Fig. 3.16. The CHN analyser for ultimate analysis

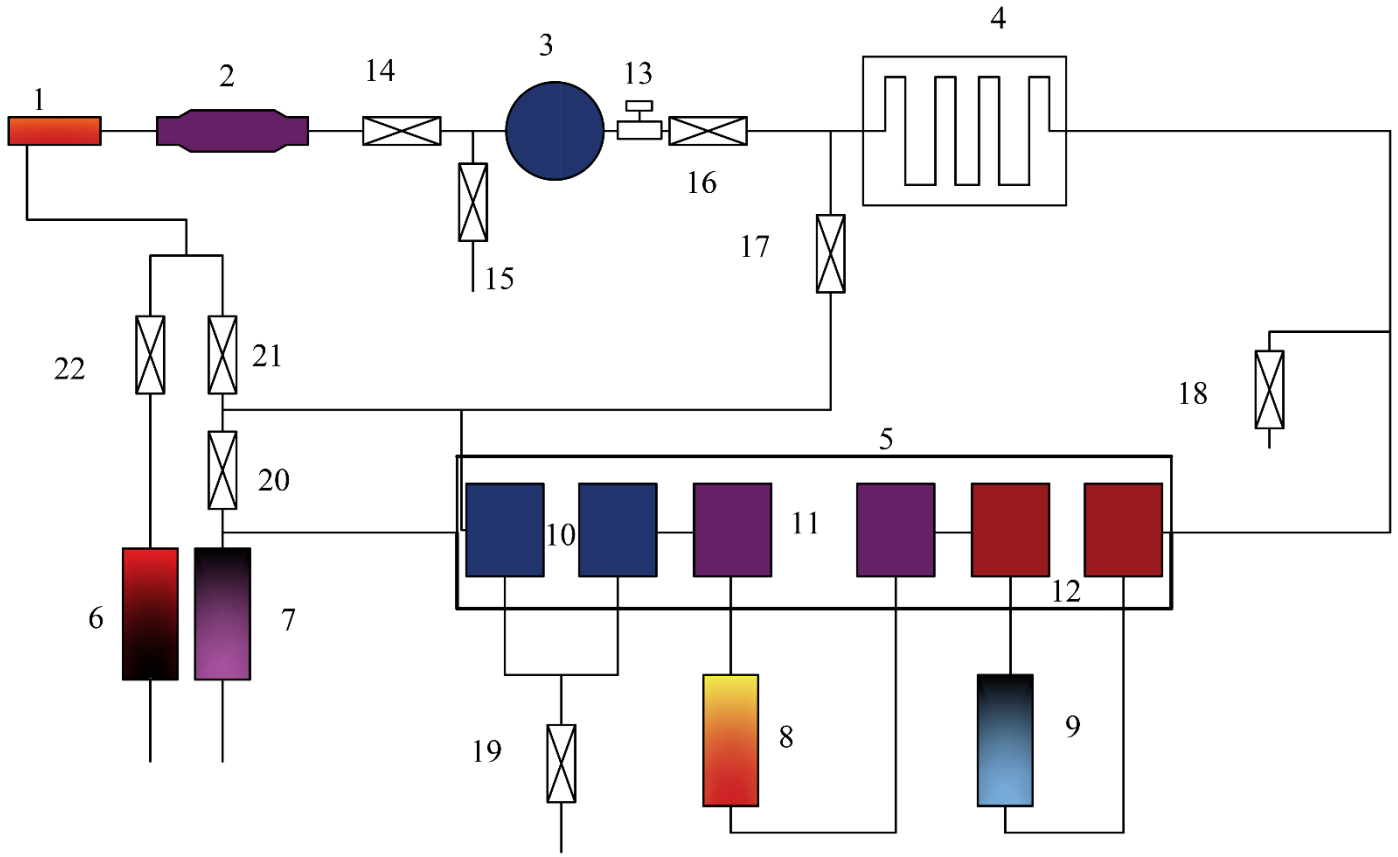

Fig. 3.17. The flow schematic diagram of CHNS analyser (1: Combustion tube, 2: Reduction tube, 3: Mixing Volume, 4: Sample volume, 5: Thermal conductivity detector, 6: Scrubber (Oxygen supply), 7: Scrubber (Helium supply), 8: CO_2 trap, 9: H_2O trap, 10: Nitrogen capture, 11: Carbon capture, 12: Hydrogen capture, 13: Pressure transducer, 14: Cut-off valve between the combustion train and the analytical system, 15 and 16: Purge valves, 17: Exhaust valve, 18: Gas control valve, 19 and 20: Automatic leak testing valves, 21: Solenoid valve, 22: Oxygen flow control valve)

For measurement of Sulphur, the combustion tube was replaced with one containing a tungstic oxide packing with a dehydration reagent. The water trap was removed and replaced with silver oxide to absorb SO. The SO_2 was detected similarly to hydrogen. The mechanism of CHN could be explained in this way that the combustion train is initially filled with oxygen. After sample injection, valve 14 was closed to seal off the combustion train from the rest of the analytical system, which was still being sent up helium gas. Combustion in the chamber occurs under the static condition in an excess of oxygen at about 975 °C. Meanwhile, the mixing volume was flooded by opening valve 15 and 16. After some time the valve 16 was closed to allow the pressure in the mixing volume to reach atmospheric pressure. At the end combustion period, a high-heat coil around the combustion tube vaporised the condensates at the entrance of the combustion tube. Due to the high influx of heat, valves 21 and 14 were reopened and the product of the combustion was allowed to flush from the combustion train into the mixing volume. The combustion train remains under positive pressure till the end of the complete cycle. During the mixing of sample gases, the carrier gas was allowed to allow from valve 17 through the sample volume and the detectors. Once the mixing is done, the valves 17 and 18 were opened to let the sample gas captured in the mixing volume expand at a constant volumetric rate to the atmosphere. The water, carbon dioxide and nitrogen concentration of the sample were measured by displacing the sample gas through the detectors to the atmosphere. The sample gas passes through TCD at constant pressure, volume and temperature so that any variation in water vapour pressure or water vapour concentration due to water adsorption was eliminated from the walls of the pneumatic system. At the end of the cycle, the exhaust valves were opened to allow the sample gases to escape to the atmosphere. It is to be noted that the oxygen (O%) was calculated by difference method Eq. 3.3.

$$\mathrm{O\%} = 100 - \mathrm{C\%} - \mathrm{H\%} - \mathrm{N\%} - \mathrm{S\%} - \mathrm{Ash\%} \quad (3.3)$$

The bomb calorimeter used during analysis is shown in Fig. 3.18. The calorific value of the samples (processed as well as raw pine waste) was obtained by the oxygen bomb calorimeter (IKA WEKE C2000).

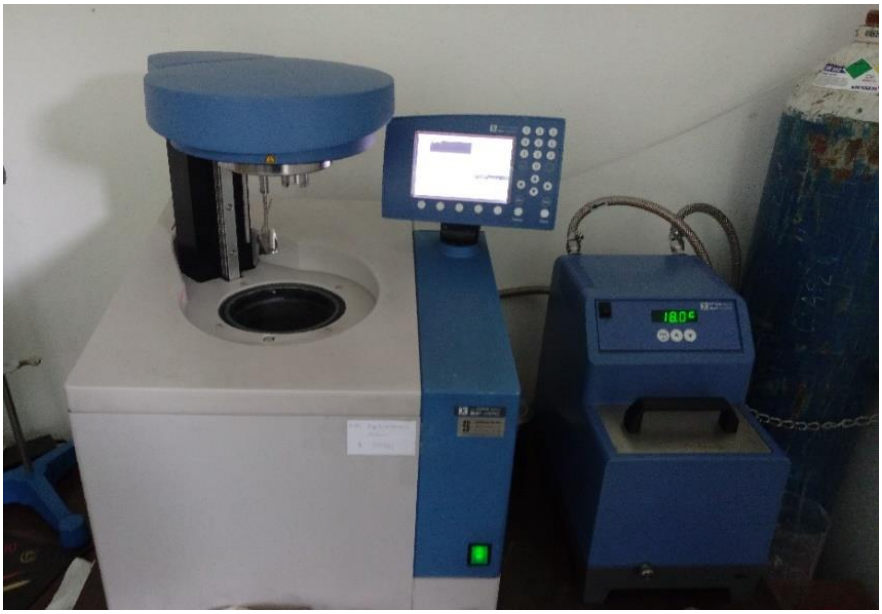

Fig. 3.18. A constant volume calorimeter

Before measurement of the calorific values, the benzoic tablets were used to calibrate the calorimeter. Once the calorimeter was calibrated, the samples were tested in a decomposition vessel. The permissible operating pressure of the calorimeter was estimated to be 23 MPa and the oxygen pressure was kept below 4 MPa in the vessel. The water inside the jacket was heated up to 25 °C before beginning the process.

The process of pyrolytic oil was performed in the Regional Knowledge Centre, Szent Istvan University. The 50 ml of isopropanol was used as a solvent to collect the pyrolytic oil, which was later distilled through a rotary evaporator (RVO 400, Boeco). The single-stage used during the process was shown in Fig. 3.19. The operating condition considered were similar to the condition provided in the literature (Dhaundiyal and Tewari, 2016). To distil the isopropanol, the vacuum pressure and temperature of the water bath were fixed at 0.137 bar and 60 °C, respectively, in a rotary evaporator. The decanter was allowed to undergo 70 revolutions per minute until no further condensation of isopropanol was noticed. The mass of the mixture along with the decanter was measured before carrying on the distillation. Upon finishing, the same decanter with the left-out sample was measured.

Fig. 3.19. The single-stage rotary evaporator for distillation

3.7. Thermo-chemical formulation

The calculation involved during thermodynamic, as well as chemical studies of the system, is divided into two parts: Dynamics of a system and chemical kinetics of the pyrolysis reactions.

3.7.1 . Dynamics of a system

It is necessary for the proper working of the unit that it might not increase the unnecessary burden on the auxiliary parts. Therefore, it must be ensured that the performance of the system must comply with the standard thermodynamic procedure. To examine the performance of the system, some thermodynamic calculations were carried out. The compressibility of the gas was neglected throughout the procedure, therefore the variation of velocity during the flow is considered to be uniform or point function. The flow is considered to be laminar in the gas pipe and the solubility of the gases was considered to be negligible at the given pressure. The procedure of testing was similar to that adopted for a gasifier (Dhaundiyal and Gupta, 2014; Dhaundiyal and Tewari, 2016; Dhaundiyal et al., 2020b).

The following expressions are used to determine the parameters associated with the performance of the thermal system.

The cold gas efficiency of the reactor was evaluated by the following equation.

$$\eta_c = \frac{HHV_g}{Total\ heat\ input(\ HHV_f + Sensible\ heat\ of\ fuel)} \times 100 \tag{3.3}$$

Likewise, the hot gas efficiency of the unit for the thermal energy system was determined through Equation 3.4.

$$\eta_h = \frac{HHV_g + enthalpy\ of\ the\ producer\ gas}{Total\ heat\ input(\ HHV_f + Sensible\ heat\ of\ fuel)} \times 100 \tag{3.4}$$

Another factor that influences the working ability of the thermal system is thermal gas efficiency that could be derived from the following expression.

$$\eta_t = \frac{HHV_g + ethalphy\ of\ water\ vapour\ in\ gas}{Total\ heat\ input(\ HHV_f + Sensible\ heat\ of\ fuel)} \times 100 \tag{3.5}$$

The specific humidity (ω) and degree of saturation (γ) were evaluated through Equation 3.6 and Equation 3.7. (Arora, 1981)

$$\omega = \frac{0.622 p_v}{p - p_v}\ \text{kg(w.v)/ kg(d.g)} \tag{3.6}$$

$$\gamma = \frac{p_v}{p_s}\left(\frac{p - p_s}{p - p_v}\right) \tag{3.7}$$

Here, p, p_v and p_s are the pressure exerted of the producer gas, the partial vapour pressure at the dew point temperature and the saturation pressure of water vapour at the dry bulb temperature, respectively.

The specific pyrolysis rate (SPR) was determined through Equation 3.8.

$$SPR = \frac{FCR}{A_{c.s}}\ \text{kg-m}^{-2}\text{-h}^{-1} \tag{3.8}$$

Here, $A_{c.s}$ denotes the cross-sectional area of the reactor and FCR is the fuel consumption rate in kg-s^{-1}

The specific gas production rate (SGPR) for the given system was calculated from the following expression.

$$SGPR = \frac{Rate\ of\ gas\ production}{A_{c.s}}\ \text{m-h}^{-1} \quad (3.9)$$

The time required to consume the biomass was determined by Equation 3.10.

$$\tau = \frac{H.\rho}{SPR}\ \text{h} \quad (3.10)$$

Here, H is the height of the reactor and ρ is the density of biomass.

The heat transfer coefficient for the producer gas flowing inside the copper tube was determined from the following empirical relation (Holmes, 2002)

$$\bar{h} = \frac{0.683k \times Re^{0.46} \times \text{Pr}^{\left(\frac{1}{3}\right)}}{D} \quad (3.11)$$

Where D is the inner diameter of the copper tube

The sphericity of the pellets was evaluated through Equation 3.12 (Dhaundiyal et al., 2020b)

$$\psi = \frac{S_s}{S_p} \quad (3.12)$$

Here, S_s is the surface area of the sphere, which has the same volume as a pellet and S_p is the surface area of a particle.

The pressure drop per unit length of the bed across the packed bed of pellets was estimated from the given Equation 3.13 (Dhaundiyal et al., 2020b)

$$\left(\frac{\Delta P}{L}\right)_b = 150\frac{(1-\varepsilon)^2}{\varepsilon^3}\left(\frac{\mu U}{(\psi d_p)^2}\right) + 1.75\frac{(1-\varepsilon)}{\varepsilon^3}\left(\frac{\rho U^2}{\psi d_p}\right) \quad (3.13)$$

Here, ε and d_p are voidage of the packed bed and the diameter of a pellet.

The mass yield (Y), energy yield (Z) and energy density enhancement factor (EDEF) obtained after the torrefaction process were determined through expression (Basu, 2013, Chen et al., 2018)

$$Y\ (\%) = \left(\frac{m_t}{m_b}\right) \times 100 \quad (3.14)$$

$$Z\ (\%) = Y \times \left(\frac{HHV_t}{HHV_b}\right) \times 100 \quad (3.15)$$

$$\text{EDEF} = \frac{\Omega_t}{\Omega_b} \quad (3.16)$$

3.7.2. Chemical kinetics of pyrolysis reactions

The methods for evaluating the chemical kinetic analysis of thermal decomposition of the torrefied pine waste is based on an isoconversional scheme. The tenet of this scheme relies on that at any extent of reaction (α), the same reactions would occur in the same ratio, which would be independent of temperature (Dhaundiyal and Singh, 2020). The isoconversional method is mainly recommended to develop a robust kinetic model (Vyazovkin et al., 2011). The scheme begins with the assumption that the function g(p) is supposed to be one in Equation 3.17.

$$-\frac{d(1-\alpha)}{dt} = f(\alpha).g(p).k(T) \quad (3.17)$$

Here, *p* and *T* represent the pressure and temperature of the chemical system, respectively.

The functions *k* (*T*) and *g* (*P)* denote the rate constant and the pressure dependence of reaction, respectively. The rate constant for a reaction can be expressed as,

$$k(T) = A.e^{-\frac{E}{RT}} \tag{3.18}$$

where *E* and *R* denote the apparent activation energy and the universal gas constant, respectively.

Keeping the reaction rate equation invariant from pressure and substitute *k* (*T*) in Equation 3.17, one can get

$$\frac{d\alpha}{dt} = f(\alpha).Ae^{-\frac{E}{RT}} \tag{3.19}$$

The terms at the right-hand side of Equation 3.19 are also called the kinetic triplet. For a non-isothermal profile, the dependence of conversion (α) on time can be expressed in terms of heating rate, β.

$$\frac{d\alpha}{dT} = f(\alpha).\frac{A}{\beta}e^{-\frac{E}{RT}} \tag{3.20}$$

Here, β is the slope of temperature profile to time.

$$\beta = \frac{dT}{dt} \tag{3.21}$$

After the rearrangement of Eq. 3.20, one can have,

$$q(\alpha) = \frac{A}{\beta} I\left(\frac{E_\alpha}{RT}\right) \tag{3.22}$$

Here, $q(\alpha) = \int_0^{\alpha_i} \frac{d\alpha}{f(\alpha)}$

The temperature integral $\left(I\left(\frac{E_\alpha}{RT}\right) = \int_{T_0}^{T_f} e^{-\frac{E}{RT}}\, dT\right)$ bears no analytical solution and it can be approximated by the numerical method proposed by Doyle (Doyle, 1961).

$$I\left(\frac{E_\alpha}{RT}\right) \cong -5.331 - \frac{1.052E_{\alpha_i}}{R.T_{\alpha_i}} \tag{3.23}$$

$$ln(\beta_i) = ln\left(\frac{A.E_{\alpha_i}}{Rg(\alpha)}\right) - 5.331 - \frac{1.052E_{\alpha_i}}{R.T_{\alpha_i}} \tag{3.24}$$

It is to be noted that the validity of Equation 3.24 depends on the $\frac{E_{\alpha_i}}{RT}$, which must be in the interval of $20 \leq \frac{E_{\alpha_i}}{RT} \leq 60$ (Dhaundiyal et al., 2018a). Here the subscript α_i denotes a fixed conversion at a different heating rate (β_i). The plot of Equation (3.24) would provide a straight line with a slope of $-\frac{1.052E_{\alpha_i}}{R}$. The expression derived in Equation 3.24 is also known as Flynn-Wall-Ozawa (FWO) method.

Apart from FWO, the more accurate version of temperature integral leads to the Kissinger-Akahire-Sunrose (KAS) method, which is also recommended by the ICTAC reports for kinetic analysis (Vyazovkin et al., 2011)

The integral approximation for KAS is provided by Equation 3.25, where $I\left(\frac{E_\alpha}{RT}\right)$ is replaced by the approximated term $I\left(\frac{E_\alpha}{RT}\right) \cong \frac{e^{-\frac{E_{\alpha_i}}{RT_{\alpha_i}}}}{\left(\frac{E_{\alpha_i}}{R.T_{\alpha_i}}\right)^2}$. This approximation is valid for the range of $20 \leq \frac{E_{\alpha_i}}{RT_{\alpha_i}} \leq 50$ (Dhaundiyal et al., 2018a).

In this way, Equation 3.23 can be rewritten as

$$ln\left(\frac{\beta_{\alpha_i}}{T_{\alpha_i}}\right) = ln\left(\frac{AR}{g(\alpha)E_{\alpha_i}}\right) - \frac{E_{\alpha_i}}{RT_{\alpha_i}} \tag{3.25}$$

The apparent activation energy can be computed by drawing a plot of $ln\left(\frac{\beta_{\alpha_i}}{T_{\alpha_i}}\right)$ versus $\frac{1000}{T_{\alpha_i}}$.

The ASTM E698 method presents a different version that lies between model-based and model-free analysis (Dhaundiyal et al., 2018a). It is not necessary to compute activation energy at each conversion as it is often performed in the isoconversional method. It focuses on the model-free approach to determine the activation energy. At the maximum reaction rate, the derivative of the reaction rate is zero, so at g (*P*) =1, differentiate Equation 3.17, and it provides the following expression

$$\frac{\beta E}{R.T_m^2} - Ae^{\left(-\frac{E}{R.T_m}\right)} = 0 \tag{3.26}$$

By taking the natural logarithm of Equation 3.26, one gets

$$ln\left(\frac{\beta_i}{R.T_m^2}\right) = ln\left(\frac{AR}{E_\alpha}\right) - \frac{E_\alpha}{R.T_m} \tag{3.27}$$

Eq. (3.27) represents the Kissinger method.

The activation energy from Equation (3.27) can be retrieved by plotting $ln\frac{\beta_i}{R.T_m^2}$ vs $\frac{1000}{T_m}$. The maximum temperature can be derived by the derivative thermogravimetric (DTG) curve of the samples. By the nature of the isoconversional methods, it is better to say that they could be able to recognize the heterogeneous reactions, which refer to the formation of miscellaneous products of the reaction at different stages of thermal decomposition of biomass. The reliability to compute the overall conversion of a starting material is also relatively good as compared to the model-fitting methods. Furthermore, the variation of activation energy *E* and the frequency factor *A* on the conversion can be more easily incorporated in the model-free method than the model-fitting scheme. The mechanism of thermal decomposition of the samples (torrefied and raw pine waste) was determined by using the master plot (Criado et al., 1989; Sanchez et al., 2013).

In this study, it is assumed that the ratio of $\frac{E}{RT} \to \infty$, so that the master curves can be plotted for the first-order differential equation of α. Here $y(\alpha)$ is generalised reduced reaction rate.

$$y(\alpha) = \frac{T}{T_{0.5}}\left(\frac{\left(\frac{d\alpha}{dt}\right)}{\left(\frac{d\alpha}{dt}\right)_{0.5}}\right) \tag{3.28}$$

Eq. (3.28) was used to plot the master curve for the experimental DTG data. For other physical processes, the master curves are obtained from Eq. (3.29).

$$y(\alpha) = \frac{f(\alpha).q(\alpha)}{f(0.5).q(0.5)} \tag{3.29}$$

The differential form of the conversion function f(α) can be retrieved by selecting the solid-state reaction (Table 3.1).

Table 3.1. Differential ($f(\alpha)$) and integral ($q(\alpha)$) forms of solid-state reaction mechanisms (Dhaundiyal et al., 2018a)

Reaction Mechanism	Code	$f(\alpha)$	$q(\alpha)$
1st Order (Random nucleation)	F_1	$(1-\alpha)$	$-ln(1-\alpha)$
Pseudo nth order (n = 2, 3)	F_n	$(1-\alpha)^n$	$\frac{[(1-\alpha)^{1-n}-1]}{n-1}$
Contracting Cylinder (Phase-boundary) controlled	R_2	$2\,(1-\alpha)^{\frac{1}{2}}$	$1-(1-\alpha)^{1/2}$
Contracting Sphere (Phase-boundary) controlled	R_3	$3\,(1-\alpha)^{\frac{2}{3}}$	$\left(1-(1-\alpha)^{\frac{1}{3}}\right)$
Power law ($k = 2,3,4$)	P_k	$k\alpha^{\left(\frac{k-1}{k}\right)}$	$\alpha^{\frac{1}{k}}$
Avrami-Erofe'ev (p= 2,3,4) (Nucleation) and	A_p	$p(1-\alpha)\,[-ln(1$ $-\alpha)]^{\left(\frac{p-1}{p}\right)}$	$[-ln(1-\alpha)]^{\frac{1}{p}}$
1D-diffusion	D_1	$0.5\alpha^{-1}$	α^2
2D-diffusion (Valensi eq.)	D_2	$[-ln(1-\alpha)]^{-1}$	$(1-\alpha)ln(1-\alpha)$ $+\alpha$
3D-diffusion (Jander eq.)	D_3	$\frac{3}{2}\,(1-\alpha)^{\frac{2}{3}}\left[1-(1\right.$	$\left[1-(1-\alpha)^{\frac{1}{3}}\right]^2$
3D-diffusion (Ginstlinge-Brounstein eq.)	D_4	$\frac{3}{2}\left[(1-\alpha)^{-\frac{1}{3}}-1\right]^{-1}$	$\left[1-\frac{2\alpha}{3}-(1-\alpha)^{\frac{2}{3}}\right]$

4. RESULTS AND DISCUSSION

The study is divided among physical and chemical characteristics of thermally pre-treated, topological changes induced due to torrefaction, and the implication of torrefaction on thermodynamic and chemical systems. The pine waste comprises pine needles and pine cones, whereas the results are compared and validated with the experimental studies conducted in non-isothermal conditions.

4.1. Investigation of physicochemical characteristic

4.1.1 Physical and chemical traits of processed pine needles

It is clear from the ultimate and proximate analysis of black pine needles that the carbon fraction is very low, whereas ample oxygen and volatile matter are available in the raw form. The ultimate and proximate analysis of pine needles is tabulated in Table 4.1. To enhance the carbon fraction, some structural reforms were performed via torrefaction or thermal pre-treatment process. The quasi-static state of the furnace has been used to torrefy the raw material so that the fibrous polymer of the pine needles was driven off from its structure and refine its parent form. The elemental composition of pine needles underwent torrefaction at different temperature scale and processing time as provided in Table 4.2. It was seen that the carbon fraction was undulating with increasing temperature and time and a trade-off relationship was seen to be established between operating conditions and the elemental composition of a material.

Table 4.1. Chemical composition of raw pine needles

C%	H%	N%	O%	S%	Ash%	FC%	VC%	HHV (MJ-kg^{-1})
49.68	5.98	0.52	41.10	0.097	2.62	7.38	90	20.53

Table 4.2. Chemical composition of torrefied pine needles

T (°C)	t_p (min.)	C%	H%	N%	S%	O%
210	5	50.30	6.54	0.33	0.09	40.03
	10	49.37	7.64	0.55	0.01	40.42
	15	49.71	7.54	0.50	0.01	39.53
220	5	51.52	6.57	0.71	0.09	39.12
	10	51.26	7.53	0.42	0.09	38.48
	15	51.20	7.40	0.71	0.01	37.13
230	5	51.60	6.63	0.69	0.09	39.74
	10	50.20	7.31	0.54	0.01	40.09
	15	50.80	7.53	0.56	0.11	38.29
240	5	52.22	6.59	0.69	0.09	40.64
	10	50.93	7.47	0.48	0.09	39.12
	15	52.13	7.43	0.58	0.10	36.67
250	5	53.40	6.54	0.68	0.09	40.53
	10	51.70	7.56	0.71	0.01	37.85
	15	52.22	7.32	0.45	0.12	36.73

Torrefaction of pine needles at 250 °C for 5 minutes could be a suitable operating condition and obtaining a better output during thermal decomposition of pine needles pellets in a pyrolysis reactor. However, it would not be pertinent to deduce a conclusion based on material. Since different biomasses have different structural form and adumbration, therefore another pine waste, pinecone, was also torrefied along with pine needles so that a common consensus could be drawn.

It was noticed that the degree of pre-treatment was a function of time and temperature. The mass yield of the pre-treated pine needles is depicted in Fig. 4.1. With the increase in temperature, it was noticed that the mass yield of pine needles was dramatically soared up. The mass yield of pine needles was computed to be reduced linearly by 2% whilst torrefying the pine needles sample at a temperature of 210 °C for 5 minutes. The gradient of mass deviation was nearly the same at the beginning of the pre-treatment process for every 10 °C rises in the temperature of the furnace when pre-treatment was scheduled for 10 to 15 minutes. It remarkably elevated upon changing the temperature of the furnace up to 240 °C, and the mass yield obtained its trough at 250 °C.

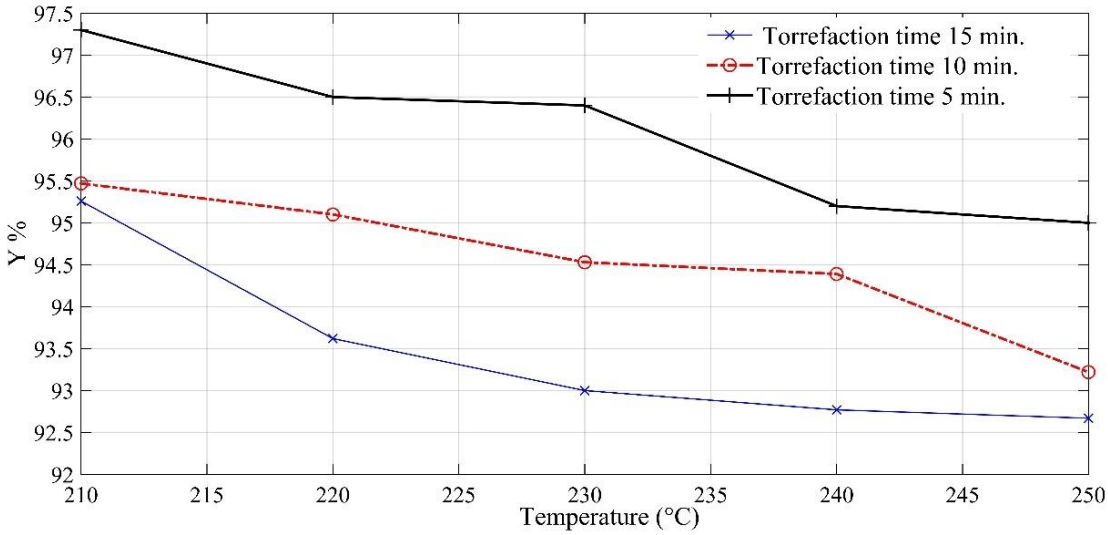

Fig. 4.1. Variation of mass yield (*Y*%) upon quasi-torrefaction in a Joule heating system at different temperature

The energy yield is another key factor to determine the appropriateness of the torrefaction process. The effect of pre-treatment on the energy yield of pine needles is illustrated in Fig. 4.2. It was contemplated that the energy yield slightly increased during the pre-treatment process of biomass at a higher temperature regime for an elongated duration. On the contrary, a higher temperature regime for a shorter duration had provided a qualitative edge in the energy yield of pine needles. The reason for this anomaly was that the energy yield is a function of mass yield and calorific content. So, there must be a quiescent point between these two factors that would lead to an outstanding solution. Pine needles were found to be highly inflammable and applying higher temperature for a prolonged period would bring drastic perturbance in the mass yield, therefore it is essential to provide thermal pre-treatment for adequate time. Likewise, mass yield, the energy yield also follows the linear pattern of variation with temperature and time.

The factor required to enhance the energy density of pine needles is the energy density enhancement factor which is shown in Fig. 4.3. A common EDEF was found at 220 °C whilst

processing pine needles for 5–10 mins. The EDEF was found to increase gradually during 210–220 °C, whereas a slight drop in energy density enhancement factor was seen when the pine needle

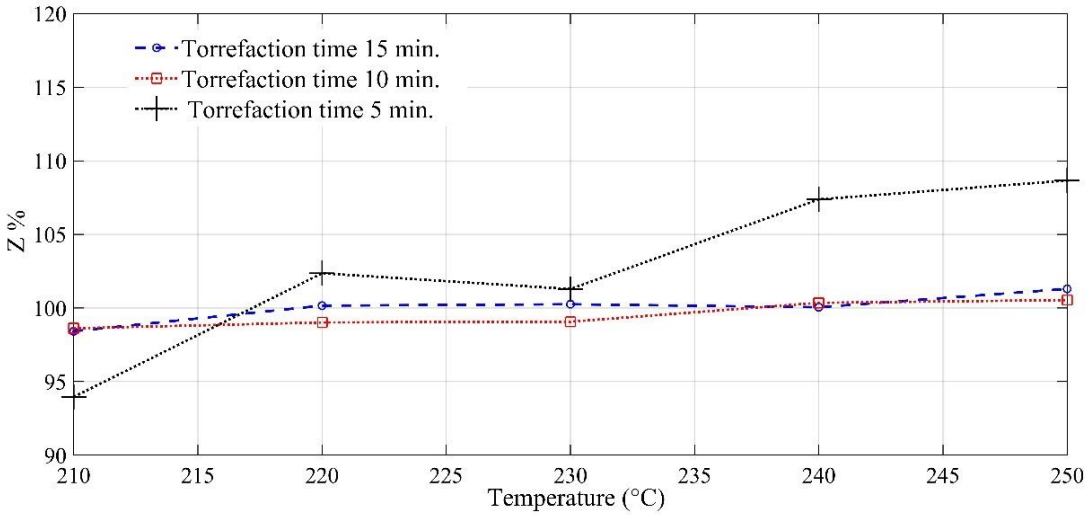

Fig. 4.2. Deviation in energy yield (*Z* %) with the pre-treatment temperature

the sample was torrefied at the temperature range of 220–230 °C. However, it is time-bound, and it would be true only when the processing of pine needles has been done for an extended period. The torrefaction for 5 minutes was found to be in good agreement with the higher temperature regime. The EDEF was observed to increase in the last quarter of 240–250 °C, but relatively, the EDEF was computed to be increased by 9% as compared to pre-treating pine needle at a constant temperature of 250 °C for 10 minutes.

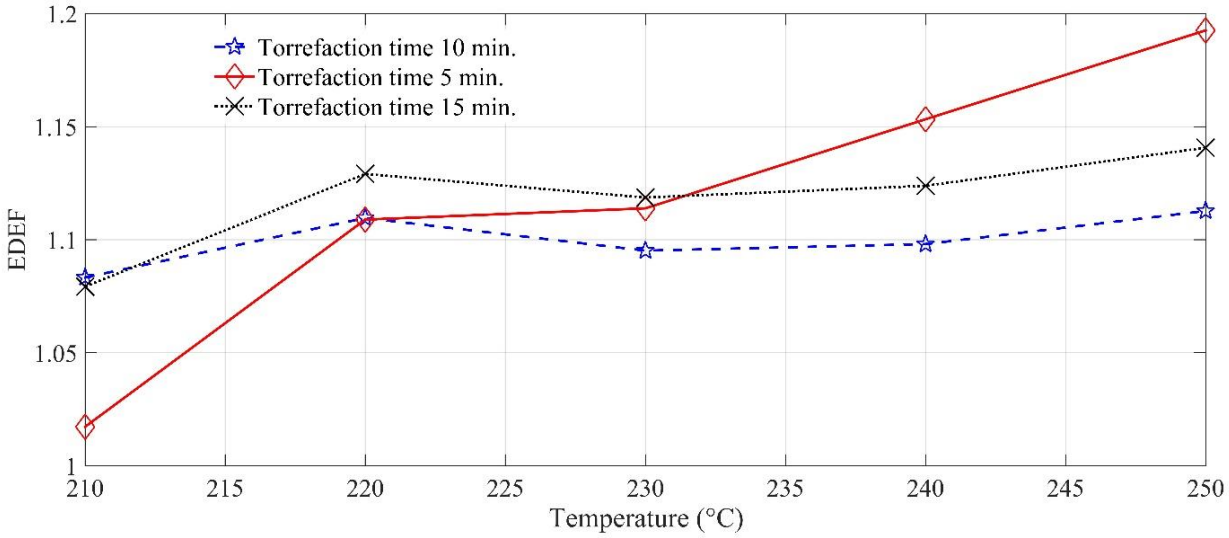

Fig. 4.3. The effect of torrefaction temperature on the energy density enhancement factor (EDEF) of processed pine needles

The maturity of pine needles upon thermal pretreatment is shown in Fig. 4.4. The higher regime of torrefaction temperature for the extended period brought a drastic deviation in the carbon percentage. The oxygen fraction in pine needles was found to be depleted remarkably as

temperature increased, and the flow of inert gas helped to increase carbon monoxide fraction by depriving the flame front of oxygen content.

Consequently, the utilisation of carbon content along with oxygen also get influenced by increasing torrefaction time and temperature. The molar ratio of H/C slightly increases, whereas the molar ratio of oxygen and carbon decreases with an increase in the degree of torrefaction. However, the oxygen is also removed from the structure during the decomposition of hemicellulose and the removal of moisture, therefore the overall drop in the oxygen content of the pine needles would be relatively higher than carbon and hydrogen. On the other hand, the higher regime of temperature would also trigger the release of H_2, which eventually allow the hydrogen fraction to drop more rapidly than the carbon fraction. There are some operating conditions where the molar of H/C would simultaneously decrease with the ratio of O/C. The suitable operating condition is to torrefy pine needles at 250 °C for 5 minutes. However, the thermal condition and duration of treatment are also subjected to the material properties of biomass. So, it may or may not be the same for another biomass. The deviation in physiochemical traits after torrefaction can also be understood by the heat transfer model and the size of the particle. The effect of particle size influences the reaction and heat transfer rates. The span of torrefaction gets minimised when the rate of heat transfer is faster than the reaction rate and it is only possible when the temperature profile across the particle is uniform.

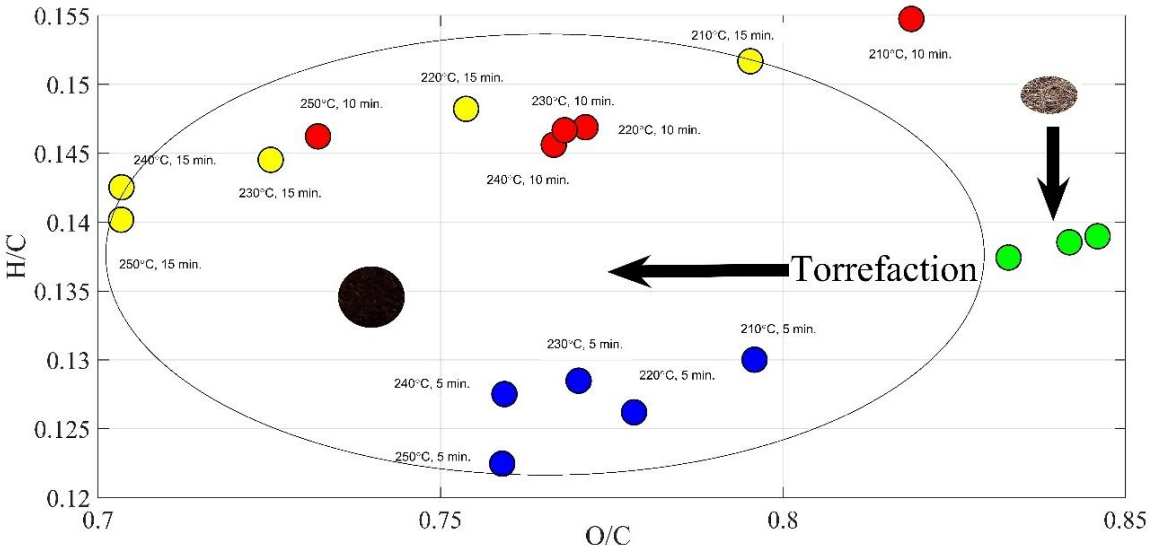

Fig.4.4. Van Krevelen diagram for the maturity of pine needles

Another important factor that has been often overlooked is the effect of torrefaction on the ash content of biomass. The ash content of biomass severely affected during the torrefaction process; therefore, it is essential to determine the deviation in the ash content of pine needles upon thermal pre-treatment. According to the literature review (chapter 2), it was found that a higher thermal regime increased the ash content of the biomass, but it is not practically correct unless the time factor is not involved. The effect of torrefaction on the ash content is depicted in Fig. 4.5. The effect of torrefaction for the shorter duration on ash content was found to have a declining trend and it was noticed that the ash content would be an acceleratory phase at the temperature range of 210–220 °C. The further increase in temperature at the same time would lead to a reduction in the ash fraction. The ash content was estimated to be lowest at 250 °C whilst pre-treating for 5 minutes. However, the literature review had confined the research specifically to the non-isothermal

condition where the furnace was subjected to follow a ramping thermal profile. On the contrary, the ash content would be maximum when the same sample is allowed to undergo torrefaction at 220 °C for a processing time of 10–15 minutes. It would all the way much higher when processing time would be extended beyond 5 minutes.

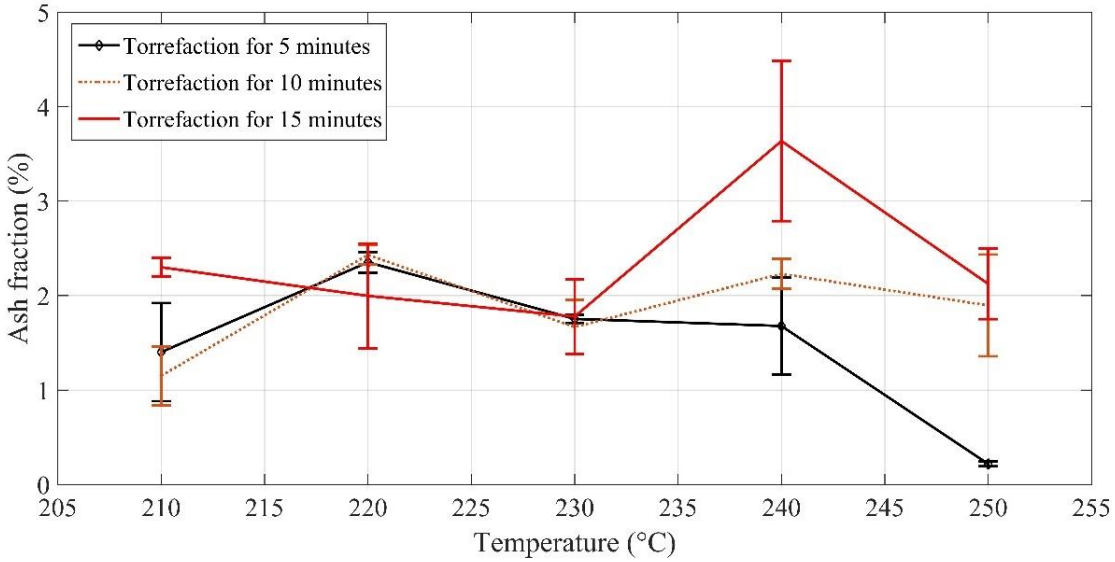

Fig.4.5. Variation in the ash content of pine needles with processing temperature

The statistical importance of governing factors, time and temperature is determined and provided in Table 4.3. The torrefaction temperature merely influences the higher heating value of pine needles or the energy density enhancement factor (EDEF). The ash content and mass yield (*Y*) would highly correlate with the processing time of pine needles rather than the temperature required for thermal pre-treatment. It can be concluded at the end that torrefaction of pine needles has a transient characteristic, and the carbon enrichment process supports a shorter span of processing time.

Table 4.3. ANOVA analysis of the obtained parameters for pine needles (alpha cut = 0.10)

Parameters	Factors	*p*-value
FC	Time	0.000799
	Temperature	0.100658
VC	Time	0.000498
	Temperature	0.396832
Ash content	Time	0.137992
	Temperature	0.250298
Y	Time	0.003338
	Temperature	0.165807
HHV	Time	0.564916
	Temperature	0.057463

4.1.2. Physical and chemical traits of processed pine cones

Likewise, pine needles, pine cones also underwent torrefaction in similar operating condition. The chemical composition of pine cones is shown in Table 4.4. As in the case of pine needles, pine cones also have similar elemental traits, that is lower carbon fraction and a higher amount of oxygen, but the ash content of raw pine cones is relatively low as compared to the ash content available in pine needles. However, the effect of torrefaction temperature and time on the elemental composition made a different opinion. The elemental composition of pine cones obtained at different torrefaction temperature and time is provided in Table 4.5. It is clear from the elemental composition that the carbon has remarkable change upon elevating temperature with time. As the role of temperature was marginalised by the duration of processing in pine needles, the time factor is slightly underplayed for pine cones. The carbon fraction was found to be continuously increasing with both torrefaction temperature and time. The oxygen content was estimated to be continuously decreasing with torrefaction temperature and time.

Table 4.4. Chemical composition of raw pine cones

C%	H%	N%	O%	S%	Ash%	FC%	VC%	HHV (MJ-kg^{-1})
48.62	5.31	0.94	44	0.10	1.22	18.42	80.355	20.14

Table 4.5. Chemical composition of processed pine cones

T (°C)	t_p (min.)	C%	H%	N%	S%	O%
210	5	48.38	5.96	0.27	0.06	44.83
	10	49.06	6.01	0.38	0.06	42.52
	15	50.02	5.97	0.39	0.07	42.72
220	5	51.41	6.56	0.52	0.07	40.78
	10	50.04	6.02	0.09	0.07	42.87
	15	50.84	5.84	0.09	0.08	41.32
230	5	52.07	6.39	0.51	0.10	40.28
	10	49.59	5.97	0.15	0.08	43.04
	15	50.16	6.03	0.15	0.07	42.27
240	5	53.54	6.1	0.71	0.09	38.74
	10	49.49	6.26	0.23	0.08	42.35
	15	54.10	5.44	0.22	0.08	37.59
250	5	49.48	6.16	0.49	0.10	42.81
	10	51.48	5.93	0.39	0.09	40.82
	15	55.48	5.49	0.39	0.09	37.25

The objective of selecting the suitable thermal condition is based on the mass and energy yield derived at the end of the torrefaction process. However, the decision-making factors might vary with the objective of energy companies, but for a sake of simplicity, mass and energy are the major concerns. The effect of operating condition on the mass yield of pine cones is shown in Fig. 4.6. The mass yield has a linear variation with the change in temperature of the furnace. Whilst processing pine cones at constant temperature 210 °C, the mass yield derived for torrefaction time of 15 minutes was estimated to be 6.5% lower than the mass yield obtained when the same sample had undergone torrefaction for 5 minutes. Conversely, concerning the mass yield derived for

carrying out torrefaction for 5 minutes, the mass yield was reduced by 43% as the duration of processing is increased by 5 minutes. With the increase in torrefaction temperature and time, the disparity in the mass yield was further extended.

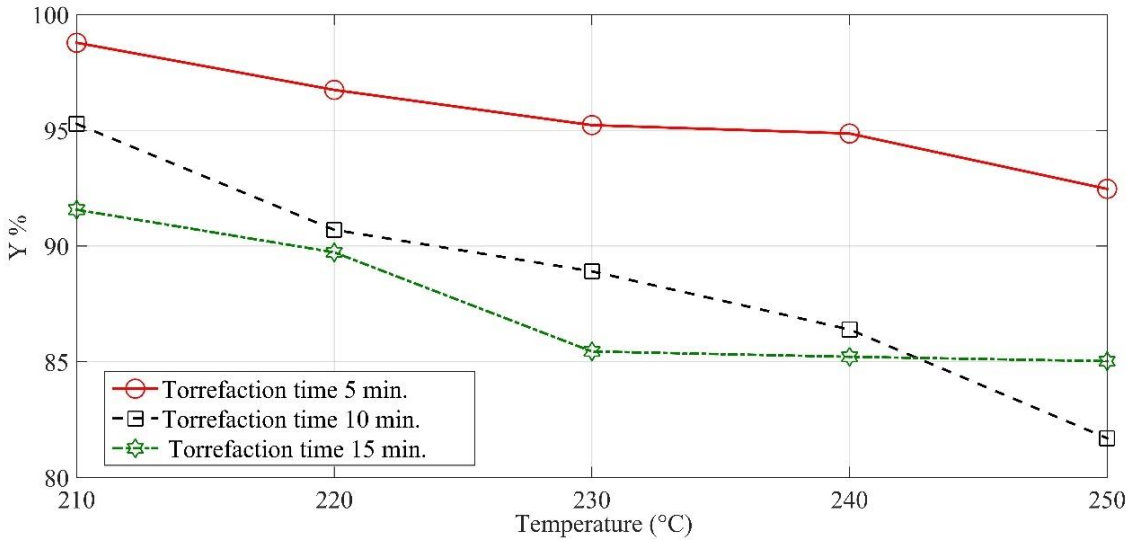

Fig. 4.6. The change in the mass yield of pine cones with temperature

The energy yield obtained at different temperature and time is shown in Fig. 4.7. A drastic increase with increasing temperature and time was noticed for pine cones. The lower thermal regime for an extended period of torrefaction was far-fetching and it was unable to showcase the magnificent change in the energy yield, instead of that it reduced the energy yield by 3.15%. At a constant temperature of 250 °C, the energy yield of pine cones was found to be 26% higher when it was torrefied for 15 minutes than that of torrefaction performed for 5 minutes, whereas it was dropped by −5.2% upon thermally treating pine cones for 10 minutes. It could be concluded that the torrefaction for a prolonged time would provide a promising energy yield. However, the gain in energy yield also relies on the initial state of pine cones. In nutshell, biomass with higher moisture content would have a higher rate of dry matter loss. The concentration of water molecules is highly correlated with the desorption process that occurs during the thermal pretreatment of pine cones.

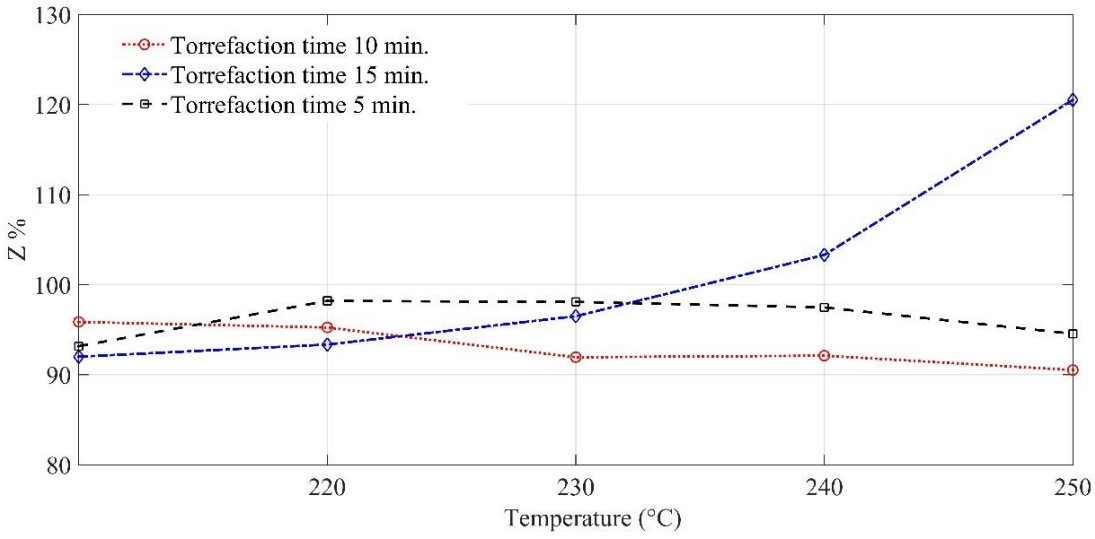

Fig. 4.7. The fluctuation in the energy yield of pine cones with the torrefaction temperature

The deviation in EDEF is illustrated in Fig. 4.8. It is clear from the energy density enhancement factor for pine cones that the higher torrefaction temperature for an extended period would enhance the energy density of pine cones. Similar to mass and energy yields, the relationship between the EDEF and the torrefaction was found to be linear. At a constant temperature of 250 °C, the EDEF was surged by 40% when the processing time was increased by 10 minutes. Similarly, a 27% rise in the EDEF was noticed whilst extending the duration from 10 minutes to 15 minutes at a constant temperature. However, the interval of deviation was seen to be shrunk as the torrefaction temperature decreases at a constant processing time. At 220 °C, the EDEF was reduced by 22% despite having a higher processing duration. So, unlike pine needles, it is clear from this fact that the carbon enrichment cannot be done unless the torrefaction temperature and duration of processing surge simultaneously.

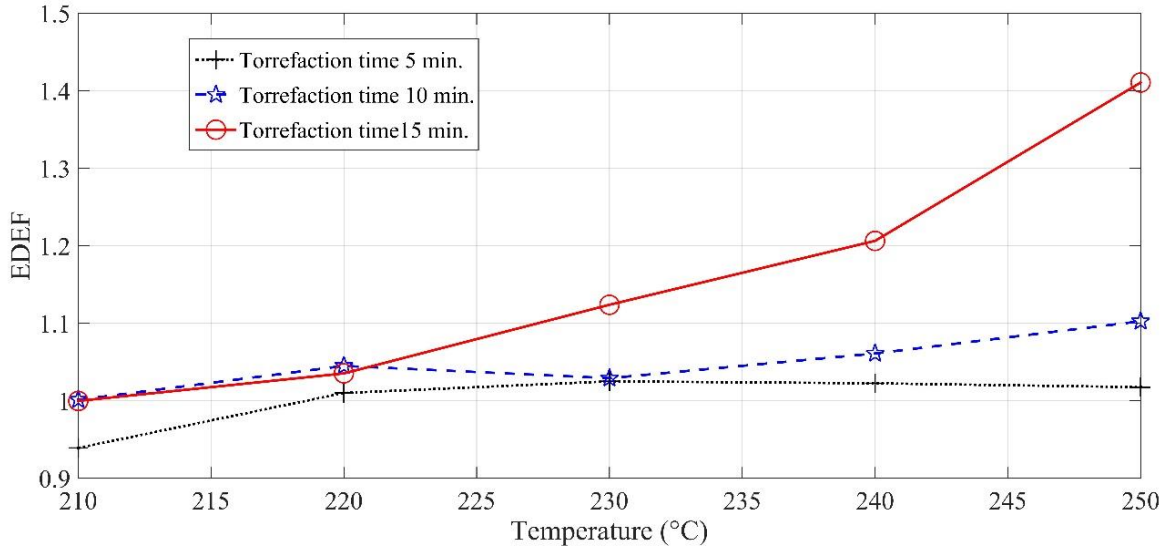

Fig. 4.8. The deviation in the EDEF with the torrefaction temperature at constant time

The Van Krevelan diagram for the maturity of pine cones is shown in Fig. 4.9. The molar ratio of H/C along with O/C decreases as the torrefaction temperature increases. However, the relative deviation in H/C as compared to O/C was found to be high. The reason for such anomaly in the behaviour is due to an increase in the fraction of H_2 with the rise in the torrefaction temperature. Another reason is the deprivation of O_2 in the flame front, which lead to an increase in the carbon monoxide and thus, some carbon gets driven off with the volatile gas in the form of soot particles. The rearrangement of molecules is also happened due to the decomposition of hemicellulose that triggers decarboxylation reactions. With these reactions, the oxygen-containing compounds such as water, CO_2, CO and oxygenated organics got liberated, thus the molar ratio of the oxygen and carbon decreases. Moreover, the inability of the OH group to make hydrogen bond imparted hydrophobicity to thermally pre-treated pine cones. With the removal of water and oxygen, the heating value of pine cones was also improved. This physical rearrangement of molecules brought a qualitative improvement in pine cones.

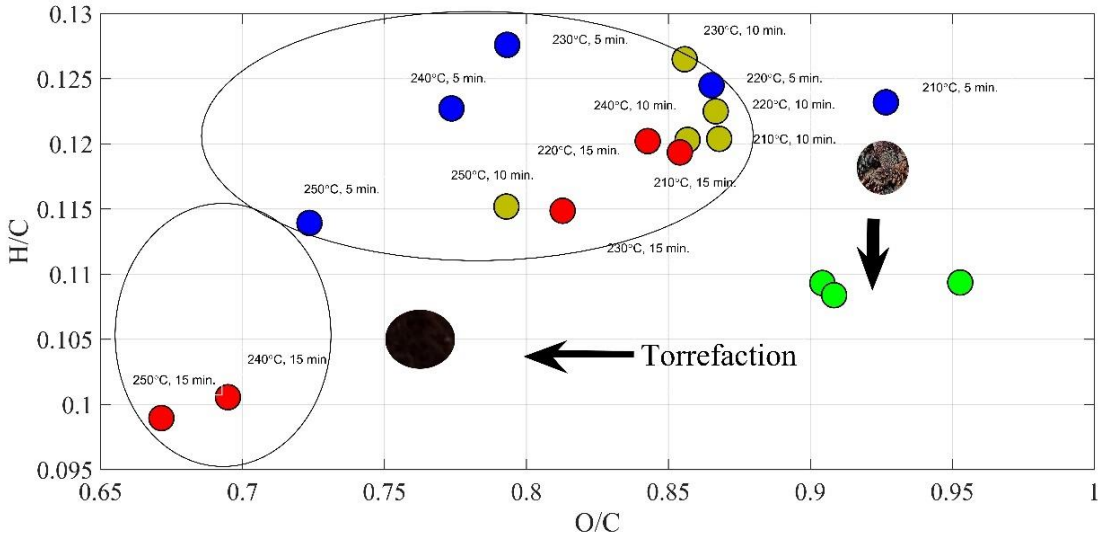

Fig.4.9. Van Krevelen diagram for the maturity of pine cones

The effect of torrefaction on the ash content of pine cones is illustrated in Fig. 4.10. The ash content obtained after torrefaction of pine cones at different temperature and time was found to increase drastically with the increase in torrefaction temperature and time. Thermal pre-treatment of pine cones for an extended period led to higher ash content, whereas the shorter duration provided the least fraction of ash at the end of the complete combustion of torrefied pine cones. It was also seen that the simultaneous increase in temperature and time would elevate the percentage fraction of ash content of torrefied pine cones. Here, a trade-off relationship was made between the energy yield and the ash content. The overall rise in the ash content was found to be all the way high if the torrefaction is conducted for 15 minutes. So, if the ash content is a criterion of selecting the torrefaction, one must choose the shortest processing duration. However, it would be discouraged if the energetic aspect has the top-most priority for the processing industry. At a constant temperature of 250 °C, the ash content was estimated to reduce by 15.39% when the processing time was increased from 10 minutes to 15 minutes. The higher processing time would be favourable only if the torrefaction is conducted at 210 °C.

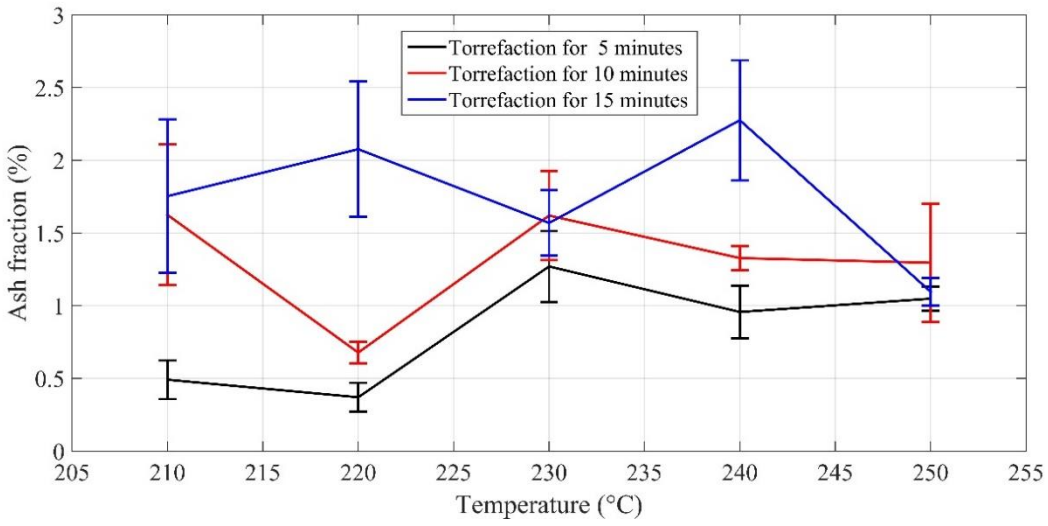

Fig.4.10. Variation in the ash content of pine cones with processing temperature

The influence of temperature and time on thermal pretreatment is shown in Table 4.6. The statistical study has shown that the time factor would have a more significant effect on the mass yield than temperature, whereas the ash content is the only parameter after the mass yield where the temperature would have some relevance in determining the course of torrefaction. So, a similar conclusion could be deduced that the duration of torrefaction would have a severe impact on the physicochemical characteristic of both pine needles and pine cones, therefore a suitable operating range for the pre-treatment of pine cones is chosen to be 250 °C, whereas the processing time should not be less than 15 minutes. Unlike pine needles, one has to meet halfway whilst selecting the physicochemical parameters for pine cones. A rift in the elemental behaviour was noticed as the physical properties of materials was changed.

Table 4.6. ANOVA analysis of the obtained parameters for pine cones (alpha cut = 0.10)

Parameters	Factors	*p*-value
FC	Time	0.492512
	Temperature	0.126046
VM	Time	0.291292
	Temperature	0.105256
Ash content	Time	0.028653
	Temperature	0.616978
Y	Time	0.000478
	Temperature	0.00855
HHV	Time	0.045349
	Temperature	0.125148

4.2. Morphological analysis of pine waste

From the physicochemical analysis, it was noticed that the torrefaction process of pine needles and pine cones accompanied some structural changes in both pine needles and pine cones. The study henceforth is focussed only on the operating condition which was obtained during elemental evaluation of pine waste.

4.2.1. Structural evaluation of pine needles

The topological changes upon thermal pre-treatment were studied with the help of FESEM. It was found that the bigger cleavage on the surface of pine needles propagated along the surface at an orientation between 13–30°, whereas the small cracks on the cellulose fibre were noticed to incline at 108–121°. The length of macro cracks formed during torrefaction varied from 8.08 μm to 20.77 μm, whereas the width was estimated to be in the range of 11.41–204.33 μm. On the other hand, the length of small cracks on the cellulose fibre falls in the domain of 4.503–30.32 μm. The effective width of small fissures was determined in the range of 1.32–3.29 μm. The recorded area of small fissures was computed to be 72% less than that of big cracks. The microfibrils were completely decomposed into small splinters. The cellulose structure was noticed to be devoid of amorphous segments (Fig. 4.11c). The FESEM images are illustrated in Fig. 4.11 (a-c: Torrefied pine needles, d-f: Raw pine needles). The macropores were noticed to be dilated in the interval of 2.82–9.65 μm. The orientation of macropores was stretched from 17° to 123°. The area of micro fibrillated cellulose was evaluated to be 2.77 μm^2, whereas its diameter was found to vary in the

range of 9.66–33.64 μm. The surface area of cellulose fibre was slightly increased due to the thermal pretreatment.

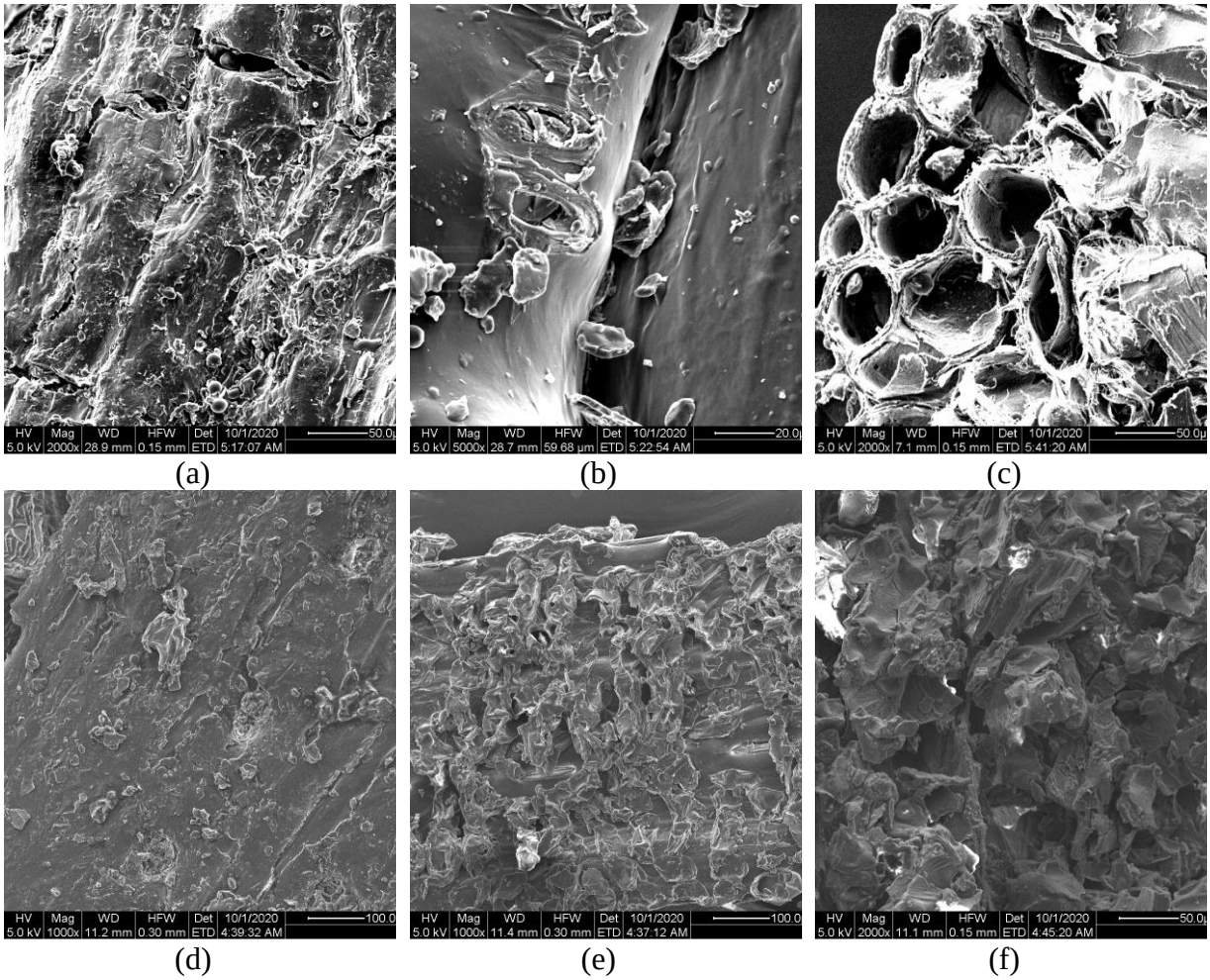

Fig. 4.11. The micrographs of torrefied as well as raw pine needles (a–c: Torrefied pine needles, d–f: raw pine needles)

4.2.2. Structural evaluation of pine cones

The morphological alteration in the torrefied pine cones after torrefaction was illustrated in Fig. 4.12. Likewise, pine needles structure, the microfibrils of raw pine cones was dilated by 198.5% after thermal pre-treatment. The diameter of the microfibril was estimated to lie in the domain of 27.72–68.88 μm. The big cracks of mean length 65.49 μm were found at the corners of cellulose fibre. A small fissure of 1.47–10.43 μm was noticed between the grain boundaries of pine cones. The orientation of the grain was deviated by 28–47° after the pre-treatment. The wall of native cellulose fibre was remained intact and there were no structural defects found (Fig. 4.12f). The cellulose fibre of thermally processed pine cones was stretched by 13%, whereas the surface area of fibre was increased by 12%. Similar to pine needles, the splinter of the amorphous region of cellulose was found during the structural investigation. All these interior failures observed during morphological analysis would affect thermogravimetric/ heating traits of material during the pyrolysis process, which has been comprehensively covered in section 4.3 and 4.4.

In this investigation, it was assessed that thermal pre-treatment affects porosity, grain size, and the propagation of cracks. It happened due to the violent escape of moisture from the surface of biomass. These structural defects mainly influence the heat transfer characteristic of biomass during pyrolytic reactions.

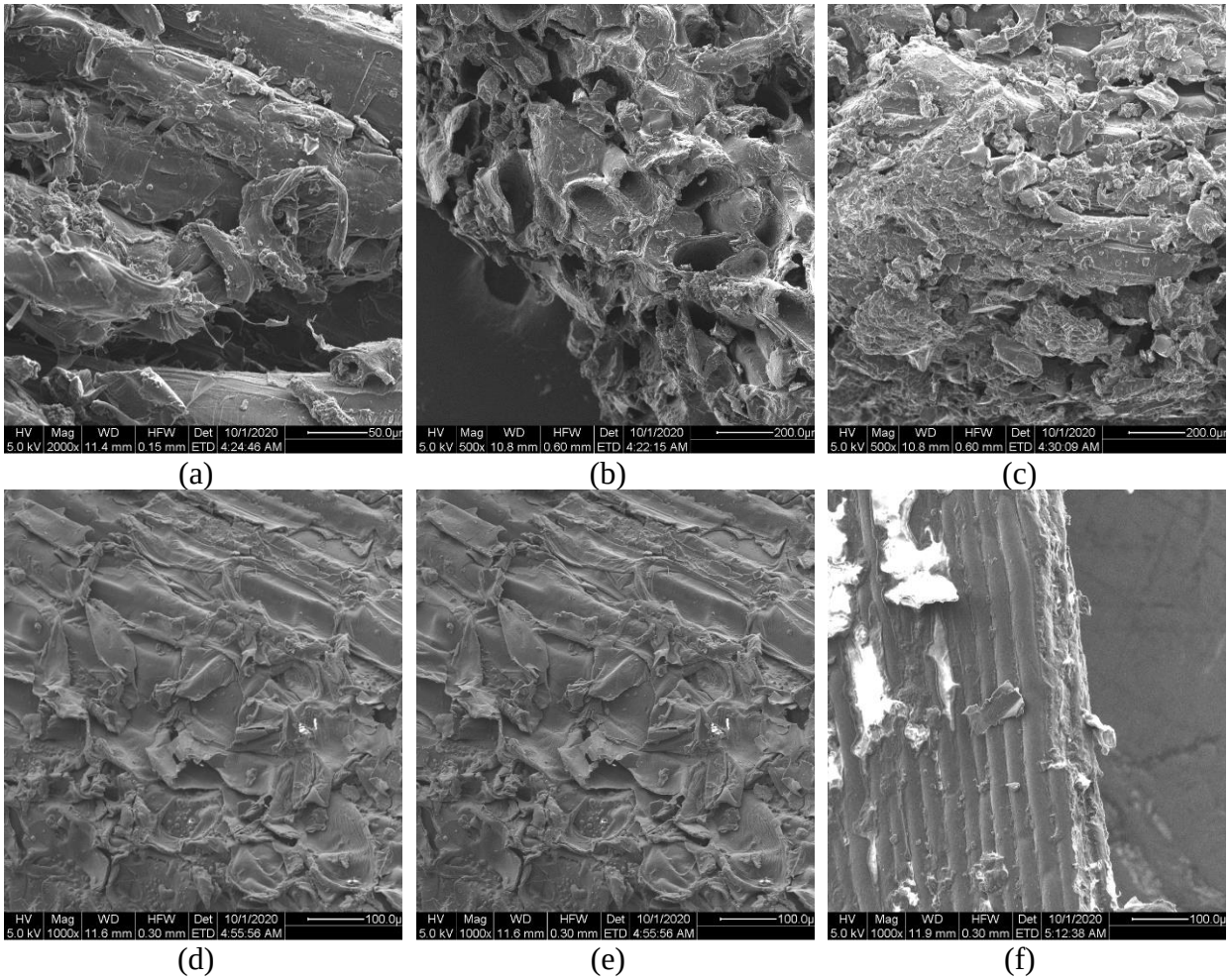

Fig. 4.12. The micrographs of torrefied as well as raw pine needles (a–c: Torrefied pine cones, d–f: raw pine cones)

4.3. Thermal analysis of torrefied material

The pellets of pine waste were processed at the operating condition derived during the physical and chemical investigation of torrefied powder of pine waste. To determine the merit of the processing technique, a test on the laboratory scale was conducted to evaluate the thermal potential of the torrefaction process. The physical feasibility of processing technology cannot be contemplated unless it is carried out in a prototype reactor. Therefore, a fixed-bed pyrolysis reactor was designed on AutoCAD and fabricated.

4.3.1. Thermal performance of pine needles in a small-scale reactor

The variation in the extensive property, mass, of pine needles pellets is shown in Fig. 4.13. The initial mass of 300 gram was chosen for experimental purpose. Each test was repeated thrice, and the average values were considered. It was noticed that the relative size of the mass plateau during dehydration was reduced by 56% for the pine pellets when it was compared with the wood chips

(Dhaundiyal et al., 2020b). The formation of ripples was observed at the onset of pyrolysis. This ripple effect was formed either due to a surge in the heating rate of the system or the formation of intermediary compounds. As the applied voltage and power supply is constant, thermal lag was noticed during the thermal degradation of pine pellets. It implicated that thermal immunity of pre-treated biomass at a lower temperature range was slightly increased due to the cross-linking or carbonization reaction. The surface adsorption in processed pine needles pellets caused a temperature drop of 15 °C at the beginning of the char formation and corresponding to this change in temperature, the dynamic pressure of the system was reduced from 0.6 Pa to 0 Pa. It was deduced from the TG curves that surface cracking during thermal pre-treatment had changed the TG behaviour of the processed pine pellets.

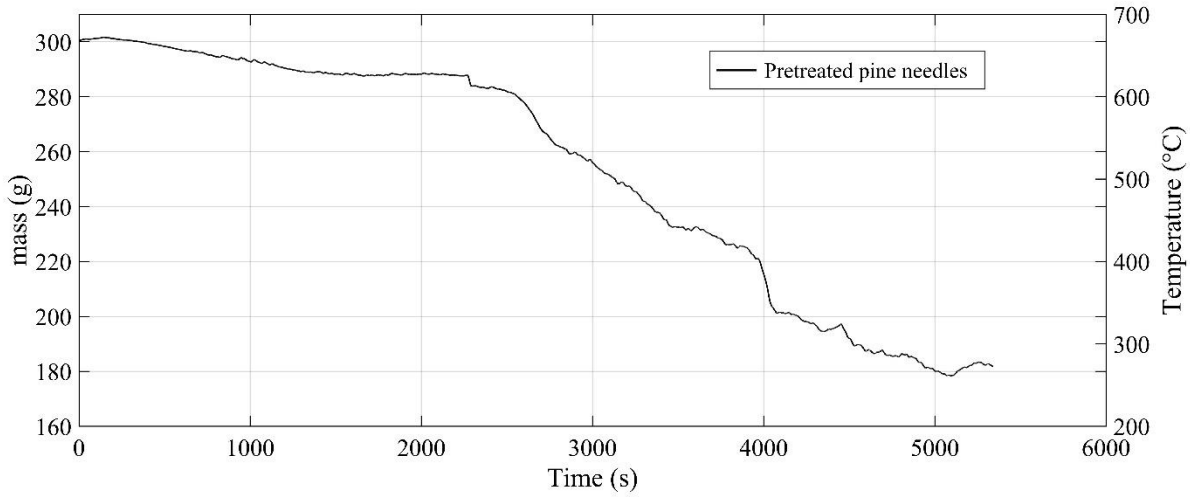

Fig. 4.13. Mass distribution of torrefied pine needles in a small-scale reactor

Apart from thermogravimetric variation in the mass of torrefied pine needles pellets, the intensive properties of the system, temperature and pressure were also got affected by the change in the course of thermal decomposition reactions. The change in the intensive properties of the fixed bed reactor is shown in Fig. 4.14. At the same electrical supply, a remarkable surge in the lower bed temperature (A) was noticed at the beginning of the thermal degradation of the pre-treated pine pellets. The heating rate was estimated to be 3.89 °C-min^{-1} during this thermal event. The sigmoidal behaviour or undulation in thermal histories signified that the dissipation of heat and pressure was taken place simultaneously within the system. As the lower bed (A) reached the cut-off point, the upper bed temperature (B) attempted to attain thermal equilibrium with the thermal profile of the lower bed (A). It was noticed that the heating rate was increased by 24.26% as desorption in the torrefied pine pellets was taken place. The desorption of moisture was carried out at the heating rate of 6.76–7 °C-min^{-1}. The drying or desorption of moisture accompanied a pressure rise of 76%, which showed that the removal of moisture content in the torrefied pine pellets drifted away from its thermal equilibrium. This was happened due to a rise in the partial vapour pressure of water content in the cellulose structure. The internal structural failure of pine needles pellets during torrefaction bolstered the pressure-driven flows across the reactor, and consequently, reduced the residence time of volatile in the reactor. The evolution of volatile was noticed to occur in a temperature interval of 406–577 °C in the torrefied pine pellets. The charring process of pine needle pellets was noticed to take place in a temperature range of 577–690 °C. The

pressure drops that occurred during char formation was estimated to be 212 Pa. After the power supply was interrupted, the thermal lag was noticed to be subdued with time.

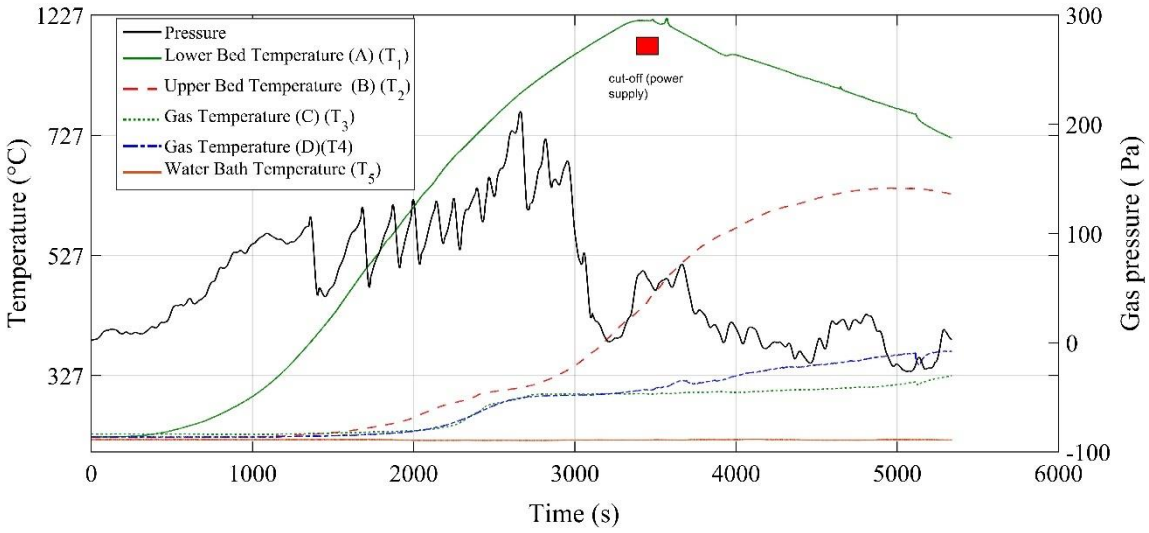

Fig. 4.14. Intensive properties of a reactor powered by the torrefied pine needles pellets

The producer gas composition derived from thermal decomposition of the torrefied pine needles pellets is shown in Fig. 4.15. It was noticed that the emission of CO_2 and CO fraction was reduced by 8.2% and 12% respectively. Likewise, the percentages of hydrogen and methane were found to increase by 91.2% and 11%, respectively. The net emission was cut by 20.2% after the pre-treatment of pine needles pellets when it was compared to the hardwood Chips (Dhaundiyal et al., 2020b). It was observed that the release of volatiles was very abrupt as time proceeds. It happened due to the reaction of carbon monoxide with the water vapour and ultimately, the increase in hydrogen gas percentage was noticed. The carbon dioxide and methane gases were saturated as the hydrogen gas began to rise.

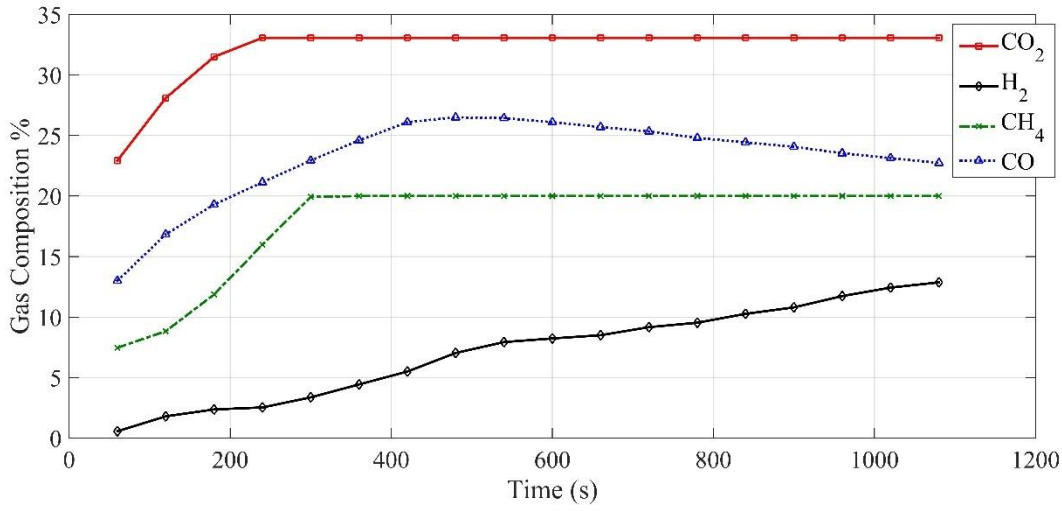

Fig. 4.15. Composition of producer gas derived from torrefied pine needles pellets

The thermal performance and miscellaneous parameters associated with the fixed-bed reactor is provided in Table 4.7. The consumption rate of the torrefied pine pellets was computed to 232 g-h^{-1}, which was found to be 51% lower than that of Wood chips (Dhaundiyal et al., 2020b). On the other hand, the specific pyrolysis rate (SPR) of the pre-treated pine pellets was estimated to be

40590 g-m^{-2}-h^{-1}, which was reduced by 25% when it was compared with wood chips (Dhaundiyal et al., 2020b). The drop in SPR was mainly happened due to the geometrical design of the reactor. Some other reason could to deviation in porosity of the pine pellets upon thermal pre-treatment. As the volatile gases penetrate the carbon particle and lead to the displacement of carbon. Consequently, the resultant gas is allowed to diffuse through the solid structure and trigger pyrolysis reactions. During the release of volatile, some materials get swollen and become more porous. These activated porous sites allow the volatile gases to react with the carbon and form the byproducts of pyrolysis. These local porosity and permeability are also affected by the presence of surface cracks that eventually causes the change in pressure during oxidation, and thus the rate of reaction is impacted. The specific gas production (SGPR) was calculated to be 7.58 m-h^{-1}, which is way too higher than that of wood chips (Dhaundiyal et al., 2020b). Owing to the volumetric flow of nitrogen, the decrease in the overall percentage of the producer gas composition was noticed during the pyrolysis of wood chips, therefore the nitrogen-based reactors are efficient enough for the gas production for the lower thermal history. The water vapour estimated to be 0.0155 kg per unit of dry producer gas generated during the thermal decomposition of pre-treated pine needles pellets. The higher rate of formation of water vapour increases the load on the auxiliary unit, therefore it must be minimized for the proper working of the power plant. The degree of saturation of processed pine pellets was computed to be 31.032%. The cold/ hot gas efficiency of the reactor powered by processed pine needles was increased by 21% when it was compared with the wood chips (Dhaundiyal et al., 2020b). However, the relative change between hot and cold gas efficiencies was marginally very low. The thermal efficiency was found to 85.42%, which is 20.63% higher than that obtained from the hardwood chips (Dhaundiyal et al., 2020b). The gas yield with respect to the wood chip was decreased by an insignificant value of 1.2%. However, the evaluated char yield was nearly 193% higher than that of wood chips (Dhaundiyal et al., 2020b). The pressure drop across the fixed bed was computed to 1.8 Pa-m^{-1}.

Table. 4.7. Thermal parameters related to thermal decomposition of processed pine needle pellets

Parameters	Values
FCR	232 g-h^{-1}
SPR	40590 g-m^{-2}-h^{-1}
SGPR	7.58 m-h^{-1}
τ	3 h
η_t	85.42%
η_c	85.25%
η_h	86%
Char yield	60%
Oil yield	10.48%
Gas yield	12%
ω	0.0155 kg w.v/kg d.a
γ	31.032%
ψ	4.73
$\left(\frac{\Delta P}{L}\right)_b$	1.8 Pa-m^{-1}

4.3.2. Thermal performance of pine cones in a small-scale reactor

The variation in the extensive and intensive properties of the system during thermal decomposition in a fixed bed reactor is shown in Fig. 4.16. Similar to torrefied pine needles, 300 g of processed pine cones pellets were used to run the small-scale reactor at the bed temperature of 700 °C. It was seen that the mass plateau formed during dehydration of water is reduced by 28% when it was compared with wood chips (Dhaundiyal et al., 2020b). Similarly, the devolatilization stage of processed pine cones was shrunken by 79% when it was compared with hardwood chips (Dhaundiyal et al., 2020b). The rate of conversion of processed pine cones at the starting of pyrolysis was reduced by 92.2%. Similar to the torrefied pine needles, thermal immunity in torrefied pine cones were also noticed. Unlike the raw pine cones, the torrefied pine cones were found to be slightly ruptured along their length during the morphological study, which made the heat transport more quickly inside the interior and influences the permeability of the volatile gases. Consequently, it allowed thermal energy to transfer through the char layer to the unreacted portion of the processed pine cones by the conduction, and thus promote the char formation reaction. The drying of processed pine cones was carried out in the temperature interval of 30–113.5 °C with a heating rate of 5 °C-min^{-1}, whereas the devolatilization of the processed pine cones occurred at 133.5–677 °C. The formation of char was taken place at 627–693 °C. The acceleratory phase accompanies the declaratory phase in the temperature profile was occurred due to a change in the pressure and heat of reaction during thermal decomposition of processed pine cones. Owing to condensation of volatile gases at macropores and dilation of grain size had increased the secondary char during pyrolysis of the torrefied pine cones. This could be enhanced if the direction of heat flow with respect to grain orientation is changed.

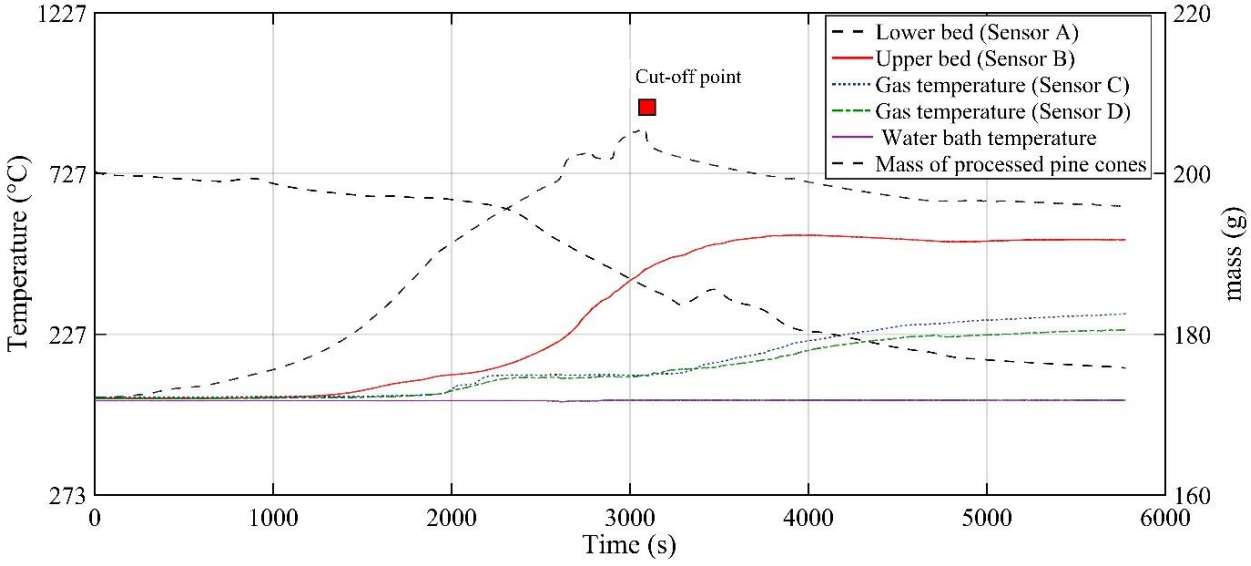

Fig. 4.16. The change in mass and temperature of torrefied pinecone pellets

The change in the pressure inside the fixed-bed reactor was shown in Fig. 4.17. The rate of change of dynamic pressure at the beginning of pyrolysis was estimated to vary from 0.06–0.07 Pa-s^{-1}. The pressure inside the reactor was reduced by 68% at the onset of char formation of processed pine cones. The peak pressure of 954 Pa was obtained at common boundaries of devolatilization and char formation regions. Besides the rapid fluctuation in the pressure of the system, the

phenomenon of surface adsorption was seen at the junction of devolatilization and char formation regions. A sharp drop of 5% was estimated for processed pine cones, which is further reduced by 55.34% as time proceeds. The pressure of volatile gases was found to be elevated by 4.2% once the surface adsorption was faded away with time.

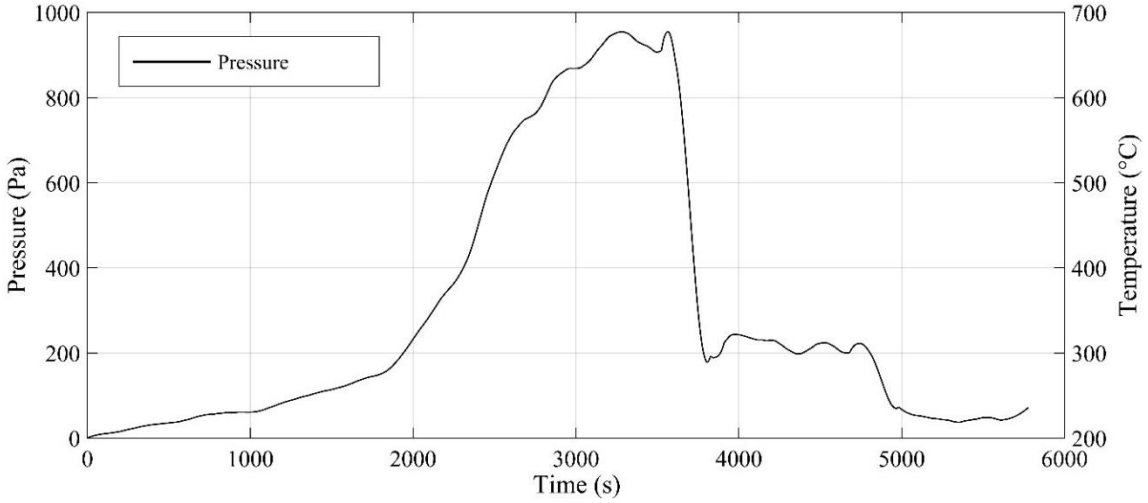

Fig. 4.17. Variation in the pressure of the producer gas generation during pyrolysis of torrefied pinecone pellets

The gas composition obtained after thermal degradation of pine cones is shown in Fig. 4.18. The emission of CO_2 from the processed pine cones pellets was dropped by 20% when it was compared with woodchips (Dhaundiyal et al., 2020b), whereas the percentage of methane in the producer gas was computed to be 6.44% higher than that of wood chips (Dhaundiyal et al., 2020b). The emission of CO and CO_2 from thermally pretreated pine needles was relatively curtailed by 11.61% and 8.17%, respectively, as compared to emission generated by the wood pellets (Dhaundiyal et al., 2021a). Similarly, the two greenhouse gases (CO and CO_2) emission (GHGs) from thermally pretreated pine cones was reduced by 3.6% (CO_2) and 3.74% (CO) as compared to raw pine cones, whereas it was decreased by 20% (CO_2) and 6% (CO) with respect to the unprocessed wood pellets (Dhaundiyal et al., 2021b). The clean gas production by thermally processed pine cones to the commercial wood pellets (Hog fuel) was increased by 6.44% (Dhaundiyal et al., 2021b), whereas it was 10.49% in the case of thermally processed pine needles (Dhaundiyal et al., 2021a). Relatively speaking, the gas content derived from processed pine waste was much cleaner than that of the wood chips and wood pellets. As compared to processed pinecones, a 63% cleaner gas was derived from thermally pretreated pine needles. The reduction in carbon monoxide during the pyrolysis was happened due to the reaction of carbon monoxide with water vapour (WGSR) and forming the carbon dioxide, therefore a sudden rise in CO_2 and hydrogen was noticed during the time interval of 800–900s.

The parameters related to the thermal performance of processed pine cones were tabulated in Table 4.8. The fuel consumption rate (FCR) of processed pine cones was computed to be 127 g-h^{-1}, which was found to be 73% lower than that of hardwood chips (Dhaundiyal et al., 2020b). The char yield derived from processed pine cones was computed to be 48% for the given design of the reactor. A 78% rise in char production was recorded as compared to the wood chips (Dhaundiyal et al., 2020b), whereas the marginal rise of 1.5% over the hardwood chips was seen in the gas yield. The SPR for the given reactor when it was run by processed pine cones was calculated to be

22280 g-m^{-2}-h^{-1}. The reactor running in the presence of nitrogen gas has an SPR of 50000 g-m^{-2}-h^{-1}, which is relatively 124.41% higher than that of a reactor running in the presence of limited air (Dhaundiyal et al., 2020b). The main reason for the drastic variation is the design of the reactor and the effect of forced convection on thermal decomposition. In the same way, the specific gas production of the reactor with processed pine cones was calculated to be 28.19 m-h^{-1}.

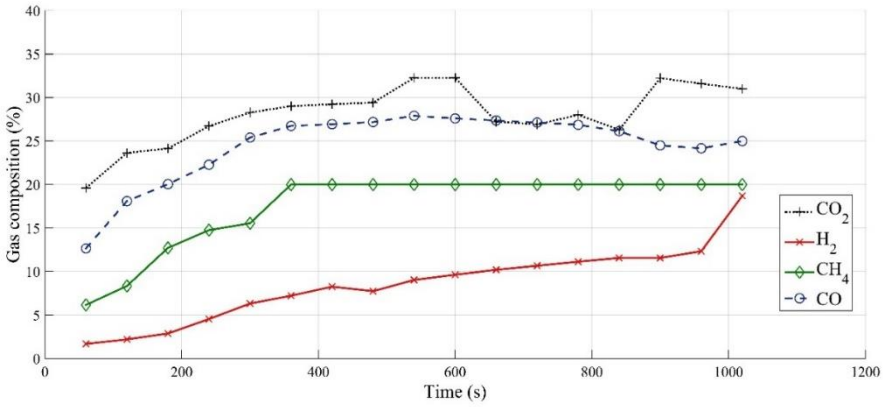

Fig. 4.18. Composition of producer gas derived from torrefied pinecone pellets

The pressure drop across the fixed bed was computed to be 5.30 Pa-m^{-1}. As compared to processed pine needles, the pressure drop across the processed pine cones was found to be 194% higher. The reason is the sphericity (ψ) of pine cones with respect to the processed pine needles pellets was reduced by 79.28%. The thermal efficiency was found to be 5.83% higher than that of processed pine needle pellets. Correspondingly, the cold and hot gas efficiencies of the reactor were estimated to be increased by 6% and 5.3% respectively when it was powered by processed pine cones. Upon comparing it with wood chips, the cold gas efficiency of the rector obtained from processed pine cones was surged by 14.30%, whereas the hot gas efficiency was increased by 6.58%.

Table. 4.8. Thermal parameters related to thermal decomposition of processed pine cones pellets.

Parameters	Values
FCR	127 g-h^{-1}
SPR	22280 g-m^{-2}-h^{-1}
SGPR	28.19 m-h^{-1}
τ	9.8 h
η_t	90.40%
η_c	90.30%
η_h	90.60%
Char yield	48%
Oil yield	13%
Gas yield	36.54%
ω	0.011 kg (w.v)/kg (d.g)
γ	37.73%
ψ	0.98
$\left(\frac{\Delta P}{L}\right)_b$	5.30 Pa-m^{-1}

The water vapour generated during the pyrolysis of processed pine cones was decreased by 29% when it was compared with the processed pine needle pellets. However, the degree of saturation of producer gas was elevated by 19%. The derived char after thermal decomposition of pine waste is shown in Fig. 4.19.

Fig. 4.19. The char derived after pyrolysis of pine waste

4.3.3. Thermo-chemistry of torrefied pine waste

Alongside the macroscopic study of torrefied pine needles pellets in a fixed bed reactor, the milled form of torrefied pine waste was also investigated in a more sophisticated way by a thermogravimetric analyser. Each pine waste milled and torrefied and was subjected to non-isothermal pyrolysis in a thermobalance. The enthalpy of pyrolysis reaction was estimated with the help of a differential thermal analyser.

4.3.3.1. Thermogravimetry of pine needles

Thermogravimetric behaviour of torrefied, as well as raw pine needle samples, was investigated on a microscopic scale in a thermogravimetric (TG) analyser. Each 10 mg sample of torrefied pine needles and its unprocessed form underwent thermal decomposition at the ramp rate of 5 °C-min−1 and 15 °C-min^{-1}, which has been illustrated in Fig. 4.20 (a & b). The heating rate is one of the main factors that influence the pyrolysis stages: dehydration, devolatilization and char formation. These stages can either be dwindled or expanded. There was no remarkable aberration in the mass loss curves noticed at the onset of the pyrolysis process in both the samples, but the domains of devolatilization and the char formation were offset to the right. The residual ash was found to be relatively low when it was compared with raw pine needles, thus it could be implicated from the TG analysis that the torrefaction brought a significant change in the ash content of the pine needles. Pyrolysis at the microscale was conducted for the temperature range of 27–600 °C, and the system was programmed for the linear thermal history. The pyrolysis domains were demarcated in the context of the raw pine needles, whereas other markers show the reduction and expansion percentage in the domain of the torrefied pine needles. The temperature range was shifted towards the right by 2.33% at the onset of devolatilization of the torrefied pine needles, whereas the shift was noticed to marginally low at the starting of char formation. The net devolatilization domain was reduced by 1.21%, whereas a 0.19% of shrinkage was seen in the char formation boundaries. The volatile yield at a low heating rate was estimated to be way too lower than the volatile yield

at a high heating rate. It was noticed that the torrefied pine needle sample offered higher thermal inertia than the raw ones, and thus the inhibition of mass transfer took place. It can be experimentally retrieved that at a higher heating rate the change in the devolatilization regime was quite refined. With the increase in the heating rate from 5 °C-min^{-1} to 15 °C-min^{-1}, it was noticed that the devolatilization zone of the torrefied pine needles was reduced by 6.31% at 15 °C-min^{-1}, whereas the domain of char formation was expanded by 0.6%. It was found from TG analysis that the torrefied sample was thermally more stable and supported the char formation even at higher ramping rates, however, the enthalpy of the system is to be computed so that the impact of torrefaction on the overall change in the heat of reaction in these domains could be seen. The ash fraction of raw pine needles was increased by 19.22% upon increasing the heating rate from 5 °C-min^{-1} to 15 °C-min^{-1}, whereas it was 6.02% for the torrefied pine needles.

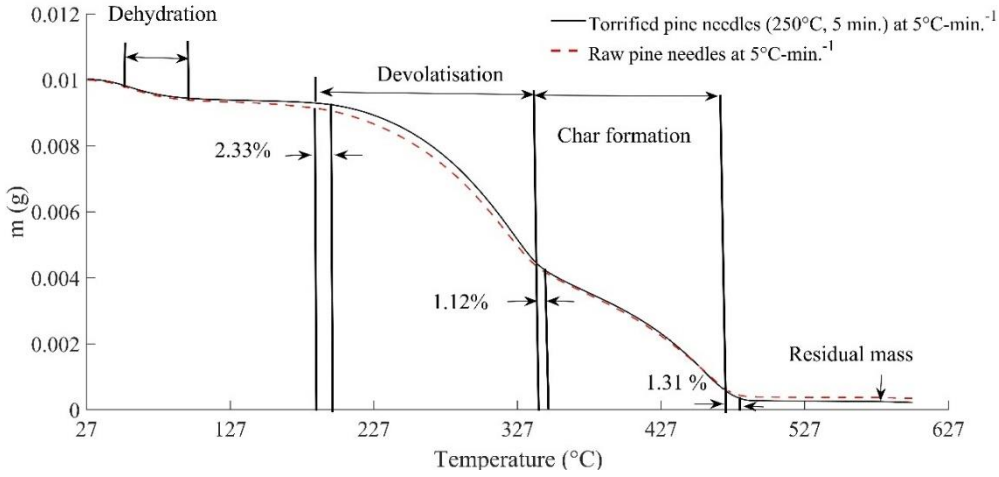

(a)

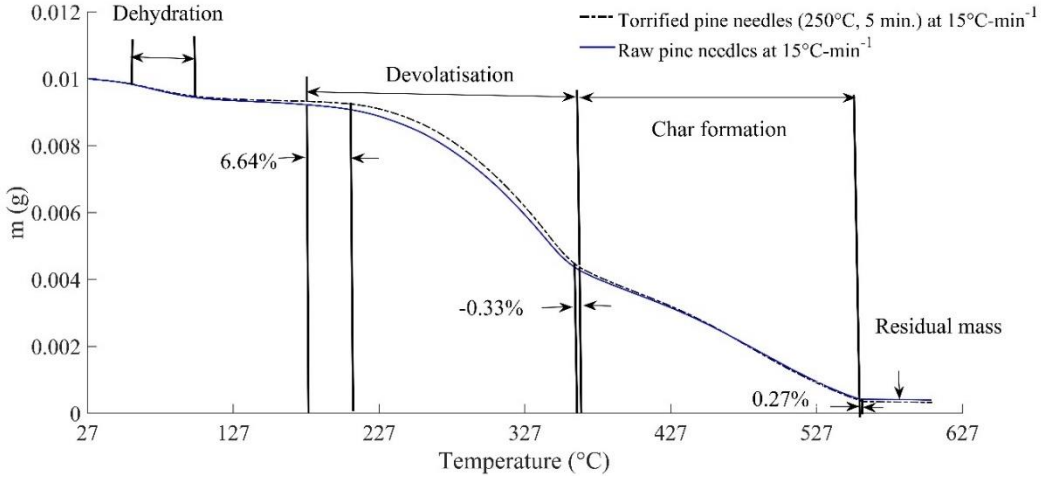

(b)

Fig. 4.20. Thermogravimetric variation in pine needles at different ramp rates (a: 5 °C-min^{-1}, b: 15 °C-min^{-1})

4.3.3.2. Enthalpy of reaction for pine needles

The distribution of heat of reaction among different regimes of pyrolysis at ramp rates of 5 °C-min^{-1} and 15 °C-min^{-1} was derived with the help of DTA curves, which are shown in Fig. 4.21 (a & b). The upward arrows denote the exothermic reactions, whereas the downward direction shows the endothermic heat of the reaction. The area under the curves was estimated by the Monte Carlo scheme (Dhaundiyal et al., 2019b), which vary with the thermal profile of the samples. For the raw pine needles, the first exothermic region was noticed to be stretched from 28.2 °C to 33.2 °C. Similarly, the second and third exothermic peaks were lying in the temperature interval of 250–336.3 °C and 337–601.89 °C, respectively. Between the first and second exothermic domain, the sunken portion denoted the endothermic domain which was estimated to lie in the domain of 33.3–57.2 °C. With the increase in the heating rates, the drifts in terms of heat of reaction and temperature range were seen. The first exothermic peak was noticed to shift by 26 °C, whereas the second and third exothermic regions are offset by 16 °C and −5 °C, respectively. Correspondingly, the change in the voltage is also demarcated in Fig. 4.21, which is proportional to the change in the heat of reaction. The positive sign indicates the rise in temperature (right) and voltage (upward), and conversely, in the case of the negative sign. Concerning raw pine needles, the exothermic heat of reactions (I) and (III) of torrefied pine needles were increased at a low heating rate, whereas the temperature range was noticed to be shifted in the left direction. On the other hand, the voltage gain at the second exothermic region was reduced. However, the overall rise in the heat of reaction was noticed for torrefied pine needles.

Likewise, the higher ramping rates characterised the peak regions of the torrefied pine needles by showing much more ripples in the magnitude of voltage and temperature than that of raw pine needles. Relatively speaking, the endothermic heat of reactions of the torrefied pine needles were seen to be decreased with increasing the heating rates and the magnitude of the exothermic heat of reaction were increased. However, for both the materials, the drop in the heat of reaction (II) (Exothermic) was noticed at the heating rate of 15 °C-min^{-1}, whereas the region (III) of the torrefied pine needles were shrunken in magnitude, which made the overall heat of the system less exothermic than that of the raw pine needles at a heating rate of 5 °C-min^{-1}. The net energy loss during the pyrolysis process takes place to decompose the hydrolysed part of the raw material. The overall capital gain is estimated to vary from 0.1 ¢ to 0.29 ¢ per kg of pine needles if torrefied pine needles are used in place of raw pine needles. The burden on the unit was noticed to be reduced by 64–88% upon using the torrefied pine needles. The enthalpy distribution along with the saving of energy is provided in Table 4.9.

Table. 4.9. The heat of the reaction (ΔH) absorbed or released during thermal decomposition

Reaction Regime	ΔH (kJ-kg^{-1}) Unprocessed pine needles		ΔH (kJ-kg^{-1}) Torrefied pine needles	
	5 °C-min^{-1}	15 °C-min^{-1}	5 °C-min^{-1}	15 °C-min^{-1}
Exothermic (I)	−4.46	−7.508	−4.66	−8.40
Endothermic(I)	2.73	0.408	0.98	0.048
Exothermic (II)	−210	−195.45	−212	−483
Exothermic (III)	−783.52	−706.89	−644.16	−706.33
Net heat of reaction (MJ/kg)	−1.00	−0.91	−0.86	−1.19
Energy saving (%)	0	0	64%	88%

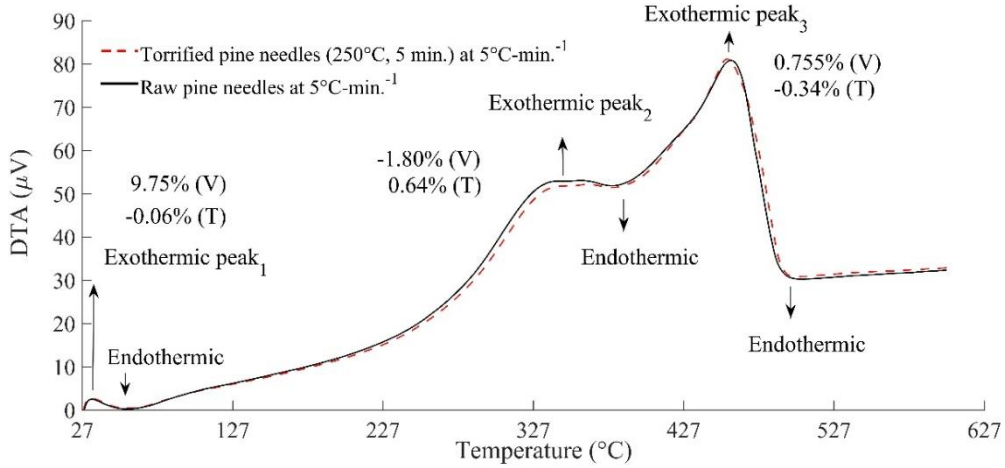

(a)

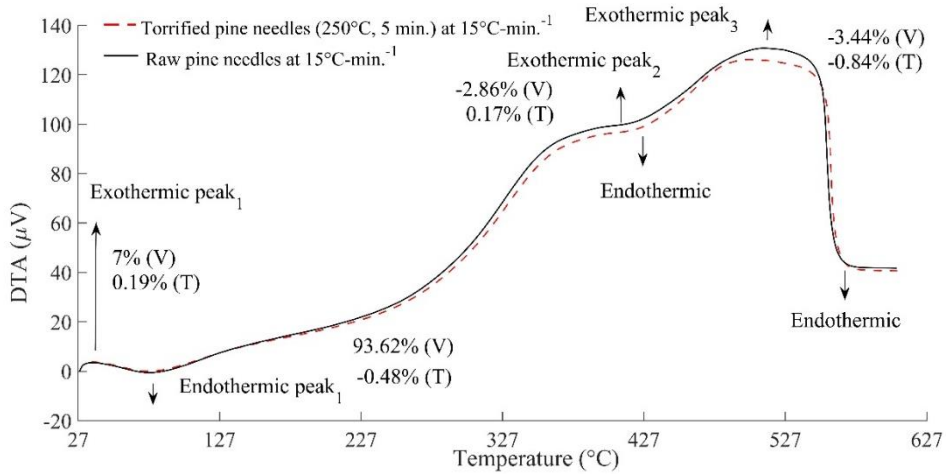

(b)

Fig. 4.21. The change in heat of reaction of pine needles at different heating rates (a: 5 °C-min^{-1}, b: 15 °C-min^{-1})

4.3.3.3. Thermogravimetry of pine cones

Similar to pine needles, the same 10 mg of pine cones samples (torrefied as well as raw pine cones) were examined in a thermogravimetric analyser at a heating rate of 5 °C-min^{-1} and 15 °C-min^{-1}. The thermogravimetric behaviour of both the materials at different ramp rates is depicted in Fig. 4.22 (a & b). At the beginning of the pyrolysis process, the mass plateau of the torrefied pine cones reduced by 28% during the dehydration when it was compared with its raw form. A shift in the temperature interval was also noticed during the same phase. The temperature range required for dehydration of moisture was also reduced by 5.09%. Relatively, the devolatilisation zone in the thermal decomposition of the torrefied pine cones was also reduced by 0.19% at the heating rate of 5 °C- min^{-1}. Similarly, the temperature range of thermal decomposition was also narrowed down by 0.41%. Correspondingly to raw pine cones, a 90.7% of mass loss of the torrefied pine cones was taken place during the char formation, whereas the share was 46% during devolatilization.

A similar trait of thermal immunity was seen in the behaviour of the torrefied pine cones as well. Conversely to the torrefied pine needles, the ash fraction relative to the raw pine cones was also increased by 35% in the torrefied pine cones. Unlike the shrinkage of devolatilization at a lower heating rate, the devolatilization zone of torrefied pine cones was stretched by 58% at a higher heating rate. Consequently, the temperature interval required for char formation was also dilated by 27% as the ramp rate was increased to 15 °C-min^{-1}. The mass loss in the torrefied pine cones was very marginal at a lower heating rate, but with the change in thermal history, the mass reduction rate of pre-treated pine cones exceeded the mass reduction rate of the raw pine cones. The swiftness in the mass loss was found to be 5% higher in the torrefied pine cones than that of the raw pine cones during the release of volatile gases. Correspondingly to the ramp rate of 5 °C-min^{-1}, the char formation at a higher ramping rate was also elevated by 6.6%. As the heating rate increased to 15 °C-min^{-1}, the mass loss gap during dehydration was increased by 33.33%. The mass variation in raw pine cones was found to be 20% higher than that of the torrefied pine cones at a higher ramp rate.

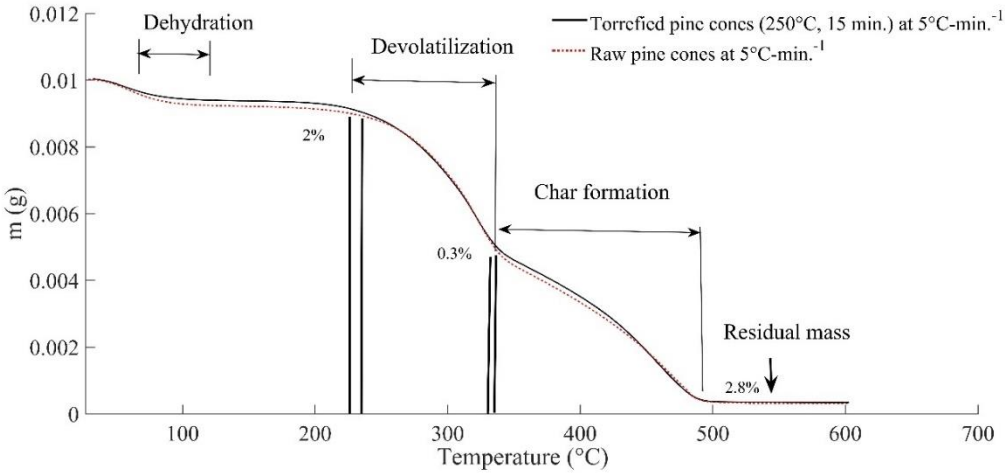

(a)

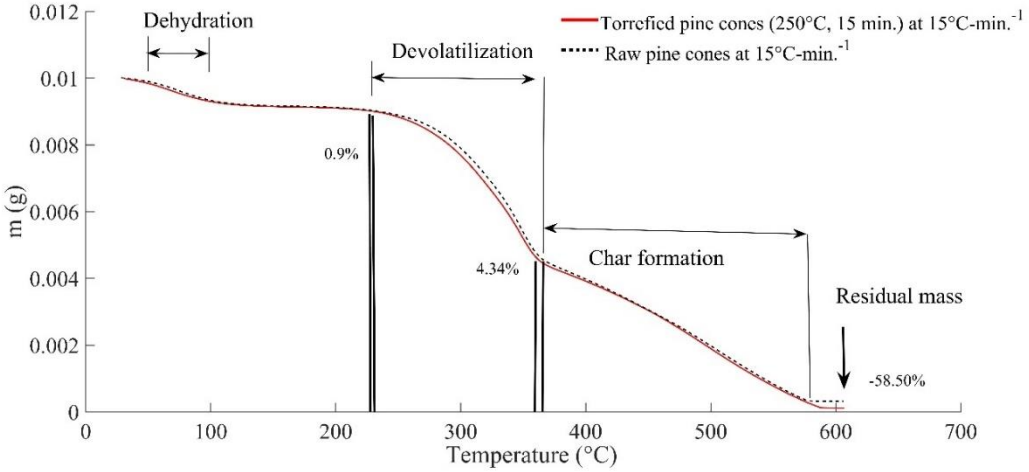

(b)

Fig. 4.22. Thermogravimetric variation in pine cones at the different ramp rates (a: 5 °C-min.$^{-1}$, 15 °C-min.$^{-1}$)

Furthermore, the char formation of raw pine cones was relatively increased at higher heating rates. The mass decomposition during the formation of ash was drastically reduced by 95% in the torrefied pine cones. This could be inferred that the char formation during thermal decomposition of the torrefied pine cones was steadier than that of raw pine cones as the heating rate increased. Conversely, the residual mass was found to be unpredictable since it depends on the extent of char formation.

4.3.3.4. Enthalpy of reaction for pine cones

Differential thermal analysis (DTA) of both the torrefied and raw pine cones at different ramp rates as illustrated in Fig. 4.23 (a & b).

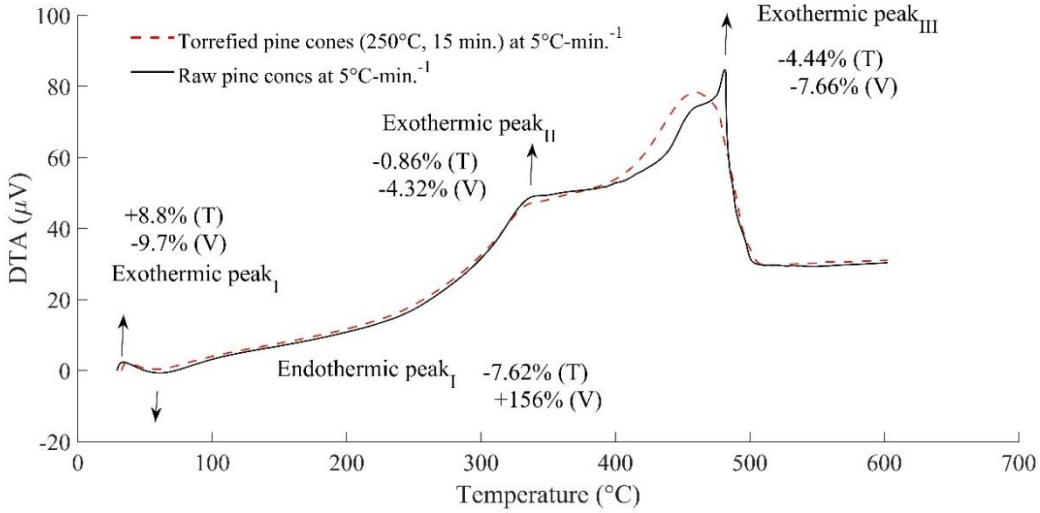

(a)

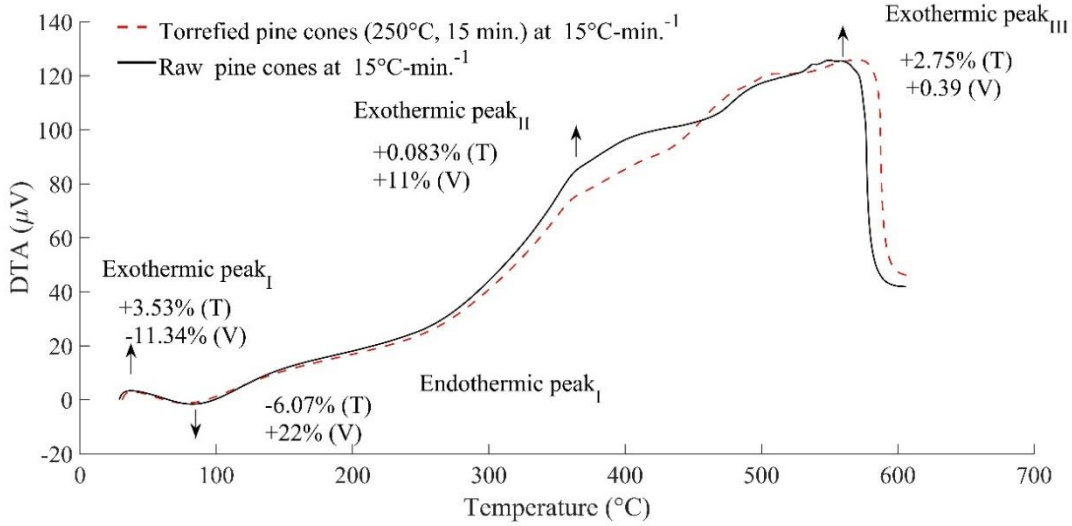

(b)

Fig. 4.23. The change in heat of reaction of pine cones at different heating rates (a: 5 °C-min^{-1}, b: 15 °C-min^{-1})

A similar notation and method were used as mentioned in section 4.3.2.2. The temperature range for the exothermic region (I) was estimated to be 8.8% higher than that of the exothermic region (I) of the raw pine cones. The voltage drop corresponding to the power of the system was computed

to be 9.7% at the onset of pyrolysis. The range of temperature during dehydration of the torrefied pine cones was reduced, which implied that the corresponding heat of reaction (Endothermic) was also mitigated by 7.62% during dehydration of the torrefied pine cones. Similarly, the heat of reaction (Exothermic II) during the release of volatiles was also curtailed by 2.55% in the case of torrefied pine cones. A marginal change of around 0.15% between the heat of reactions of the raw and the torrefied pine cones was noticed as both the materials underwent the char formation at a heating rate of 5 °C-min^{-1}. Likewise, the deviation in the local maxima and minima over a given range of temperature was seen at higher ramping rates. The distribution of heat of reaction among different stages of pyrolysis was found to be disrupted due to the formation of the intermediate products, which resulted in the formation of an additional number of peaks in the given stage. This phenomenon was noticed at 15 °C-min^{-1}. These additional peaks encompassed 12% of the total heat of reaction whilst carrying out pyrolysis of raw pine cones at a higher ramping rate, whereas, in the case of torrefied pine cones, this share was augmented by 19.2% at the same heating rate. The relative variation of temperature range at Endothermic peak I was reduced by 30% as the heating rate increased from 5 °C-min^{-1} to 15 °C-min^{-1}. Similarly, the temperature over which devolatilisation was taken place, was also increased by 34.88–110% with the increase in the heating rate, which was estimated to be 84 to 162% during char formation. The energy released during the charring process to the ambience was found to be 50–52% lesser at 15°C-min^{-1} than that of 5 °C-min^{-1}. The overall heat of reaction was reduced 0.8–32% for the torrefied pine cones, whereas it was 0.6–41% for the raw pine cones. The conclusion can be drawn from this fact that the variation of the reaction heat in the torrefied is lower than that of its raw form. The energy burden on the system was increased at a higher ramping rate.

The heat of reaction obtained during thermal decomposition is provided in Table 4.10. The energy burden during the pyrolysis was curtailed whilst carrying out the thermal decomposition of the torrefied pine cones at a lower heating rate. The torrefaction process had reduced the indirect outlay inflicted to tackle the energy-intensive process. The total saving per kg of fuel was estimated to vary from 0.08 ¢ to 1.5 ¢.

Table. 4.10. The heat of the reaction (ΔH) absorbed or released during thermal decomposition

Reaction Regime	ΔH (kJ-kg^{-1}) Unprocessed pine cones		ΔH (kJ-kg^{-1}) Torrefied pine cones	
	5 °C-min^{-1}	15 °C-min^{-1}	5 °C-min^{-1}	15 °C-min^{-1}
Exothermic (I)	−3.83	−6.74	-	−5.59
Endothermic(I)	1.88	2.36	0.016	1.77
Exothermic (II)	−697.85	−455	−680	−426
Exothermic (III)	−839.26	−450	−838	−412.35
Net heat of reaction (MJ/kg)	−1.54	−0.91	−1.52	−1.04
Energy saving (%)	0	0	99.14%	25%

4.4. Chemical kinetics of thermally processed pine waste

Among the different aspects of torrefaction, the chemical kinetics of pyrolysis reaction also hold the key place. To examine the effect of torrefaction on the reaction scheme and the activation energies of pyrolysis reactions, derivative thermogravimetric (DTG) analysis of the torrefied as

well as raw pine waste was performed. The objective of chemical kinetics to determine the change in the pathway of thermal decomposition reactions.

4.4.1. Chemical kinetics of pine needle

The DTG curve of the torrefied and raw pine needles samples is depicted in Fig. 4.24 (a & b). The active and passive stages of both the materials are demarcated by the global and local minima on the DTG curves drawn at different ramp rates.

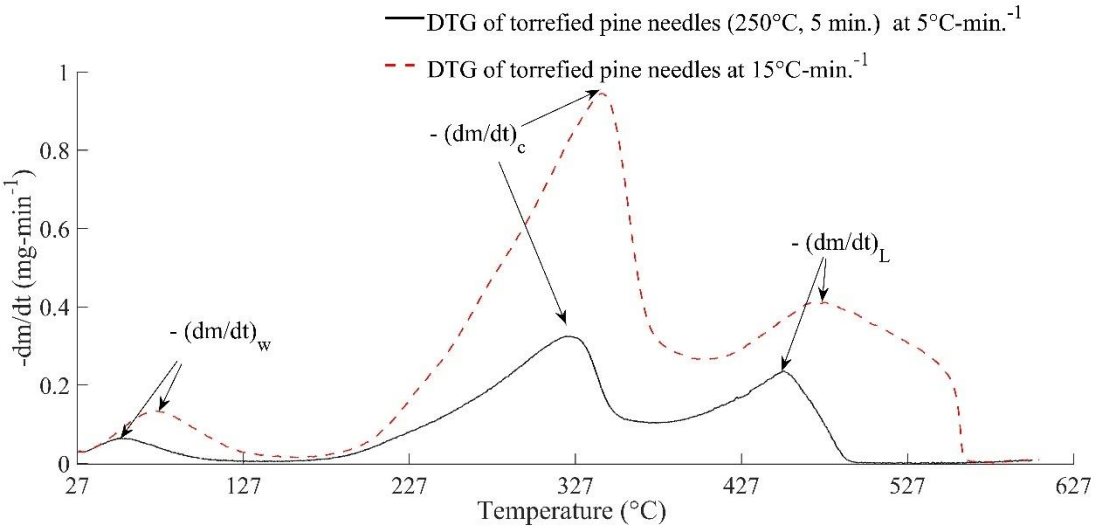

(a)

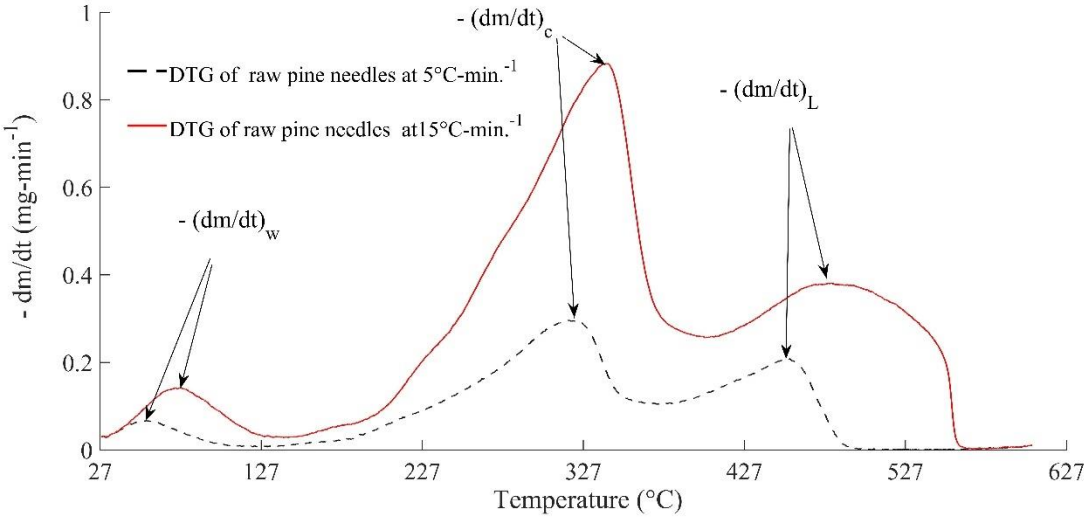

(b)

Fig. 4.24. The DTG curves of pine needles at the heating rates of 5 °C-min^{-1} and 15 °C-min^{-1} (a: Torrefied pine needles, b: raw pine needles)

The rate of mass loss during evaporation of moisture $\left(\frac{dm}{dt}\right)_w$ was taken place at a temperature interval of 54.3–74 °C, whereas the cellulose $\left(\frac{dm}{dt}\right)_c$ was noticed to degrade in a range of 323.4–343.2 °C. The decomposition of lignin was seen to occur during the active as well as passive

pyrolysis, however, the local minimum $\left(\frac{dm}{dt}\right)_L$ was found to be more distinct at 452.6–470.6 °C for the torrefied pine needles. It was evaluated that the temperature range for lignin was relatively stretched as compared to cellulose and hemicellulose, but the rate of mass loss was seen to be more steady and slower than the mass loss that took place during degradation of cellulose and dehydration. It is important to know that the peaks of the hemicellulose decomposition were significantly overlapped with the cellulose peaks for both materials (torrefied and raw form of pine needles). In the case of pre-treated as well as raw pine needles, the decomposition of hemicellulose was taken place simultaneous with cellulose. Consequently, it decomposed alongside cellulose.

Likewise, for the raw pine needles, similar traits in the DTG curves except for the shift in temperature range as well as the magnitude of the rate of decomposition was noticed. Correspond to the temperature range required for dehydration in the torrefied pine needles, a marginal rise of 56–74 °C in the temperature range was estimated for raw pine needles. Furthermore, the mass loss during dehydration of raw pine needles was computed to be 4.45–5.70% higher than the corresponding mass loss of torrefied pine needles. The decomposition of cellulose in raw pine needles was taken place at 318.8–340.9 °C, which was relatively slackened as compared to the torrefied pine needles. Also, the rate of cellulose decomposition in raw pine needles was computed to 6.5–8.8% lower than that of torrefied pine needles. The range of temperature over which the decomposition of lignin took in raw pine needles was 452.8–477.5 °C. The scale of temperature was shifted to the right during the thermal decomposition of lignin. Corresponding to torrefied pine needles, the lignin decomposition was reduced by 7.58–11.76%. It could be inferred from the DTG analysis that the cellulose and lignin decomposition had increased the overall char formation in torrefied pine needles.

The parametric information about pyrolysis of the torrefied and the raw pine needles were tabulated in Table 4.11 and Table 4.12, respectively. Evaluation of kinetic parameters was carried out by using the model-free methods (Kissinger, FWO, KAS). The apparent activation energies estimated during the pyrolysis of the torrefied pine needles by FWO and KAS were 157.08 kJ-mol^{-1} and 160.54 kJ-mol^{-1}, respectively. On the other hand, the derived value was 137 kJ-mol^{-1} by the Kissinger method. Likewise, for raw pine needles, the estimated activation energies by FWO and KAS methods were 155 kJ-mol^{-1} and 158.43 kJ-mol^{-1}. A 1.34% rise in the activation energy of torrefied pine needles was seen whilst determining it from the FWO and KAS methods. The frequency factor (A) derived from FWO, KAS and Kissinger for the torrefied pine needle was 2.95×10^{19} min^{-1}, 4.41×10^{16} min^{-1}, and 2.46×10^{8} min^{-1}, respectively. The derived value of activation energy by the Kissinger method for the torrefied pine needles was found to be 7.3% higher than that of the raw pine needles. This shows that the apparent activation energy estimated at the maximum reaction rate was remarkably high for torrefied pine needles.

Furthermore, the change in the activation energy with the degree of conversion (α) also shown that the reaction mechanism would not be the same throughout the thermal degradation of both the materials.

Table. 4.11. Activation energy and frequency factor derived for the torrefied pine needles

Conversion (α)	FWO			KAS		
	E_a (kJ-mol^{-1})	A (min^{-1})	R^2	E_a (kJ-mol^{-1})	A (min^{-1})	R^2
0.05	69.07	4.17×10^{11}	0.99	69.68	1.43×10^{8}	0.99
0.10	144.83	1.01×10^{17}	0.99	148.23	1.10×10^{14}	0.99
0.15	161.92	1.17×10^{18}	0.99	165.96	1.53×10^{15}	0.99
0.20	175.14	1.07×10^{19}	0.99	179.71	1.27×10^{16}	0.99
0.25	179.64	1.03×10^{19}	0.99	184.33	1.56×10^{16}	0.99
0.30	180.17	5.99×10^{18}	0.99	184.79	8.98×10^{15}	0.99
0.35	178.22	2.30×10^{18}	0.99	182.65	3.31×10^{15}	0.99
0.40	175.24	7.75×10^{17}	0.99	179.43	1.05×10^{15}	0.99
0.45	172.20	2.77×10^{17}	0.99	176.31	3.78×10^{14}	0.99
0.50	171.56	1.70×10^{17}	0.99	176.15	4.18×10^{14}	0.99
0.55	167.78	5.53×10^{16}	0.99	171.37	6.62×10^{13}	0.99
0.60	153.65	1.87×10^{15}	0.99	156.37	1.83×10^{12}	0.99
0.65	139.32	4.92×10^{13}	0.99	141.11	3.79×10^{10}	0.99
0.70	130.47	4.29×10^{12}	1	131.58	2.78×10^{9}	1
Average	157.08	2.95×10^{19}		160.54	4.41×10^{16}	
Kissinger	137	2.46×10^{8}	0.97			

Table. 4.12. Activation energy and frequency factor derived for the raw pine needles

Conversion (α)	FWO			KAS		
	E_a (kJ-mol^{-1})	A (min^{-1})	R^2	E_a (kJ-mol^{-1})	A (min^{-1})	R^2
0.05	74	2.92×10^{12}	1.00	74.98	1.18×10^{9}	1
0.10	149.67	1.53×10^{18}	0.98	153.48	1.90×10^{15}	0.98
0.15	152.58	3.44×10^{17}	0.99	156.26	4.13×10^{14}	0.99
0.20	162.58	1.05×10^{18}	0.99	166.59	1.37×10^{15}	0.99
0.25	173.72	5.27×10^{18}	0.99	178.18	7.64×10^{15}	0.99
0.30	176.07	4.15×10^{18}	0.99	180.05	6.01×10^{15}	0.99
0.35	174.13	1.47×10^{18}	0.99	178.40	2.05×10^{15}	0.99
0.40	172.50	6.33×10^{17}	0.99	176.60	8.49×10^{14}	0.99
0.45	170.36	2.60×10^{17}	0.99	174.26	3.34×10^{14}	0.99
0.50	170.00	1.59×10^{17}	0.99	173.72	2.01×10^{14}	0.99
0.55	170.20	9.79×10^{16}	0.99	174.94	1.40×10^{14}	0.99
0.60	161.03	1.02×10^{16}	1.00	164.19	1.11×10^{13}	1.00
0.65	138.89	5.86×10^{13}	1.00	140.70	4.52×10^{10}	1.00
0.70	124.16	1.72×10^{12}	1.00	125.78	1.23×10^{9}	1.00
Average	155	1.49×10^{18}		158.43	2.09×10^{16}	
Kissinger	127.66	4.21×10^{7}	1.00			

The change in the activation energy to the conversion is shown in Fig.4.25. As compared to the torrefied pine needles, it was noticed that the degree of variation in activation energy of raw pine needles was quite more erratic. On the contrary, a uniform change in the activation energy of the torrefied pine needles was noticed. The reason for the shift in the characteristic peaks in the DTG plot could also be related to the variation in physical and thermal properties of the material, which led to the drastic change in the chemical kinetics of the material.

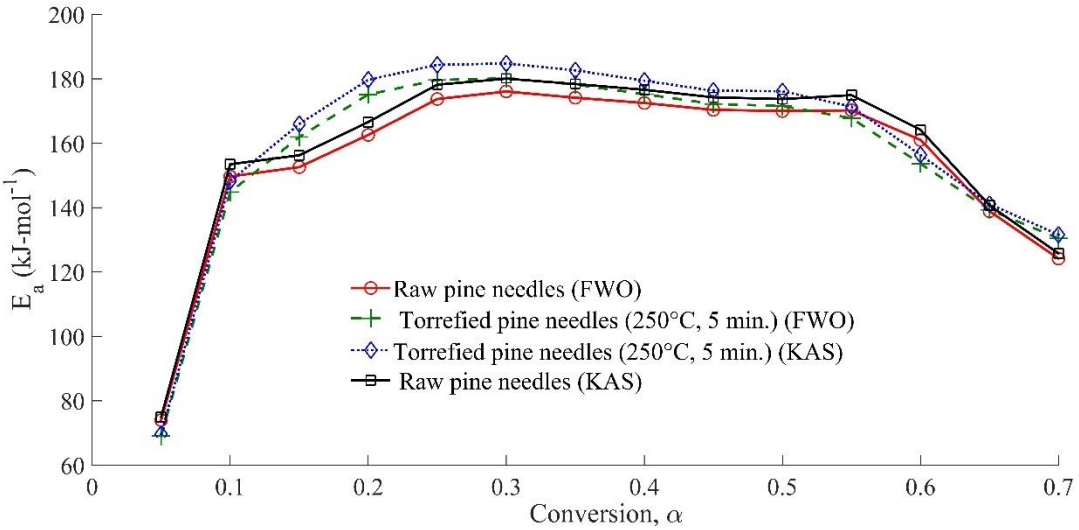

Fig. 4.25. The variation in apparent activation energy of torrefied as well as raw pine needles with the extent of conversion, α

The change in course of the reaction was assessed by the master curves which was based on the first derivative of thermal conversion. The generalised reaction rate for different reaction regime was shown in Fig. 4.26. It was assumed that the $\frac{E}{RT} \rightarrow \infty$, and thus it became easier to make the reaction mechanism independent of the heating rate and it mainly relied on thermal conversion for a given range of temperature. The pattern of variation of the experimental curves for both the material is essentially the same, but the deviation was noticed after the reference point (α = 0.5) of torrefied pine needles.

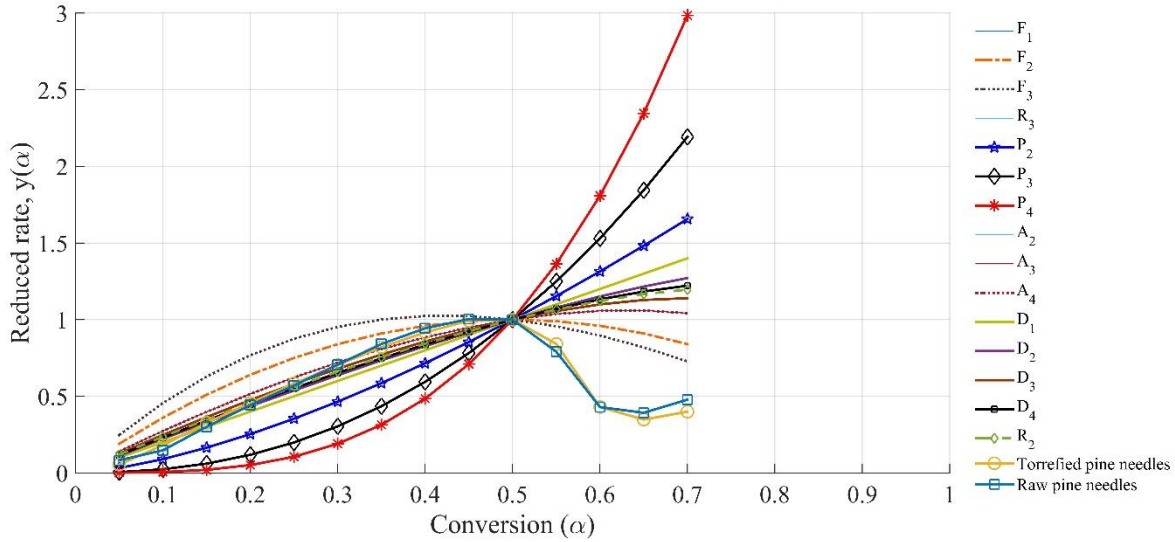

Fig. 4.26. Generalised reduced reaction rate, $y(\alpha)$ for torrefied as well as raw pine needles with the extent of conversion, α

The reference point is the point where all the curves intersect. The generalised rate of reactions marginally deviated until 50% conversion of both the materials. The reaction mechanism was found to be D_1 for pre-treated and raw pine needles till 10% conversion. As the conversion of both materials increases with temperature, the reaction regime was noticed to shifted to the higher order of diffusion reactions D_2. With the further change in conversion from 30% to 50%, the course of

pyrolysis reactions adopted a 'nucleation and growth' regime (A_p) for both the material. In other terms, the system is tending to be more irreversible, and the Gibbs free energy will be maximised. The deviation in the order of nucleation and growth was the only difference seen in both materials. The torrefied pine needles were noticed to be drifted to a higher order of nucleation and growth than the raw pine needles, whereas the pattern was changed after the reference point. The torrefied, as well as raw pine needles, was found to follow the multi-reaction regimes. The reaction regime details are provided in Chapter 3.

4.4.2. Chemical kinetics of pine cones

The DTG analysis of torrefied, as well as raw pine cones, is illustrated in Fig. 4.27 (a & b).

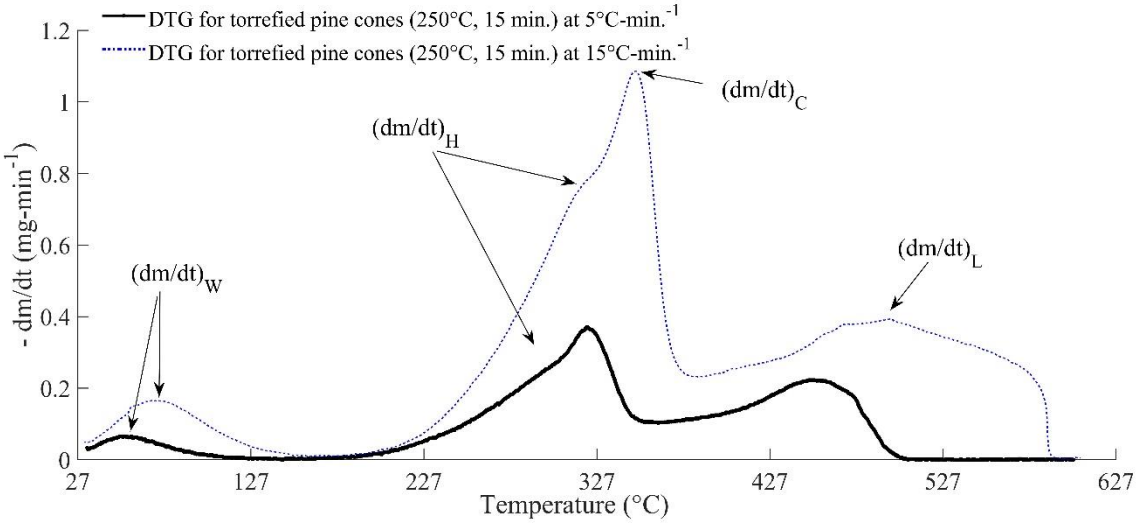

(a)

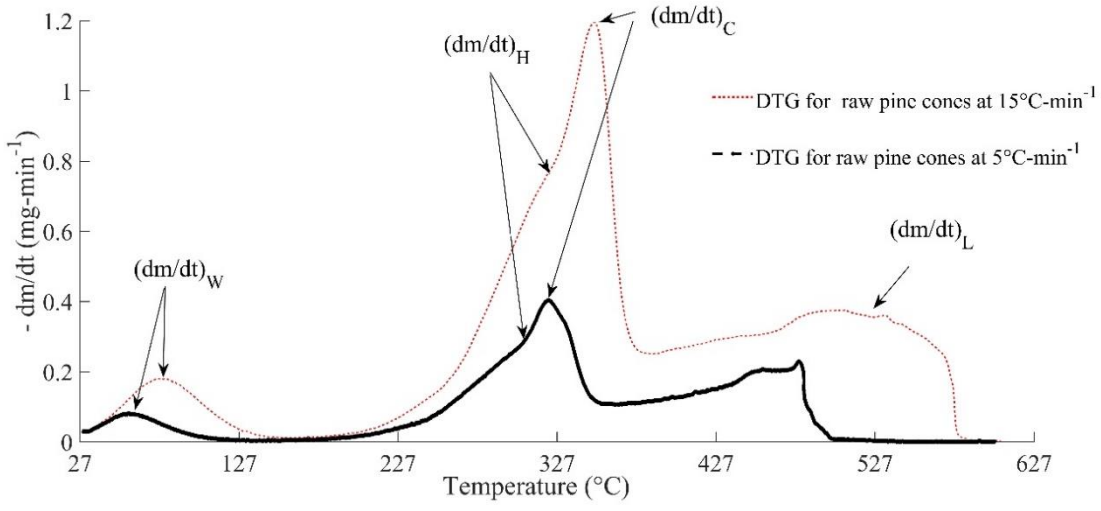

(b)

Fig. 4.27. The DTG curves of raw pine cones at heating rates of 5 and 15 °C-min^{-1} (a: Torrefied pine cones, b: Raw pine cones)

The local minima for the given temperature range indicate the decomposition rates of hemicellulose and lignin, whereas the global minimum denotes the degradation of cellulose. The maximum decomposition rate during dehydration of processed pine cones was taken place at 57.4–72.1 °C. It was seen that the mass loss during the removal of moisture was increased with the increasing heating rate. The relative rise in the mass loss rate due to the elevated heating rate was in the range of 35–92%. The maximum decomposition rate of cellulose was seen to occur at 321.3–350.5 °C, whereas it was 310.5–323.7 °C for hemicellulose, and 454.6–496.4 °C at the maximum decomposition rate of lignin. However, lignin simultaneously decomposes with cellulose and hemicellulose and therefore it also influences the degradation rates of cellulose and hemicellulose during pyrolysis. But its decomposition is more distinct at the end of pyrolysis as cellulose and hemicellulose are exhausted and thus lignin peak becomes easier to demarcate. The lignin decomposition can be characterised by its lower decomposition rate. Thus, it is completely overlapped with the decomposition rates of hemicellulose and cellulose.

The relative change in the maximum decomposition rate of the hemicellulose with the rise in the heating rate is 42–85% for raw pine cones, whereas it was found to be 60–82% and 25–40% for cellulose and lignin, respectively. It also shows that the degradation rate of lignin relative to cellulose and hemicellulose is rather slow and decomposes over a wide range of temperature. The change in mass loss during removal of moisture occurred over 60–78.9 °C, which was noticed to be 0.9–2.9% higher than that of the torrefied pine cones, whereas the mass loss during dehydration was estimated to be 25.1–46.5% higher than that of torrefied pine cones. The mass loss at the onset of pyrolysis was found to be increased with the increasing ramp rate for both torrefied and raw pine cones. Conversely, the temperature range over which cellulose decomposed was insignificantly dilated by 0.016–0.0064% for torrefied pine cones, but the relatively, the decomposition rate was estimated to be dropped by 7.9–9.2%. An insignificant difference between the temperature ranges over which decomposition took place was seen, which was merely 0.08–0.5% higher in the case of torrefied pine cones.

The kinetic parameters were computed by using the model-free methods. The parametric information for torrefied pine and raw pine cones were provided in Table 4.13 and Table 4.14, respectively. The estimated value of activation energy was found to be different for all the methods (KAS, FWO and Kissinger), which shows the occurrence of a complex multi-step mechanism in a solid-state. The average apparent activation energy computed from FWO and KAS methods for torrefied pine cones was 165.87 kJ-mol^{-1} and 169.66 kJ-mol^{-1}, respectively. Similarly, it was estimated to be 121 kJ-mol^{-1} by the Kissinger method. On the opposite, the average value of activation energy derived from integral methods (FWO and KAS) for raw pine cones was reduced by 7.9–8.2%. Correspondingly, a17% drop in activation energy of raw pine cones was estimated from the Kissinger scheme. The obtained value of frequency factor (A) from FWO and KAS for torrefied pine cones was found to be in the range of 1.39×10^{6}– 2.26×10^{21} min^{-1} and 3.28×10^{8}–2.59×10^{21} min^{-1}, respectively. Similarly, the obtained value of A from the Kissinger scheme was 10^{9} min^{-1} for torrefied pine cones and 1.3×10^{10} min^{-1} for raw pine cones. The variation in the Arrhenius parameters happened due to the variation in the reactivity of the major constituents of the pine cones. The change in activation energy to conversion is shown in Fig. 4.28. It was seen that the apparent activation energy was not the same for each method, and it indicated that there was no reaction mechanism able to portray the thermal decomposition of torrefied and raw pine

cones. The pattern of variation was found to be similar, although the quantitative distinctions were observed.

Table. 4.13. Activation energy and frequency factor derived for the torrefied pine cones

Conversion (α)	FWO			KAS		
	E_a (kJ-mol^{-1})	A (min^{-1})	R^2	E_a (kJ-mol^{-1})	A (min^{-1})	R^2
0.05	68.31	1.39×10^{6}	1.00	68.97	6.65×10^{11}	1
0.10	209.67	1.00×10^{19}	0.98	216.41	6.51×10^{25}	0.98
0.15	197.86	2.26×10^{21}	0.99	203.67	4.23×10^{15}	0.99
0.20	182.81	1.71×10^{19}	0.99	187.70	5.77×10^{14}	0.99
0.25	179.74	5.75×10^{18}	0.99	184.38	2.10×10^{14}	0.99
0.30	179.37	3.00×10^{18}	0.99	183.87	9.30×10^{13}	0.99
0.35	177.01	1.13×10^{18}	0.99	181.30	2.18×10^{13}	0.99
0.40	167.76	1.14×10^{17}	0.99	171.50	3.69×10^{12}	0.99
0.45	163.33	3.40×10^{16}	0.99	166.78	1.86×10^{12}	0.99
0.50	172.04	1.44×10^{17}	0.99	175.87	4.67×10^{12}	0.99
0.55	207.38	9.10×10^{19}	0.99	212.95	9.13×10^{12}	0.99
0.60	171.85	2.54×10^{16}	1.00	175.36	2.52×10^{10}	1.00
0.65	132.14	6.23×10^{12}	1.00	133.37	4.62×10^{8}	1.00
0.70	112.99	1.17×10^{11}	1.00	113.04	4.99×10^{7}	1.00
Average	165.87	1.83×10^{20}	-	169.66	1.85×10^{20}	-
Kissinger	121	1.00×10^{9}	1.00			

Table. 4.14. Activation energy and frequency factor derived for the raw pine cones

Conversion (α)	FWO			KAS		
	E_a (kJ-mol^{-1})	A (min^{-1})	R^2	E_a (kJ-mol^{-1})	A (min^{-1})	R^2
0.05	82.54	1.30×10^{15}	1.00	83.94	6.65×10^{11}	1
0.10	247.06	1.97×10^{28}	0.98	255.8	6.51×10^{25}	0.98
0.15	170.30	2.98×10^{18}	0.99	174.67	4.23×10^{15}	0.99
0.20	166.23	4.42×10^{17}	0.99	170.23	5.77×10^{14}	0.99
0.25	164.64	1.69×10^{17}	0.99	168.43	2.10×10^{14}	0.99
0.30	163.20	7.73×10^{16}	0.99	166.84	9.30×10^{13}	0.99
0.35	158.46	1.95×10^{16}	0.99	161.78	2.18×10^{13}	0.99
0.40	151.72	3.67×10^{15}	0.99	154.62	3.69×10^{12}	0.99
0.45	149.63	1.93×10^{15}	0.99	152.35	1.86×10^{12}	0.99
0.50	155.06	4.55×10^{15}	0.99	158.02	4.67×10^{12}	0.99
0.55	160.04	8.48×10^{15}	0.99	163.18	9.13×10^{12}	0.99
0.60	136.00	3.38×10^{13}	1.00	137.68	2.52×10^{10}	1.00
0.65	120.19	8.29×10^{11}	1.00	120.86	4.62×10^{8}	1.00
0.70	111.90	1.08×10^{11}	1.00	111.91	4.99×10^{7}	1.00
Average	152.64	1.41×10^{27}		155.74	4.65×10^{24}	
Kissinger	100.41	1.3×10^{10}	0.98			

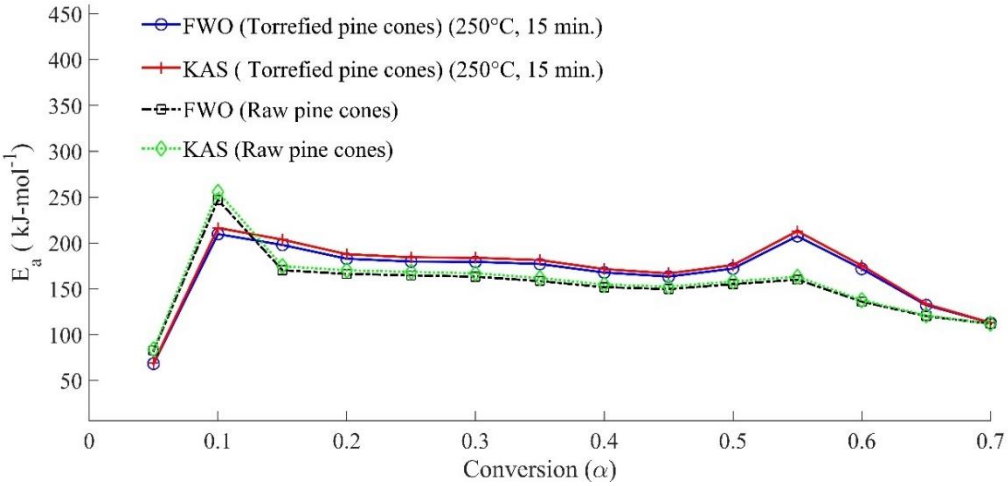

Fig. 4.28. The variation in apparent activation energy of torrefied as well as raw pine cones with the extent of conversion, α

To determine the reaction mechanism of torrefied as well as raw pine cones, a master plot was drawn, which is illustrated in Fig. 4.29. The trend of the experimental curve was found to be similar for both materials, but the exponential deviation was noticed. Unlike the pine needles, the pathway of pyrolysis reactions in the pine cones was found to follow a complex multi-step reaction mechanism from the beginning of the pyrolysis. It was found that until 10% of conversion, torrefied and raw pine cones followed the power-law regime (P_n). The only difference between reaction regimes of materials was that the torrefied pine cones were more inclined to the lower order of reactions than the raw pine cones. Within 20–30%, the reaction regime was noticed to shifted from P_n to the diffusion-reaction regime (D_n). It was noticed that pretreated pine cones supported higher order of diffusion reactions. Though diffusion-reaction would follow by nucleation and grow regime at the same time. During 30 to 50% conversion of both the material, the reaction mechanism again shifted to sigmoidal reactions (F_n). So, it is clear that the decomposition of pine cones and pine needles have a similar complex multi-step reaction characteristic. It is a different matter that the variabilities in reaction regime were found to be least in pine needles and it was predominately following the diffusion reactions.

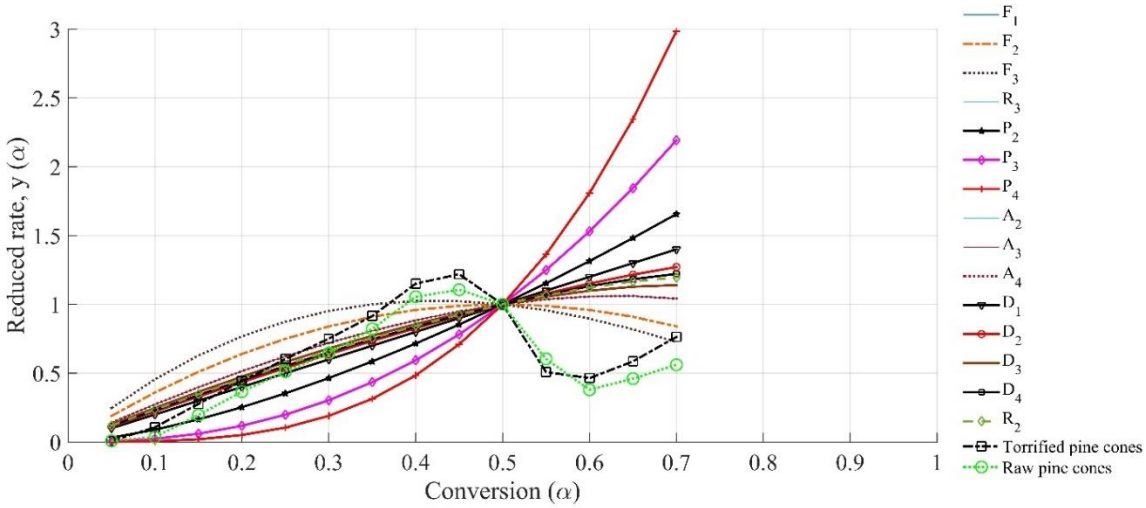

Fig. 4.29. The generalised reduced reaction rate for torrefied as well as raw pine cones with the extent of conversion, α

4.5. Energy distribution and economic feasibility of the pre-treatment process

Torrefaction and its implication related to economic development can be estimated by predicting the net profit a pyrolysis unit can provide at the end of the operation. Here, merely, the energy distribution and incentives that could be earned from the obtained is studied.

4.5.1. Energy allocation of end products derived from pine needles

The energy required to enrich the raw pine needles was assessed by the overall cost of production. The recorded data based on energy load is provided in Table 4.15. A marginal rise in power consumption was seen during milling the raw pine needles with a sieve size of 1.05 mm. Apart from milling, a steep change in power consumption was observed whilst the densification process was carried out. This happened due to a change in friction loss and pressure during pushing the material across the ring die. The energy quota of 49.4% was exhausted during pelletisation, whereas the quasi-static torrefaction required merely 14% of the total energy for thermal pre-treatment of pine needles pellets. The energy needed for pyrolysis of torrefied pine needles was found to be 25% of the total energy quota, which was found to be 52% lower than the required energy for processing wood chips (Dhaundiyal et al., 2020b). The overall cost of production for processing pine pellets was estimated to be 2.8¢ per kg of raw pine needles, whereas it was around 7.8¢ per kg for wood chips (Dhaundiyal et al., 2020b). On the other hand, the char production through torrefied pine was found to be 122% higher than that of the hardwood chips (Dhaundiyal et al., 2020b). The market value of char was decided according to the Hungarian energy market (UNComtrade, 2020). So, the overall benefit of $1.01 was estimated per kg of torrefied pine needles pellets. However, the assumed price of charcoal could have bull-and-bear in the energy market, therefore it was quoted as an expected cost. The energy distribution for the torrefied pine pellets was estimated by the Sankey diagram, which is illustrated in Fig. 4.30. The net gain from the torrefied pine pellets came from char production. The energy budget of 79.5% were retrieved from the charcoal, whereas it was 15.9% for gas, and 13.9% for oil, respectively. In the context of the thermal potential of produced char, the estimated energy content is 40% higher than that of wood chips (Dhaundiyal et al., 2020b).

Table 4.15. Power distribution during preparation and processing of the raw pine needles pellets

Parameters	Milling (Sieve ϕ = 1.5 mm)	Pelletisation	Torrefaction	Pyrolysis	Cost ($)	Expected Revenue
Actual Power	0.21 kW	0.95 kW	0.28 kW	0.48 kW	0.28	$ 1.01
Voltage	389.59 V	393.69 V	230 V	174 V	-	
Power factor	0.23	0.18	1	1	-	
Mass	8.75 kg	8.14 kg	7.5 kg	-	-	
Power % share	11%	49.4%	14%	25%	-	
η_p	87.5%	93.11%	93%	-	-	

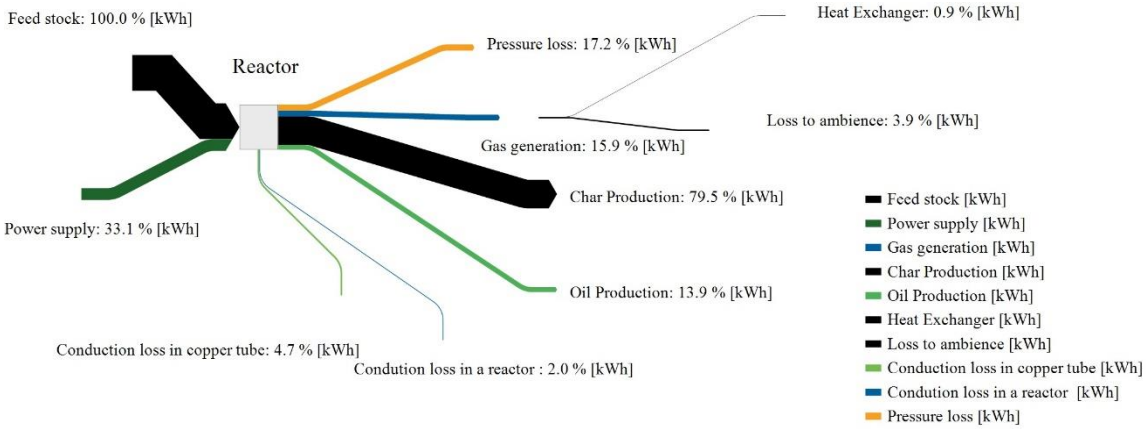

Fig. 4.30. Energy distribution across the pyrolysis reactor for torrefied pine needles pellets

4.5.2. Energy allocation of end products derived from pine cones

The energy utilisation at different processes conducted on raw pin cones is provided in Table 4.15. The compacting process was noticed to drained the major amount of energy, whereas the quasi-static torrefaction through the Joule heating system imbibed a 2.4% share of the total energy budget. The energy involved in milling raw pine cones was found to be 64% lower than the energy spent during the densification process. The energy required for the thermal decomposition of processed pine cones was reduced by 54% when it was compared with the wood chips (Dhaundiyal et al., 2020b). The process efficiency during the preparation of raw pine cones was estimated to be 53%, whereas the pre-treatment process had shown the highest efficiency of 97%. The char gain over wood chip was estimated to be 78%, which could bag an incentive of 20 ¢. The rise in the power consumption during the milling process primarily caused by a higher percentage of moisture content in raw pine cones. Likewise, the Sankey plot for the torrefied pine cones is shown in Fig. 4.31. The energy quota of pine cones was remarkably shifted to the charring process. The net thermal energy of charcoal obtained from pine cones was found to be 173% higher than that of the hardwood chips (Dhaundiyal et al., 2020b). Correspondingly, the energy share of producer gas was also enhanced by 19% when it was compared with the gas production capacity of the hardwood chips (Dhaundiyal et al., 2020b). The net thermal energy loss was noticed 96% lesser than that of hardwood chips.

Table 4.16. Power distribution during preparation and processing of the raw pine cones pellets

Parameters	Milling (Sieve ϕ = 1.5 mm)	Pelletisation	Torrefaction	Pyrolysis	Cost ($)	Expected Revenue
Actual Power	0.52 kW	1.46 kW	0.06 kW	0.46 kW	0.37	$ 0.20
Voltage	387.91 V	391.25 V	230 V	142 V	-	
Power factor	0.37	0.26	1	1	-	
Mass Input	7.5 kg	4 kg	3.12 kg	-	-	
Power % share	21%	58.4%	2.4%	18.4%	-	
η_p	53%	78%	97%	-	-	

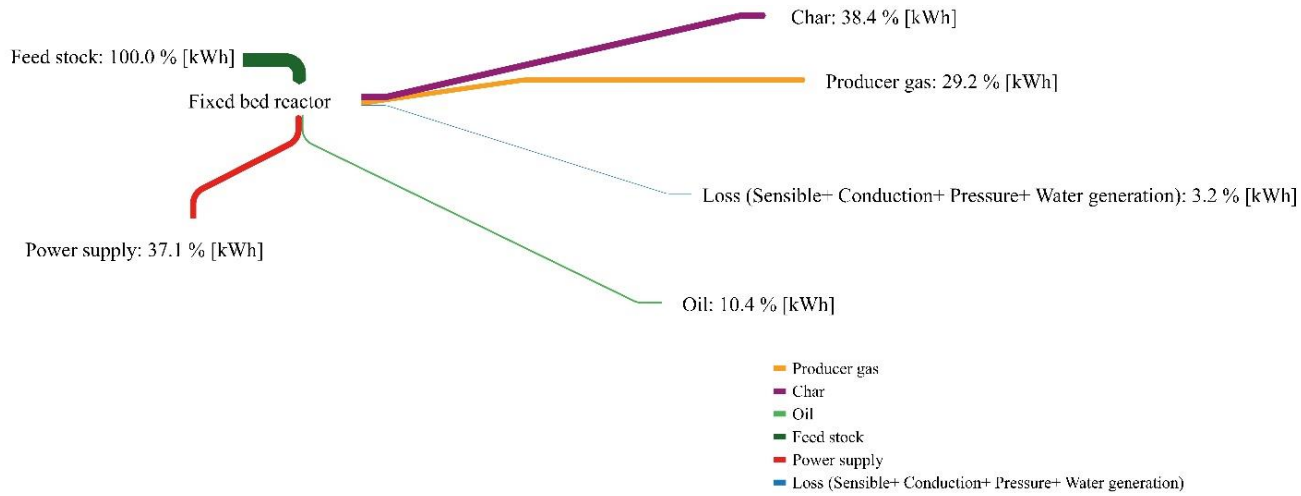

Fig. 4.31. Energy distribution across the pyrolysis reactor for torrefied pinecone pellets

4.6. Validation of experimental results

The obtained solution at different aspects of torrefaction was compared to determine whether it was in good agreement with the literature or not. But before that, the reliability of experimental work on the pyrolysis reactor was determined with the help of standard error of measurement. The reliability of any data vacillates in the interval of [0, 1]. The reliability of data at a different point is tabulated in Table 4.17. It could be seen that the reliability of pyrolysis in the small-scale reactor was found to vary from 0.76–0.99 for torrefied pine cones pellets, whereas it was noticed to be far more consistent for the torrefied pine needles pellets.

Table 4.17. Reliability of the obtained experimental value

Parameters		T_A (°C)	T_B (°C)	T_C (°C)	T_D (°C)	P (Pa)	Mass (kg)
Reliability	Torrefied pine cones	0.98	0.98	0.99	0.97	0.76	0.99
	Torrefied pine needles	0.99	0.99	0.98	0.99	0.99	0.99

Torrefaction of eucalyptus wood and bark was carried out and it was found that the molar of H/C and O/C was decreased with increasing torrefaction temperature (Almeida et al., 2010). Similarly, whilst conducting experiments on the herbaceous residue, Liquorice, and it was noticed that the oxygen content was decreased within 210–240 °C (Xin et al., 2018). Similarly, the torrefaction of rice husk led to a reduction in the volatile content and a rise in fixed carbon of material (Chen et al., 2018). With the increase in carbon content, it was noticed that the calorific value of the agricultural bagasse was increased (Pach, 2002). The torrefaction of beech wood made the heat of reactions less endothermic (Strandberg, 2015). Upon drawing a comparative scale, a similar trend was found whilst performing torrefaction on pine waste. However, the quantitative difference is indispensable since the technique and methodology are completely different. The obtained experimental results completely complied with the literature review and the recent research have been made in the last 10 years.

4.7. New scientific results

The torrefaction process on the pine waste was exhaustively investigated and the various elements were highlighted in the different sub-heading. The following points were found to be noteworthy:

1. Physico-chemical analysis

According to physical and chemical evaluation, I observed that it was not necessary that the hydrogen and oxygen would simultaneously decrease with increasing torrefaction temperature. So far, it was reported in the literature that both hydrogen and oxygen would decrease, but to what extent a fall takes place. I evaluated that the higher thermal history would only allow the hydrogen molecules to disintegrate from the structure. In fact, on the contrary, in some cases, the overall hydrogen fraction would increase and only oxygen would be driven off the structure. I noticed that the different material would showcase anomaly in the elemental behaviour. I had investigated that the material with higher volatile content could not withstand a higher duration of processing and mass yield drop would be phenomenal. Comparatively, I noticed that pine cones would support temperature orientated torrefaction, whereas the leaf part, pine needles, would largely rely on torrefaction time. I ferreted out the fact that both time and temperature would govern the thermal event associated with the torrefaction process. The ash content would increase with increasing both time and temperature for pine cones. On the other hand, it would only decrease with increasing torrefaction temperature and reducing the processing period. The calorific value for pine needles would only be increased if torrefaction is conducted for a higher temperature regime, whilst it is governed by the processing period in pine cones.

2. Morphological investigation of pine waste

I noticed that the grain shifting, dilation of boundaries and the propagation of surface cracks were predominant on both pine needles and pine cones, which changed the heating characteristic of torrefied pine waste and influence the char yield upon pyrolysis. I found the dilation of grain boundary would increase the residence time of volatile gas and support the intermolecular condensation reaction that ultimately impacts the char formation reaction. With the change in the heating characteristic, the pressure-driven flow is reduced, and intra-particle residence time is increased, which finally encourage condensation reaction and char formation. To confirm this finding, I compared the results with G50 chips, and I noticed that the pressure was continuously rising from 10 Pa to 30 Pa during the devolatilisation phase, whilst it was not true in the case of torrefied pine waste. It was decreased from 100 Pa to 0 Pa during the devolatilisation of torrefied pine waste. Thus, I confirmed that the condensation reaction would take a lead. The structural defect would bear upon the alternation in the reaction pathway.

3. Thermo-economic analysis of pine waste

I investigated that thermal decomposition of thermally pre-treated pine waste (unconventional biomass) mitigated emission of CO_2 by 8.17–20% and CO by 6–11.61% as compared to the commercial wood pellets (conventional biomass). Similarly, the clean energy production was increased by 6.44–10.49% after thermal pretreatment of pine waste. After the torrefaction process, I found that the loose biomass generated 63% much cleaner energy than the commercial wood pellets. I confirmed that the major emission reduction was during the water-gas shift reactions. I noticed the catalytic effect of flying ash, which ultimately bolstered the methanation of products of WGSR. I also found that the overall financial gain would be highest with those materials which

have higher volatile content and the least processing cost. The percentage of CH_4 was significantly increased while carrying out the thermal decomposition of pre-treated pine cones and pine needles in a pilot-scale reactor. The drop in carbon emission and improvement in methane content showed that the torrefaction process provided a clean and less polluted source of energy. The torrefied pine needle pellets were seen to be lesser energy-intensive than that of torrefied pine cones. I estimated the relative financial incentive obtained from torrefied pine cones could be 81.83% lower than that of torrefied pine needles. Furthermore, I also observed that the processing of torrefied pine needles would be 30.20% lesser energy-intensive than that of torrefied pinecones. During the milling process, I noticed that the loose biomass, pine needles, would be 60% lesser energy-drain process than the solid biomass, pine cones. On the other hand, pelletisation of loose biomass would relatively require 35% less energy as compared to solid biomass. As compared to the commercial wood pellets, the electrical energy required by the pine waste was decreased by 11–21%. I estimated that the expected revenue generation from the pine waste char over the commercial biomass was $0.31–1.37.

4. Thermochemistry of the torrefied pine waste

I validated via the microscopic analysis that the shift in energy balancing would be predominant, and I had noticed that the torrefied pine waste would be more exothermic in nature than its raw form. A torrefied material derived from a highly volatile material, such as pine leaves, would have a higher heat of reaction if they are decomposed at a higher ramping rate, whilst the torrefaction of hard material, pine cones, would be more exothermic at a lower ramping rate than higher ramping rate. It happened due to a change in the grain orientation of pine waste upon torrefaction. I had seen that the lower heating rate in torrefied pine cones increased the residence time of volatile. Consequently, it triggered the autocatalytic reactions which are highly exothermic in nature.

5. Chemical kinetics of torrefied pine waste

I had seen that the multi-step reaction mechanism was followed by both the material. Pyrolysis of torrefied pine needles was shifted to higher-order diffusion-reaction along with nucleation and growth reaction regime. Unlike torrefied pine needles, torrefied pine cones were found to have more drastic variation in the reaction pathway. The higher-order power law, followed by higher orders of diffusion, nucleation and growth, and sigmoidal regimes would be the sequence of pyrolysis reaction in the torrefied pine cones. The nucleation was found to be more predominant in torrefied pine needles than that of torrefied pine cones, which eventually influenced the activation energies of the reaction.

5. CONCLUSION AND SUGGESTIONS

It was found that torrefied pine waste, pine cones and pine needles, had a severe impact on their physical, chemical and morphological characteristics. The time and temperature played a pivotal role to determine the calorific content of the torrefied pine waste. The torrefaction duration was found to have a phenomenal impact on the ash content and mass yield of torrefied pine needles, whereas temperature played a major role to decide the optimum energy yield. Alongside loose biomass, pine needles, a hard form of biomass was also torrefied. The torrefaction temperature was seen to have a hegemony over torrefaction duration when the constant sample of raw pine cones was thermally processed at 210–250 °C. Conversely, the ash content, the mass yield was found to be affected by both the operating time and temperature. Unlike, the torrefied pine needles, the energy yield was influenced by the duration of processing rather than torrefaction temperature. It can be suggested that time and temperature must go hand-in-hand whilst performing thermal pre-treatment. The physical properties of material influence the torrefaction, therefore mechanical properties must be taken into consideration whilst processing the material.

From the relative morphological study of pine needles, the longitudinal cracks of around 8.08–20.77 μm were formed after the torrefaction. The microfibrils were found to be disintegrated into small splinters. The pore size was dilated by 2.82–9.65 μm. The grain orientation was changed by 17° to 123°. The dilation of surface area was also noticed. Similarly, in torrefied pine cones, the holes of cellulose microfibrils of raw pine cones were stretched by 198.5%. The fissures of around 1.47–10.43 μm were formed between the grain boundaries of pine cones. The orientation of grain was deviated by 28–47°. Relatively speaking, the orientation of grain would impact the heating fluxes and the heat of reaction. Therefore, the structural changes are essential to examine before performing thermal decomposition in a pyrolysis reactor. It could be suggested that the effect of residence time with grain orientation would fortify the fact that the torrefaction also influences the energy balancing during the thermochemical processes.

As compared to commercial wood pellets, the emission of CO_2 from torrefied pine needles and pine cones pellets was estimated to be dropped by 8.17% and 20%, respectively, and the methane gas percentage was increased by 6.44–10.49%. It was noticed that CO_2 and CO were saturated as the hydrogen gas was elevated. Similarly, the methane obtained from torrefied pine cones was reduced by 70% when it was compared with the torrefied pine needle pellets. The consumption rate of torrefied pine pellets was computed to be 232 g-h^{-1}, which was noticed to 83% higher than that of torrefied pine cones. The water generation per kg of the dry gas was found to be 41% higher with the torrefied pine needles pellets than that of the torrefied pine cones. The net exothermic heat of reaction for torrefied pine needles at a ramp rate of 5 °C-min^{-1} was decreased by 43% when it was compared with torrefied pine cones, whereas a 14% rise in exothermic heat of reaction was recorded as the ramp rate was increased to 15 °C-min^{-1}. The net endothermic heat of reaction for the torrefied pine cones was reduced by 98% as compared to the torrefied pine cones at a heating rate of 5 °C-min^{-1}, whereas it was reduced by 97% for the torrefied pine needles with the increase in the heating rate to 15 °C-min^{-1}. The net energy saving for torrefied pine needles was found to be decreased by 35% at lower heating, whereas it was surged by 252% at a higher heating rate. It can be concluded that the higher thermal history is favourable for torrefied pine needles, whereas the torrefied pine cones support a lower thermal profile for pyrolysis.

6. SUMMARY

PRE-TREATED PINE WASTE AS AN ALTERNATIVE ENERGY SOURCE

A comprehensive as well as qualitative analysis of one of biomass processing technologies, torrefaction, was carried out with the help of the quasi-static technique. Unlike the predominant studies carried out on the micro-wave oven, this work was performed on the joule heating system, where the existing furnace was improvised to serve the desired purpose. The objective of the study to determine the effect of operating condition on the torrefaction process. It was found in the study that the physical characteristic of biomass influenced the mass and energy yield of the torrefied materials. The material used in this study is different in physical structure. It was a combination of loose biomass and regular biomass. The effect of time and temperature on the elemental composition, molar ratio of H/C and O/C was found to be different. A breakthrough finding in the context of physiochemical analysis emphasises that it is not essential that hydrogen and oxygen would simultaneously decrease with a rise in processing temperature. The thermal events that took place at higher thermal history would only allow the hydrogen molecules to break apart from the structure. The material with higher volatile content cannot withstand higher torrefaction temperature, and thus, the loss of mass would be remarkably high. The ash content was noticed to be decreased with increasing torrefaction temperature for torrefied pine needles when torrefaction was done for a shorter duration. Conversely, the simultaneous increase in time and temperature increased the ash content for raw pine cones.

According to structural analysis, surface cracks, dilation of grain boundary, the change in grain orientation was taken place for both pine needles and pine cones. As a result of morphological distortion, the heating trait of the torrefied pine waste was also changed, which consequently, influenced the char formation. The dilation of grain boundary increased the residence time of volatile gas in a solid matrix and supported the intermolecular condensation reaction. Not only pathway of pyrolysis reaction was changed but also the pressure-driven flow was impaired. A pressure drop from 100 Pa to 0 Pa was noticed during devolatilisation. The emission of CO_2 and CO was reduced by 20%, whereas the percentage increase of 11% was estimated in Methane. The char yield obtained from torrefied pine needle pellet was found to be 60%, whereas it was 48% for the torrefied pine cones.

The effect of torrefaction on the heat fluxes of pine waste was also seen. The torrefied pine waste was found to be more exothermic in nature. However, the heat of the reaction was seen to be a function of the heating rate. The higher heating rate was seen to be favourable for the torrefied pine needles, whereas it was the lower ramp rate that enhanced the exothermic heat fluxes of the torrefied pine cones. The reason for the rise in heat fluxes was owing to a change in the grain orientation.

According to chemical kinetics, the generalised reaction rate depicted that both torrefied pine needles and pine cones would follow the higher-order reaction regime. However, the raw and torrefied pine waste would have a similar trend of variation, but the quantitative deviation was observed. The higher order of nucleation and growth reaction regime was seen to be predominant in the torrefied pine needles, whereas it was predominantly a multi-step reaction mechanism for torrefied pine cones. Therefore, the char, gas and oil yields of both the materials had drastic variation.

7. ÖSSZEFOGLALÁS (SUMMARY IN HUNGARIAN)

ELŐKEZELT FENYŐHULLADÉK, MINT ALTERNATÍV ÜZEMANYAG AZ ENERGIATERMELÉSHEZ

A biomassza energetikai átalakításának, a hőbontásának átfogó, valamint kvantitatív elemzését végeztük a kvázi statikus technika segítségével. A mikrohullámú sütővel végzett kísérletekkel ellentétben joule fűtőrendszerrel alkalmaztunk, és a kísérleti berendezést a kívánt cél érdekében alakítottuk ki. A tanulmány célja meghatározni a gyakorlati, üzemi állapothoz hasonló hőbontás lefolyását. A kísérletek során megállapítottam, hogy az anyagok előkezelése, a biomasszák fizikai jellemzői, az anyagok tömegállapota hatással van az energiahozamokra. A kisérletek során felhasznált anyagok fizikai jellemzői eltérőek voltak. Megállapítottam, hogy a kezelési idők és a hőmérsékletek az elemi összetételre, a H/C és az O/C moláris arányaira eltérő hatással volt. A fizikokémiai elemzéssel kapcsolatos új megállapításaimnál hangsúlyozom, hogy nem feltétlenül szükséges, hogy a hidrogén és az oxigén egyidejűleg csökkenjen a folyamat hőmérsékletének emelkedésével. A nagyobb termikus hatások a magasabb hőfokú előkezelések időszakában történnek, később csak a hidrogénmolekulák szabadulnak fel az anyagi szerkezetből. A nagyobb illóanyag tartalomnál a magasabb kezelési hőmérsékleten a tömegveszteség kiemelkedően nagy volt. Megállapítottam, hogy a hamutartalom az előkezelés (pörkölés) hőmérsékletének növekedésével csökkent és akkor is, ha a pörkölést rövidebb ideig végeztem. Ezzel szemben az idő és a hőmérséklet egyidejű növelése a nem előkezelt fenyőtű hamutartalmát növelte.

Szerkezeti elemzés szerint a nagyobb felületi egyenetlenségek, tehát a szemcse felület növekedése, mind a fenyőtűk, mind a tobozok esetében kimutatható voltt.

A fizikai előkezeléssel járó morfológiai elváltozások következtében változnak az előkezelt fenyőhulladékok fűtési tulajdonságai, amelyek befolyásolták a szénképződést is. A szemcsefelület növekedése hatott az illékony gázok tartózkodási idejére a szilárd anyagban, és ez támogatta az intramolekuláris kondenzációs reakciót. Nem csupán a hőbontási reakció lefolyása változott, hanem a tér nyomásviszonyai által vezérelt gázáramlás is. A folyamat nyomáselemzése során 100 Pa-ról 0,0 Pa-ra történő nyomásesést figyeltem meg. A CO_2- és CO kibocsátás 20%-kal csökkent, míg a metánban 11% -os növekedést tapasztaltam. Megállapítottam, hogy a pörkölt fenyőtű-pelletnél a szénképződés 60%, míg a pörkölt fenyőtoboz pelletnél csupán 48% volt.

Az pörkölés hatása a fenyőhulladékok hőáramainál is megfigyelhető volt. A pörkölt anyagot exotermebb jellegűnek találtam. A reakció hőmérsékletének lefolyása a fűtési sebesség függvényében alakult. A nagyobb fűtési sebesség kedvezőbbnek bizonyult az pörkölt fenyőtűknél, míg az alacsonyabb fűtési -sebesség növelte a pörkölt fenyőtűk exoterm hőáramát. A hőáramok emelkedésének oka a szemcsék összetételének (kémiai és fizikai) megváltozása volt.

A kémiai kinetika elemzés alapján az átlagos reakciósebességnél azt tapasztaltam, hogy mind a pörkölt fenyőtűnél, mind a pörköletlen anyagnál a magasabb rendű volt a reakció folyamata. Ugyanakkor a nem pörkölt és az pörkölt anyagok hasonló tendenciákat mutatott, de a mennyiségnél eltérést tapasztaltam. A magasabb rendű nukleációs és növekedési jellegű reakciós-folyamatot láttam dominánsnak az előkezelt fenyőtűknél, míg az előkezelt fenyőtoboznál a perdominálisan többlépcsős reakciómechanizmus volt a jellemző. Ezért az anyagok szén-, gáz- és olajhozama jelentősebb különbséget mutatott.

8. APPENDICES

A1. Bibliography

1. Almeida, G., Brito, J.O., and Perré, P. (2010): Alterations in energy properties of eucalyptus wood and bark subjected to torrefaction: The potential of mass loss as a synthetic indicator, Bioresource Technology,101(24), pp.9778–9784.
2. Arora, C. P (1981): Refrigeration and air conditioning : (in SI units). Tata McGraw-Hill Pub. Co, New Delhi.
3. Asmadi, M., Kawamoto, H., and Saka, S. (2017): Characteristics of softwood and hardwood pyrolysis in an ampoule reactor, Journal of Analytical and Applied Pyrolysis,124, pp.523–535.
4. Bach, Q.V., Tran, K.Q., and Skreiberg, Ø. (2017): Comparative study on the thermal degradation of dry- and wet-torrefied woods, Applied Energy,185, pp.1051–1058.
5. Basu, P. (2010): Pyrolysis and torrefaction. In: Biomass gasification and pyrolysis, practical design and theory (pp. 65-96). Elsevier Inc., New York.
6. Basu, P. (2018): Biomass gasification, pyrolysis and torrefaction: practical design and theory.
7. Ben, H. and Ragauskas, A.J. (2013): Comparison for the compositions of fast and slow pyrolysis oils by NMR characterization, Bioresource Technology, 147, pp. 577-584.
8. Ben, H. and Ragauskas, A.J.(2011b): NMR characterization of pyrolysis oils from kraft lignin. Energy Fuels, 25 (5), pp. 2322–2332.
9. Benke, A.C., and Huryn, A.D. (2007): Secondary production of macroinvertebrates, In Methods in Stream Ecology, pp. 691–710.
10. Bergman, P.C.A., Boersma, A.R., Zwart, R.W.H., and Kiel, J.H.A. (2005): Development of torrefaction for biomass co-firing in existing coal-fired power stations (ECN-Ce05e013), ECN Report, Retrieved from https://www.ecn.nl/docs/library/report/2005/rx05180.pdf.
11. Bilgic, E., Yaman, S., Acma, H.H., and Kucukbayrak, S. (2016): Limits of variations on the structure and the fuel characteristics of sunflower seed shell through torrefaction, Fuel Processing Technology, 144, pp. 197-202.
12. Blasi, C. D.(1993): Modelling and simulation of combustion processes of charring and noncharring solid fuels. Progress of Energy Combustion. Science,19 (1), pp. 71-104.
13. BP (2014): BP energy outlook 2035. BP, London, UK. http://www.bp.com/ content/dam/bp/pdf/Energyeconomics/EnergyOutlook/Energy_Outlook_2035_booklet.pdf.
14. Bradbury, A.G.W., Sakai, Y. and Shafizadeh, F.A. (1979): Kinetic model for pyrolysis of cellulose, Journal of AppliedPolymer Science., 23 (11), pp. 3271-3280.
15. Bridgeman, T.G., Jone, J.M. and Shield, I. (2008): Torrefaction of reed canary grass, wheat straw and willow to enhance solid fuel qualities and combustion properties, Fuel, 87(6), pp. 844-856.
16. Briggs, J. L., Maier, D. E, Watkins, B. A, and Behnke, K. C. (1999): Effects of ingredients and processing parameters on pellet quality, Poultry Science, 78, pp.1464–1471.
17. Brown HP, Panshin AJ., and Forsaith CC. (1952): Textbook of wood technology, vol. II. New York: McGraw-Hill, p. 643.
18. Carlson, T.R., Vispute, T.P., and Huber, G.W. (2008): Green gasoline by catalytic fast pyrolysis of solid biomass-derived compounds. ChemSusChem, 1(5), pp. 397-400.

19. Chai, L., and Saffron, C.M. (2016): Comparing pelletization and torrefaction depots: Optimization of depot capacity and biomass moisture to determine the minimum production cost. Appl. Energy, 163, pp. 387–395.
20. Chaikumpollert, O., Methacanon, P., and Suchiva, K. (2004): Structural elucidation of hemicelluloses from vetiver grass, Carbohydrate. Polymer., 57 (2), pp. 191–196.
21. Chaiwat, W., Hasegawa, I., Kori, J., and Mae, K. (2008): Examination of degree of crosslinking for cellulose precursors pretreated with acid/hot water at low temperature. Industrail Engineering and Chemical Rsearch., 47 (16), pp. 5948–5956.
22. Chan W. C. R., Kelbon M., and Krieger, B. (1985): Modelling and experimental verification of physical and chemical processes during pyrolysis of a large biomass particle, Fuel, 64 (11), pp.1505–1513.
23. Chen, G.-B., Li, Y.-H., Chen, G.-L., and Wu, W.-T. (2017): Effects of catalysts on pyrolysis of castor meal, Energy, 119, pp.1–9.
24. Chen, W., Lickfield, G. C., and Yang, C. Q. (2004): Molecular modeling of cellulose in amorphous state Part I: Model building and plastic deformation study, Polymer, 45, pp. 1063–1071.
25. Chen, W.H., and Kuo, P.C. (2011): Isothermal torrefaction kinetics of hemicellulose, cellulose, lignin and xylan using thermogravimetric analysis, Energy, 36 (11), pp. 6451–6460.
26. Chen, W.H., Cheng, W.Y., Lu, K.M., and Huang, Y.P. (2011): An evaluation on improvement of pulverized biomass property for solid fuel through torrefaction. Applied Energy, 88 (11), pp. 3636–3644.
27. Chen, W.-H., Lu, K.-M., Liu, S.-H., Tsai, C.-M., Lee, W.-J., and Lin, T.-C. (2013): Biomass torrefaction characteristics in inert and oxidative atmospheres at various superficial velocities, Bioresource. Technology., 146, pp.152–160.
28. Chen, W.H., Zhuang, Y.Q., Liu, S.H., Juang, T.T., and Tsai, C.-M. (2016): Product characteristics from the torrefaction of oil palm fiber pellets in inert and oxidative atmospheres, Bioresource Technology, 199, pp. 367–374.
29. Chen, W-H, Peng, J, and Bi, X.T. (2015): A state-of-the-art review of biomass torrefaction, densification and applications. Renewable and Sustainable Energy Review., 44, pp. 847–66.
30. Chena, D., Gao, A., Mab, Z., Feia, D., Changa, Yu., and Shena, C. (2018): In-depth study of rice husk torrefaction: characterization of solid, liquid and gaseous products, oxygen migration and energy yield, Bioresource Technology, 253, pp. 148–153.
31. Chew, J.J., and Doshi, V. (2011): Recent advances in biomass pre-treatment-torrefaction fundamentals and technology, Renewable and Sustainability . Energy Review., 15(8), pp. 4212–4222.
32. Ciolkosz, D., and Wallace, R. (2011): A review of torrefaction for bioenergy feedstock production, Biofpr.,5, pp. 317–329.
33. Commandré J.M., and Leboeuf, A. (2014): Volatile yields and solid grindability after torrefaction of various biomass types. Environment Progress and.Sustainable, Energy, 34(4), pp. 1180–1186.
34. Couhert, C., Salvador, S., and Commandré, J.M. (2009): Impact of torrefaction on syngas production from wood, Fuel, 88(11), pp. 2286–2290.
35. Criado, J. M., Málek, J., and Ortega, A. (1989): Applicability of the master plots in kinetic analysis of non-isothermal data', Thermochimica Acta, 147(2), pp. 377–385.

36. Czernik S. (2013): Catalytic Pyrolysis of Biomass. In: Lee J. (eds), Advanced Biofuels and Bioproducts (pp.119-127), Springer, New York, NY.
37. Debdoubi, A., El amarti, A., Colacio, E., Blesa, M.J., and Hajjaj, L.H. (2006): The effect of heating rate on yields and compositions of oil products from esparto pyrolysis, International. Journal of Energy Research., 30 (15), pp.1243–1250.
38. Demirbas, A, Akdeniz, F, Erdogan, Y., and Pamuk, V. (1996): Kinetics for fast pyrolysis of hazel nutshell, Fuel Science and Technology International, 14 (3), pp. 405–415.
39. Deng, J., Wang, G.J., Kuang, J.H., Zhang, Y.L., and Luo, Y.H. (2009): Pretreatment of agricultural residues for co-gasification via torrefaction. Journal of Analytical and Applied Pyrolysis, 86, pp. 331–337.
40. Department of Materials Science and Engineering, University of Illinois Urbana-Champaign (2017). Polymers. Retrieved from http://matse1.mse.uiuc.edu/polymers/prin.html.
41. Dhaundiyal, A, Singh, S.B., Hanon, M.M., and Rawat, R. (2018a): Determination of kinetic parameters for the thermal decomposition of parthenium hysterophorus, Environmental and Climate Technologies, 22(1), pp. 5–21.
42. Dhaundiyal, A. and Singh, S. B. (2020): The generalisation of a multi-reaction model for polynomial ramping of temperature, Journal of Thermal Analysis and Calorimetry, 143(4), pp.1–13.
43. Dhaundiyal, A., and Gupta, V. K. (2014): The analysis of pine needles as a substrate for gasification, Hydro Nepal: Journal of Water, Energy and Environment, 15, pp. 73–81.
44. Dhaundiyal, A., and Tewari, P. C. (2016): Performance evaluation of throatless gasifier using pine needles as a feedstock for power generation, Acta Technologica Agriculturae, 19(1), pp. 10–18.
45. Dhaundiyal, A., and Tewari, P.C. (2017): Kinetic Parameters for the Thermal Decomposition of Forest Waste Using Distributed Activation Energy Model (DAEM), Environmental and Climate Technologies, 19(1), pp. 15–32.
46. Dhaundiyal, A., Singh S.B., and Hanon, M.M. (2018b): Study of distributed activation energy model using bivariate distribution function, f (E_1, E_2), Thermal Science and Engineering Progress, 5, pp. 384–404.
47. Dhaundiyal, A., Singh S.B., Atsu, D. and Toth, L. (2021): Comprehensive analysis of pre-treated Austrian pine, Fuel, 287, pp.1–13.
48. Dhaundiyal, A., Singh, S.B., and Hanon, M.M. (2019a): Application of Archimedean copula in the non-isothermal n^{th} order distributed activation energy model, Biofuels, 10(2), pp.259–270.
49. Dhaundiyal, A., Singh, S.B., Atsu, D., and Dhaundiyal, R. (2019b): Application of Monte Carlo simulation for energy modelling, Journal of American Chemical Society, 4(3), pp. 4984–4990.
50. Dhaundiyal, A., Toth, L., Bacskai, I., and Atsu, D. (2020b): Analysis of pyrolysis reactor for hardwood (Acacia) chips, Renewable Energy,147, pp.1979–1989.
51. Dhaundiyal, A., Bercesi, G., Atsu, D., and Toth, L.(2021a): Development of a small-scale reactor for upgraded biofuel pellet, Renewable Energy, 170, pp.1197–1214.
52. Dhaundiyal, A., Singh, S.B., and Toth, L. (2021b): Experimental investigation of a small-scale reactor with processed biofuel pellets, Biofuels, Bioproducts and Biorefining. Available at: http://dx.doi.org/10.1002/bbb.2256.

53. Dhungana, A., Basu, P. and Dutta, A. (2012): Effects of Reactor Design on the Torrefaction of Biomass. Journal of Energy Resources Technology, 134(4), 1-11.
54. Emmons, H.W. and Atreya, A. (1982): The Science of Wood Combustion, Proc. Indian Academy of Sciences, 24, pp. 259–268.
55. Eseltine, D., Thanapal, S.S., Annamalai, K., and Ranjan, D. (2013): Torrefaction of woody biomass (Juniper and Mesquite) using inert and non-inert gases, Fuel,113, pp.379–388.
56. Esteban, L.S., and Carrasco, J.E. (2006): Evaluation of different strategies for pulverization of forest biomasses. Powder Technology, 166 (3), pp.139–151.
57. Gallagher, P.K. (1998): Handbook of Thermal Analysis and Calorimetry, Vol.1, (Ed. M.E.Brown), Elsevier, Amsterdam, Ch.3.
58. Gayubo, A.G., Aguayo, A.T., Atutxa, A., Aguado, R., and Bilbao, J. (2004): Transformation of oxygenate components of biomass pyrolysis oil on a HZSM-5 zeolite. I. Alcohols and phenols. Industrial & Engineering Chemistry Research, 43(11), pp. 2610–2618.
59. Granada, E., López González, L.M., Míguez, J.L., and Moran, J. (2002): Fuel Lignocellulosic Briquettes, Die Design, and Products Study, Renewable Energy, 27, pp. 561–573.
60. Grimm, A., Skoglund, N., Bostrom, D., and Ohman, M. (2011): Bed agglomeration characteristics in fluidized quartz bed combustion of phosphorus-rich biomass fuels, Energy and Fuels, 25(3), pp. 937–947.
61. Holman, J. P. (2002): Heat transfer 9th Edition, New York, Boston, McGraw-Hill, Inc.
62. Hon, D. N. S. (1989): Cellulosic Adhesives," in R.W. Hemmingway and A.H. Conner (Eds.), Adhesives from Renewable Resources, Washington, DC: American Chemical Society, 1989, pp. 289–304.
63. Houghton, R.A. (2008): Biomass, In *Encyclopedia of Ecology, Five-Volume Set*: pp. 448–453.
64. Huang, Y.F., Sung, H. Te, Chiueh, P. Te and Lo, S.L. (2017): Microwave torrefaction of sewage sludge and Leucaena, Journal of the Taiwan Institute of Chemical Engineers,70, pp.236–243.
65. Iyer, P.V.R., Rao, T.R., Grover, P.D., and Singh, N.P. (Eds). Biomass: Thermochemical Characterisation. Second edition, Biomass Gasification Action Research Centre, Dept. of Chemical Engg, IIT, New Delhi, 1997.
66. Jae, J., Tompsett, G.A., Foster, A.J., Hammond, K.D., Auerbach, S.M., Lobo, R.F., and Huber, G.W. (2011): Investigation into the shape selectivity of zeolite catalysts for biomass conversion., Journal of Catalysis, 279(2), pp. 257–268.
67. Jiménez, S., and Ballester, J. (2005): Influence of operating conditions and the role of sulfur in the formation of aerosols from biomass combustion, Combustion and Flame, 140(4), pp. 346–358.
68. Kansa, E.J., Perlee, H.E., and Chaiken R.F. (1977): Mathematical model of wood pyrolysis including internal forced convection, Combustion and Flame, 29, pp. 311–324.
69. Kelbon M. (1983): Conditions that favour tar production from pyrolysis of large, moist wood particles, M.S. Thesis, University of Washington, Seattle, Washington.
70. Kihedu J. (2015): Torrefaction and combustion of lignocellulosic biomass, Energy Proc., 75, pp.162–167.
71. Koufopanos, C.A., Papayannakos, N., Maschio, G., and Lucchesi, A. (1991): Modelling of the pyrolysis of biomass particles. studies on kinetics, Thermal and Heat Transfer Effects. The Canadian Journal of Chemical Engineering, 69(4), pp. 907–915.

72. Krishna K. P., Sangen, E., and Visser, P. (1985): Woodburning cookstoves, Advances in Heat Transfer, 17, pp. 159–317.
73. Kung, H.C. (1972): A mathematical model of wood pyrolysis, Combustion and Flame, 18(2), pp.185–195.
74. Kurkela, E., Kurkela, M., and Hiltunen, I. (2016): Steam-oxygen gasification of forest residues and bark followed by hot gas filtration and catalytic reforming of tars, Fuel Processing Technology, 141, pp.148–158.
75. Lampart-Szczapa, E., P. Konieczny, M. Nogala-Kalucka, S. Walczak, I. Kossowska, and M. Malinowska. (2006): Some functional properties of lupin proteins modified by lactic fermentation and extrusion," Food Chemistry, 96, pp. 290–296.
76. Lédé, J. (2012): Cellulose pyrolysis kinetics: An historical review on the existence and role of intermediate active cellulose, Journal of Analytical and Applied Pyrolysis, pp. 17–32.
77. Lee, C.K., Chaiken, R.F., and Singer, J.M. (1976): Charring pyrolysis of wood in fires by laser simulation. Symposium (Intl.) on Combustion, 16(1), pp.1459–1470.
78. Lehtikangas, P.(1999): Quality properties of fuel pellets from forest biomass, Licentiate Thesis, Department of Forest Management and Products, Report 4, Uppsala.
79. Lewellen P.C., Peters W.A., and Howard J.B. (1977): Cellulose pyrolysis, kinetics and char formation mechanism, Symposium (International) on Combustion, 16(1), pp.1471–1480.
80. Li, X.T., Grace, J.R., Lim, C.J., Watkinson, A.P., Chen, H, P., and Kim, J.R. (2004): Biomass gasification in a circulating fluidized bed, Biomass and Bioenergy, 26 (2), pp. 171–193.
81. Lorio, P.L., Stephen, F.M., and Paine, T.D. (1995): Environment and ontogeny modify loblolly-pine response to induced acute water deficits and bark beetle attack. For. Ecol. Manag, 73(1-3), pp. 97–110.
82. Lv, P., Almeida, G., and Perré, P. (2015): TGA-FTIR Analysis of torrefaction of Lignocellulosic Components (Cellulose, xylan, lignin) in Isothermal Conditions over a wide range of time durations, Bioresour, 10 (3), pp. 4239–4251.
83. Maa, P.S., and Bailie, R.C. (1973): Influence of particle sizes and environmental conditions on high-temperature pyrolysis of cellulosic material -I (Theoretical), Combustion Science and Technology, 7(6), pp. 257–269.
84. Mani, S., Tabil, L.G., and Sokhansanj, S. (2004): Grinding performance and physical properties of wheat and barley straws, corn stover and switchgrass, Biomass and Bioenergy, 27 (4), pp. 339–352.
85. Matsumoto, T., Fujiwara, T., and Kondo, J. (1969): Non-steady thermal decomposition of plastics, Symposium (International) on Combustion, 12(1), pp.515–531.
86. Mattsson, J. E. (1989): Basic handling characteristics of wood fuels, angle of repose, friction against surfaces and bridging', in VTT Symposium (Valtion Teknillinen Tutkimuskeskus), pp. 399–410.
87. McKendry, P. (2002): Energy production from biomass (part 1): overview of biomass., Bioresource Technology, 83(1), pp. 37–46.
88. Melkior, T., Jacob, S., Gerbaud, G., Hediger, S., Pape, L.L., Bonnefois, L., and Bardet, M. (2012): NMR analysis of the transformation of wood constituents by torrefaction. Fuel, 92(1), pp. 271–280.
89. Mohan, D., Pittman, C.U., and Steele, P.H. (2006): Pyrolysis of wood/biomass for bio-oil: a critical review, Energy and Fuels, 20(3), pp. 848–889.

90. Møller, H.S., and Esbensen, K.H. (2005): Representative sampling of wood chips - A contribution to fulfil the Kyoto protocol, In Australasian Institute of Mining and Metallurgy Publication Series. pp. 205–207.
91. Morf, P., Hasler, P., and Nussbaumer, T. (2002): Mechanisms and kinetics of homogeneous secondary reactions of tar from continuous pyrolysis of wood chips, Fuel, 81, pp. 843–853.
92. Murphy, J. D., and K. McCarthy K. (2005): Ethanol production from energy crops and wastes for use as a transport fuel in Ireland, Applied Energy, 2005, 82, pp.148–166.
93. Murty, K.A., and Blackshear, Jr. P.E. (1967): Pyrolysis effects in the transfer of heat and mass in thermally decomposing organic solids, Symposium (International) on Combustion, 11(1), pp. 517-523.
94. Nanou, P., Carbo, M.C., and Kiel, J.H.A. (2016): Detailed mapping of the mass and energy balance of a continuous biomass torrefaction plant, Biomass and Bioenergy, 89, pp. 67-77.
95. Nassar, M.M., and Mackay, G.D.M. (1984): Studies on the mechanism of flame retarding, Thermochimica Acta, 81, pp. 9-14.
96. Nelson, D. L., Cox, MM. and Lehninger, M.M. (2005): Principles of biochemistry, New York, NY: W. H. Freeman and Company.
97. Nhuchhen, D., Basu, P. and Acharya, B. (2014): A Comprehensive Review on Biomass Torrefaction. International Journal of Renewable Energy and Biofuels, 2014, 1–56.
98. Nikolaisen, L. S., and Jensen, P. D. (2013): Biomass feedstocks: categorisation and preparation for combustion and gasification, in biomass combustion science, Technology and Engineering, pp. 36–57.
99. Nunes, L.J.R., Matias, J.C.O., and Catalão, J.P.S. (2014): Mixed biomass pellets for thermal energy production: A review of combustion models, Applied Energy,127, pp.135–140.
100. Nyanzi, F. A. and Maga, J.A. (1992): Effect of processing temperature on detergent-solubilized protein in extrusion-cooked cornstarch/soy protein subunit blends, Journal of Agricultural and Food Chemistry, 40, pp.131–133.
101. Pach, M, Zanzi, Z, and Bjornbom, E. Torrefied biomass a substitute for wood and charcoal. 6th Asia-Pacific International Symposium on Combustion and Energy Utilization, 20 May 2002 – 22 May 2002, Kuala Lumpur.
102. Panton, R.L., and Rittman, J.G. (1971): Pyrolysis of a slab of porous material, Symposium (International.) on Combustion, 13(1), pp. 881-891.
103. Pastorova, I., Arisz, P.W., and Boon, J.J. (1993): Preservation of D-glucose-oligosaccharides in cellulose chars, Carbohydrate Research, 248, pp. 151-165.
104. Phanphanich, M., and Mani, S. (2011): Impact of torrefaction on the grindability and fuel characteristics of forest biomass, Bioresource Technology, 102(2), pp.1246-1253.
105. Piskorz, J., Radlein, D.S.A, Scott, D.S., and Czernik, S. (1989): Pre-treatment of wood and cellulose for production of sugars by fast pyrolysis, J. Anal. Appl. Pyrolysis, 16, pp. 127–142.
106. Prins, M.J, Ptasinski, K.J., and Janssen, F.J.J.G. (2006): Torrefaction of wood: part 1. Weight loss kinetics, Journal of Analytical and Applied Pyrolysis, 77(1), pp.28-34.
107. Pushkaraj, R., Patwardhan, Brown, R.C., and Shanks, B.H. (2011): Product distribution from the fast pyrolysis of hemicellulose, ChemSusChem, 4(5), pp. 636-643.
108. Pyle D.L., and Zaror C.A. (1984b): Thermochemical processing of biomass, Butterworths and Co. Pub. Ltd., London.
109. Pyle, D.L., and Zaror, C.A. (1984a): Heat transfer and kinetics in the low-temperature pyrolysis of solids, Chemical Engineering Science, 39(1), pp. 147–158.

110. Radlein, D., Piskorz, J., and Scott, D.S. (1991): Fast pyrolysis of natural polysaccharides as a potential industrial process, Journal of Analytical and Applied Pyrolysis, 19, pp. 41–63.
111. Rehan, M., Miandad, R., Barakat, M.A., Ismail, I.M.I., Almeelbi, T., Gardy, J., Hassanpour, A., Khan, M.Z., Demirbas, A., and Nizami, A.S. (2017): Effect of zeolite catalysts on pyrolysis liquid oil, International Biodeterioration & Biodegradation, 119, pp.162-175.
112. Saadon, S, Uemura, Y., and Mansor, N. (2014): Torrefaction in the presence of oxygen and carbon dioxide: the effect on yield of oil palm kernel shell, Procedia Chemistry, 9, pp.194-201.
113. Saleh Al, Arni (2018): Comparison of slow and fast pyrolysis for converting biomass into fuel, Renewable Energy, 2018, 124, pp. 197-201.
114. Samolda M.C., and Vasalos L.A. (1991): A kinetic approach to the flash pyrolysis of biomass in a fluidized bed reactor, Fuel 70(7), Fuel 70(7), pp. 883-889.
115. Sánchez-Jiménez, P. E. et al. (2013): Generalized master plots as a straightforward approach for determining the kinetic model: The case of cellulose pyrolysis, Thermochimica Acta, 552, pp. 54–59.
116. Scott, D.S., Paterson, L., Piskorz, J., and Radlein, D. (2001): Pre-treatment of poplar wood for fast pyrolysis: rate of cation removal, Journal of Analytical and Applied. Pyrolysis, 57, pp. 169–176.
117. Shafizadeh, F. (1982): Introduction to pyrolysis of biomass, Journal of Analytical and Applied Pyrolysis, 3(4), pp. 283-305.
118. Shafizadeh, F. and McGinnis, G.D. (1971): Chemical composition and thermal analysis of Cottonwood, CarbohydrateResearch., 16 (2), pp. 273-277.
119. Shafizadeh, F., and Stevenson, T.T. (1982): Saccharification of douglas-fir wood by a combination of pre-hydrolysis and pyrolysis, Journal of Applied Polymer Science, 27(12), pp. 4577-4585.
120. Shaw, M. (2008): Feedstock and process variables influencing biomass densification, PhD thesis submitted to Department of Agricultural and Bioresource Engineering, University of Saskatchewan, Saskatoon, Saskatchewan, Canada, 2008.
121. Shen, D.K., Gu, S., and Bridgewater, A.V. (2010): Study on the pyrolytic behaviour of xylan-based hemicellulose using TG–FTIR and Py–GC–FTIR, Journal of Analytical and Applied Pyrolysis, 88(2), pp. 199-206.
122. Siedlecki, M., and Jong, W.D. (2011): Biomass gasification as the first hot step in clean syngas production process e gas quality optimization and primary tar reduction measures in a 100-kW thermal input steam oxygen blown CFB gasifier, Biomass and Bioenergy, 35, 40-62.
123. Sierra, R, Smith, A, Granda, C, and Holtzapple, M.T.(2008): Producing fuels and chemicals from lignocellulosic biomass, Chemical Engineering Process, Society of Biological Engineering Special Section: Biofuels, 104, S10–S18.
124. Sluiter, A., Hames, B., Ruiz, R., Scarlata, C., Sluiter, J., Templeton, D., and Crocker, D. (2008): Determination of structural carbohydrates and lignin in biomass. Laboratory Analytical Procedure (NREL/TP-510-42618), National Renewable Energy Laboratory. Retrieved from https://www.nrel.gov/docs/gen/fy13/42618.pdf.
125. Sokhansanj, S., Mani, S., X. Bi, X., Zaini, P. and Tabil, L. Binderless Pelletization of Biomass, Presented at the ASAE Annual International Meeting, Tampa, FL, ASAE Paper No. 056061. ASAE, 2950 Niles Road, St. Joseph, MI 49085-9659 USA, July 17–20, 2005.
126. Soltes, E.J., and T.J. Elder (1981): Pyrolysis in Organic Chemicals from Biomass, ed. I.S. Goldstein, 63-100. Boca Raton, FL: CRC Press In.

127. Stamm, A.J., and Harris, E.E. (1953): Chemical processing of wood, Chemical Publishing co., inc., New York, p.595.B.
128. Steenari, B. M., and Lindqvist, O. (1998): High-temperature reactions of straw ash and the anti-sintering additives kaolin and dolomite, Biomass and Bioenergy, 14(1), pp. 67–76.
129. Steenari, B. M., Lundberg, A, Pettersson, H, Wilewska-Bien, M., Andersson, D. (2009): Investigation of ash sintering during combustion of agricultural residues and the effect of additives, Energy and Fuels, 23(11), pp. 5655–5662.
130. Strandberg, M., Olofsson, I., Pommer, L., Lindström, S.W., Åberg, K., and Nordin, A. (2015): Effects of temperature and residence time on continuous torrefaction of spruce wood, Fuel Processing Technology, 134, pp. 387-398.
131. Strom, B.L., Goyer, R.A., Ingram, L.L., Jr. Boyd, G.D.L., and Lott, L.H. (2002): Oleoresin characteristics of progeny of loblolly pines that escaped attack by the southern pine beetle. Forest Ecology and Management. 157, pp.169–178.
132. Tabil, Jr., L. G. (1996): Binding and pelleting characteristics of alfalfa," Unpublished PhD. Thesis, Saskatoon, Saskatchewan: Department of Agricultural and Bioresource Engineering, University of Saskatchewan.
133. Tan, I.A.W., Shafee, N.M., Abdullah, M.O., and Lim, L.L.P. (2017): Synthesis and characterization of bio coal from Cymbopogon citrates residue using microwave-induced torrefaction, Environmental Technology and Innovation, 8, pp. 431–440.
134. Tang, W.K. and Neikl, KJ. (1964): Effect of flame retardants on pyrolysis and combustion of α-cellulose, Journal of Polymer Sci, Part C: Polymer symposia, 2(1), pp. 65-81.
135. Thanapal, S.S, Annamalai K., Sweeten, J. and Gordillo, G. (2012): Fixed bed gasification of dairy biomass with enriched air mixture. Applied Energy, 97, pp. 525–31.
136. Thangalazhy-Gopakumar, S., Adhikari, S., Gupta, R.B., and Fernando, S.D. (2011): Influence of pyrolysis operating conditions on bio-Oil components: A microscale study in a pyroprobe, Energy and Fuels,25(3), pp.1191–1199.
137. Thomas, M., Van Vliet, T. and Van der Poel, A.F.B. (1998): Physical quality of pelleted animal feed 3. Contribution of Feedstuff Components, Animal Feed Science Technology, 70, pp. 59–78.
138. Thunman, H., and Leckner, B. (2005): Influence of size and density of fuel on combustion in a packed bed', Proceedings of the Combustion Institute, 30 II, pp. 2939–2946.
139. Thy, P., Jenkins, B.M., Grundvig, S., Shiraki, R. and Lesher, C.E. (2006): High-temperature elemental losses and mineralogical changes in common biomass ashes, Fuel, 85(5–6), pp. 783–795.
140. Tinney, E.R. (1965): The combustion of wood dowels in heated air, Symposium (International) on Combustion, 10(1), pp. 925-930.
141. Tobiasen, L., Skytte, R., Pedersen, L.S., Pedersen, S.T. and Lindberg, M.A. (2007): Deposit characteristic after injection of additives to a Danish straw-fired suspension boiler, Fuel Processing Technology, 88(11–12), pp. 1108–1117.
142. Tran, K.-Q., Luo, X., Seisenbaeva, G., and Jirjis, R. (2013): Stump torrefaction for bioenergy application. Appl. Energy, 2013, 112, pp. 539-546.
143. Tsalidis, G.A., Marcello, M.D., Spinelli, G., Wiebren de Jong, W.D., and Kiel, J.H.A. (2017): The effect of torrefaction on the process performance of oxygen-steam blown CFB gasification of hardwood and softwood, Biomass and Bioenergy, 106, pp. 155-165.

144. Turner, I, Rousset, P, Rémond, R., and Perré, P. (2010): An experimental and theoretical investigation of the thermal treatment of wood (Fagus sylvatica L.) in the range 200–260 C. International Journal of Heat Mass Transfer, 53(4), pp. 715-725.
145. Uberoi, M., Punjak, W. A., and Shadman, F. (1990): The kinetics and mechanism of alkali removal from flue gases by solid sorbents, Progress in Energy and Combustion Science, pp. 205–211.
146. Uemura, Y, Omar, WN, Tsutsui, T, and Yusup, SB. (2011): Torrefaction of oil palm wastes, Fuel, 2011, 90, pp.2585–2591.
147. UN Comtrade (2020, November). Annual International Trade Statistics by Country. *Trend economy*. https://trendeconomy.com/data/h2/Hungary/4402 (Accessed 06-12-2020)
148. Van Dam, J. E. G., Van den Oever, M.J.A., Teunissen, W., Keijsers, E.R.P. and A. G. Peralta, A.G. (2004): Process for Production of High Density/High Performance Binderless Boards from Whole Coconut Husk—Part 1: Lignin as Intrinsic Thermosetting Binder Resin, Industrial Crops and Products, 19(3), pp. 207–216.
149. Várhegyi, G., Antal, M.J., Jakab, E., and Szabo, P. (1997): Kinetic modeling of biomass pyrolysis. Journal of Analytical and Applied Pyrolysis, 42(1), pp.73–87. Available at: http://dx.doi.org/10.1016/s0165-2370(96)00971-0.
150. Vuory A., and Bredenberg, J.B.S. (1988): Liquefaction of Kraft Lignin: 1. Primary Reactions under Mild Thermolysis Conditions, Holzforschung, 42(3), pp.155-161.
151. Vyazovkin, S., Burnham, A.K., Criado, J.M., Pérez-Maqueda, L.A., Popescu, C., and Sbirrazzuoli, N. (2011): ICTAC Kinetics Committee recommendations for performing kinetic computations on thermal analysis data, Thermochimica Acta,520(1–2), pp.1–19.
152. Wang, L., Skjevrak, G., Hustad, J.E., and Gronli, M.G. (2011): Effects of sewage sludge and marble sludge addition on slag characteristics during wood waste pellets combustion, Energy and Fuels, 25(12), pp. 5775–5785.
153. Werner, K., Pommer, L., and Brostrom, M. (2014): Thermal decomposition of hemicelluloses, Journal of Analytical and Applied. Pyrolysis, 110, pp.130–137.
154. Williams, O., Newbolt, G., Eastwick, C., Kingman, S., Giddings, D., Lormor, S., and Lester, E. (2016): Influence of mill type on densified biomass comminution. Applied Energy, 182, pp. 219–231.
155. Wood, J. F. (1987): The functional properties of feed raw materials and the effect on the production and quality of feed pellets, Animal Feed Science and Technology, 18, pp. 1–17.
156. Woytiuk, K., Campbell, W., Gerspacher, R., Evitts, R.W. and Phoenix, A. (2017): The effect of torrefaction on syngas quality metrics from fluidized bed gasification of SRC willow, Renewable. Energy, 101, pp. 409-416.
157. Xiao, W, Zhang, X., Wang, X., Niu, W., and Han, L. (2015): Rapid Liquefaction of Corn Stover with Microwave Heating, BioResources, 10(3), pp. 4038–4047.
158. Xin, S., Mi, T., Liu, X., and Huang, F. (2018): Effect of torrefaction on the pyrolysis characteristics of high moisture herbaceous residues, Energy, 152, pp. 586–593.
159. Yang, H, Yan, R., Chen, H, Lee, D.H., and Zheng, C. (2007): Characteristics of hemicellulose, cellulose and lignin pyrolysis, Fuel, 86 (12-13), pp. 1781–1788
160. Yu, H., Zhang, Z., Li, Z., and Chen, D. (2014): Characteristics of tar formation during cellulose, hemicellulose and lignin gasification, Fuel, 118, pp. 250–256.

161. Zandersons, J., Gravitis, J., Zhurinsh, A., Kokorevics, A., Kallavus, U., and Suzuki, C.K.(2004): Carbon Materials Obtained from Self-Binding Sugar Cane Bagasse and Deciduous Wood Residues Plastics, Biomass and Bioenergy, 2004, 26, 345–360.
162. Zheng, A., Zhao, Z., Chang, S., Huang, Z., Wang, X., He, F., and Li, H. (2013): Effect of torrefaction on structure and fast pyrolysis behaviour of corncobs, Bioresource Technology, 128, pp. 370–377.
163. Zhi, W.J., Wang, L.F., and Hu, X.J. (2017): Recent advances in the effects of microwave radiation on brains, Military Medical Research, 29, 4(1), 1–14.

A2. Publications related to the dissertation.

Refereed papers in foreign languages:

1. **Dhaundiyal, A.**, and Toth, L. (2021): Modelling of a torrefaction process using thermal model object, Energies, 14, 9, pp. 1-24. DOI: 10.3390/en14092481 (IF: 2.702)
2. **Dhaundiyal, A**., Bercesi, G., Atsu, D., and Toth, L. (2021): Development of a small-scale reactor for upgraded biofuel pellet, Renewable Energy, 170, pp.1197–1214. DOI: 10.1016/j.renene.2021.02.057 (IF: 7.387)
3. **Dhaundiyal, A**., and Atsu, D. (2020): Exergy analysis of a pilot-scale reactor using wood chips. Journal of Cleaner Production, 279, pp. 1-11. DOI: 10.1016/j.jclepro.2020.123511. (IF: 8.41)
4. **Dhaundiyal, A.**, Atsu, D. and Toth, L. (2020): Physico-chemical assessment of torrefied Eurasian pinecones. Biotechnology for Biofuels 13, 199, pp.1–20. DOI: 10.1186/s13068-020-01840-7. (IF: 5.47)
5. **Dhaundiyal, A**., Bercesi, G., and Backsai, I. (2020): The effect of torrefaction on the thermo-kinetics of thermally processed black pine. Canadian Journal of Chemical Engineering., pp. 1–16. DOI: 10.1002/cjce.23933. (IF: 1.687)
6. **Dhaundiyal, A**., Singh, S. B., Atsu, D., and Toth, L. (2020): Comprehensive analysis of pre-treated Austrian pine. Fuel, 287, pp. 1–13. DOI: 10.1016/j.fuel.2020.119605. (IF: 6.593)
7. **Dhaundiyal, A.,** and Singh, S. (2020): Optimisation of the performance of a pyrolysis reactor for G50 chips, Archive of thermodynamics, 41(1), pp. 245–263. DOI: 10.24425/ather.2020.132957.
8. **Dhaundiyal, A.**, and Toth, L. (2020): Modeling of hardwood pyrolysis using the convex combination of the mass conversion points. Journal of Energy Resources Technology, Transactions of the ASME, 142(6), pp. 1–10. DOI: 10.1115/1.4045458. (IF: 3.183)
9. **Dhaundiyal, A**., Toth, L., Bacskai, I., and Atsu, D. (2020): Analysis of pyrolysis reactor for hardwood chips, Renewable Energy, 147, pp.1979–1989. DOI: 10.1016/j.renene.2019.09.095. (IF: 7.387)
10. **Dhaundiyal, A.**, Mohammad, A. T., and Laszlo, T. (2019): Thermo-kinetics of forest waste using model-free methods. *Universitas Scientiarum*, *24*(1), pp.1–31. DOI: 10.11144/Javeriana.SC24-1.tofw.
11. **Dhaundiyal, A**., Singh, S. B., Hanon, M. M., and Schrempf, N. (2018): Clayton copula as an alternative perspective of multi-reaction model. Environmental and Climate Technologies, *22*(1), pp.83–106. DOI: 10.2478/rtuect-2018-0006.
12. **Dhaundiyal, A**., and Hanon, M. M. (2018): Calculation of kinetic parameters of the thermal decomposition of residual waste of coniferous species: Cedrus deodara. Acta Technologica Agriculturae, *21*(2), pp.75–80. DOI: 10.2478/ata-2018-0014.
13. **Dhaundiyal, A**., and Singh, S. B. (2018): Approximation to distributed activation energy model for residual logging of Cedrus deodora using Weibull distribution. Turkish World Mathematical Society Journal of Applied and Engineering Mathematics, 8(1), pp.8–19. DOI: 10.26837/jaem.395481.
14. **Dhaundiyal, A**., Singh, S. B., and Hanon, M. M. (2018): Study of distributed activation energy model using bivariate distribution function, f (E1, E2). Thermal Science and Engineering Progress, 5, pp.388–404. DOI: 10.1016/j.tsep.2018.01.009

International conference proceedings:

1. **Dhaundiyal, A**., and Toth, L. (2019): Calculation of kinetic parameters of thermal decomposition of forest waste using the Monte Carlo technique. Environmental and Climate Technologies, 24(1), 162–170. DOI: 10.2478/rtuect-2020-0010 Conference of Environmental and Climate Technologies (CONECT), Riga, Latvia (Held at Riga Technical University in May 2019).
2. **Dhaundiyal, A**., and Toth, L. (2021): Thermal Modelling of Torrefaction Process Using Finite Element Method The 3R International Scientific Conference on Material Cycles and Waste Management (3RINCs), (Held at National Institute for Environmental Studies, Tsukuba, Japan in March 2021)

Book chapter in foreign languages:

1. **Dhaundiyal, A.** and Singh, S.B. (2020): Distributed activation energy modeling by the transmutation of different density functions. (2020). Soft Computing, pp.67–104. DOI: 10.1515/9783110628616-005.
2. **Dhaundiyal, A**., Singh, S. B., and Hanon, M. M. (2019): Application of Transmuted Gumbel Copula for Energy Modeling. In Mathematics Applied to Engineering and Management (pp. 155–185**).** DOI: 10.1201/9781351123303-6.
3. **Dhaundiyal, A.**, Singh, S. B., and Hanon, M. M. (2018): Comparative Evaluation of Crisp and Fuzzy Schemes to Solve Chemical Kinetic Models (pp. 132–161). DOI: 10.4018/978-1-5225-5709- 8.ch007.
4. **Dhaundiyal, A**. and Atsu, D. (2020): Thermo-economic study of öNORM M7 133 Chips in a Pilot Scale Reactor. Production Technologies for Gaseous and Solid Biofuel. (Accepted)

9. ACKNOWLEDGEMENT

Many others support the tenure of human in this world. Acknowledgement for a few might be just a trifle thing written on a piece of paper. Nevertheless, in the true essence, it allows us to remember and express our feelings to those, whom we love, revere, and share our secrets. Here I get a great chance to express my token of thanks to people who helped and supported me to complete this record.

It is my sublime duty to express my most profound sense of gratitude and veneration to my supervisor, Professor Dr (Emeritus) Laszlo Toth, Doctoral school of Mechanical Engineering, Szent Istvan University, for his earnest exhortation, indelible inspiration, constant encouragement and constructive criticism, meticulous guidance and sustained interest, immense patience and supporting attitude throughout the investigation of the present research problem and preparation of this manuscript.

I express my most profound sense of reverence and indebtedness to the esteemed members of Doctoral School of Mechanical Engineering, Professor Dr Istvan Farkas, Head of the doctoral school of Mechanical Engineering, Professor Istvan Seres, Department of Mechanical Engineering, and Professor Peter Kiss, Head of Institute of Process Engineering, for their valuable suggestions and eternal encouragement at various stages of the investigation and thesis writing.

I am also thankful to Dr Norbert Schrempf, co-supervisor, Department of Mechanical Engineering, Dr Gabor Halasz, Head of Chemistry department, and Professor Daood Hussein, Department of Agriculture and Food Industry Machinery, Szent Istvan University, Godollo, for providing the necessary facilities to carry out the study.

I am grateful to my Indian mentor and co-researcher, Professor Suraj Bhan Singh, Department of Mathematics, Statistics and Computer Science, College of Basic Science and Humanities, Govind Ballabh Pant University of Agriculture and Technology, Pantnagar, Uttarakhand, India; Assistant Professor Csaba Feher, Department of Biotechnology, Budapest University of Technology and Economics, Budapest, Hungary; Mr Gabor Bercesi, Institute of Process Engineering, Szent Istvan University; Mr Istvan Bacskai, Mr Gabor Magyar, and Mr Laszlo, Institute of Agricultural Mechanization, National Agriculture and Innovation Centre; and Mr Laszlo Havas, Kaloria Hotechnikai Kft, Budapest, Hungary, for providing the logistic assistance. I am also thankful to the Indian Instrumentation Centre, Indian Institute of Technology, Roorkee, Uttarakhand, India for providing a testing facility.

Also, I would like to express my sincere gratitude to Professor Dr Klaus Gottshchalk, Leibniz Institute of Agricultural Engineering and Bioeconomy, Potsdam, Germany, and Professor Dr Zoltan Vargy, Department of Mathematics, Szent Istvan University, for providing me with valuable information about the modelling tool, which somehow assisted in the completion of my dissertation work.

Words will fall short to express the gravity of feelings for my colleague and research co-workers, Mr Muammel M. Hanon, Mr Divine Atsu and Mr Gedion Gabremichael Habtay, Doctoral school of Mechanical Engineering, whose helping attitude and suggestions have always been a source of energy at times of despair.

With a sense of gratitude and great pleasure, I acknowledge the wholehearted cooperation extended by Mrs Tassy Zsuzsanna and Mrs Monika Hajdu Torokne, Doctoral Office of Szent Istvan University.

My other teaching and non-teaching staff, the Department of Mechanical Engineering and my mates whilst carrying out experiments, Mr Taha Ibrahim, and Miss Bulgan Andryei, deserve a special word of thanks for supporting and encourage me.

At this juncture of time, my heart is full, and I feel short of words at my command to express my respect to my mother and father, whose invaluable love and support have brought me to this position.

My kind regards go to the Ministry of Human Resources Development, the University grant commission, New Delhi, India, and the Tempus Foundation, Hungary, to award me the Stipendium Hungaricum Fellowship. This list is incomplete but allows me to submit that the omissions are inadvertent. I once again record my heartfelt gratitude to all those who cooperated with me in this endeavour.

Gödöllő Alok Dhaundiyal

June 2021